GLOBAL IRRIGATION MAPPING – THE ROLE OF SPATIAL RESOLUTION OF CURRENT AND FUTURE EARTH OBSERVATION MISSIONS

Jonas Meier

München 2023

GLOBAL IRRIGATION MAPPING – THE ROLE OF SPATIAL RESOLUTION OF CURRENT AND FUTURE EARTH OBSERVATION MISSIONS

Jonas Meier

DISSERTATION ZUR ERLANGUNG DES DOKTORGRADES AN DER FAKULTÄT FÜR GEOWISSENSCHAFTEN DER LUDWIG-MAXIMILIANS-UNIVERSITÄT MÜNCHEN

VORGELEGT VON

JONAS MEIER

AUS LÖRRACH

eingereicht am 11. Januar 2023, München

Erstgutachter**:**	Prof. Dr. Wolfram Mauser
Zweitgutachter**:**	PD Dr. Florian Zabel
Tag der mündlichen Prüfung:	02. März 2023

“The breath I’ve taken and the one I must.”

- Johnny Flynn -

ZUSAMMENFASSUNG

Für die globale Nahrungsmittelproduktion sind bewässerte landwirtschaftliche Flächen von hoher Bedeutung. Ca. 20 % der globalen landwirtschaftlichen Flächen werden bewässert, jedoch werden 40 % der weltweit geernteten Nahrungsmittel auf diesen bewässerten Flächen produziert. Die globale Landwirtschaft ist mit 69 % der größte Süßwasserverbraucher und aufgrund des sich ändernden Klima wird erwartet, dass die bewässerten Flächen zunehmen werden. Ein höherer Wasserverbrauch der Landwirtschaft würde zu Interessenkonflikten zwischen unterschiedlichen Sektoren wie Energiewirtschaft, Industrie und private Haushalte führen. Daher ist ein effizienterer Umgang der Landwirtschaft mit der Ressource Wasser notwendig. Die aktuellen Bewässerungstechniken bestehen zumeist aus Oberflächenbewässerung im Stau- oder Rieselverfahren oder Sprinklerbewässerung. Diese Techniken nutzen die Ressource Wasser nur sehr ineffizient, da ein hoher Anteil am Wasser von der Oberfläche in die Atmosphäre verdunstet und nicht von der Pflanze genutzt werden kann. Um bei einer Verknappung der Ressource Wasser durch ein sich änderndes Klima und den damit einhergehenden landschaftlichen Veränderungen, wie dem Abschmelzen der Gletscher, die landwirtschaftliche Produktion dieser Flächen zu erhalten, wird eine Erhöhung der Wassernutzungseffizient notwendig. Der Wasserkreislauf wird hinsichtlich des Anteils des in den Pflanzen gebundenen Wassers (grünes Wasser) und dem Wasser, welches zurück in den Wasserkreislauf geführt wird, verändern. Um Wasserflüsse dieser Art Modellieren und damit Handlungsempfehlungen für politische Entscheidungen aussprechen zu können, werden Informationen über die bewässerten Flächen und Bewässerungstechniken in einer möglichst hohen räumlichen Auflösung benötigt. Bestehende Datensätze unterscheiden sich in ihrer Aussage über die bewässerten landwirtschaftlichen Flächen. Dies liegt vor allem an der unterschiedlichen Definition („bewässert“ oder „ausgestattet für Bewässerung“), an den Zeitpunkten der ermittelten Flächen und an den unterschiedlichen Methodiken und verwendeten Eingangsdaten. In der vorliegenden Arbeit wird eine neue Methodik entwickelt, die verschiedene Eingangsdaten kombiniert und bewässerte Flächen von nicht bewässerten Flächen unterscheidet. Hierfür werden nationale und sub-nationale Statistiken verwendet, die von den Ländern an die Food and Agriculture Organisation (FAO) gemeldet werden. Die Statistiken werden mit einer räumlichen Auflösung von 0,008333 Grad (ca. 1 km am Äquator) auf landwirtschaftlichen Flächen verteilt.

Zusätzlich zu den Statistiken wurde mittels Satellitendaten das Pflanzenwachstum global untersucht und mit einem von Klima- und Bodendaten abgeleiteten Datensatz in Bezug auf

die landwirtschaftliche Eignung verglichen. Entspricht die Vegetationsentwicklung auf landwirtschaftlichen Flächen nicht dem von Klima- und Bodendaten zu erwartendem Pflanzenwachstum wird davon ausgegangen, dass landwirtschaftliches Management in Form von Bewässerung zu dem beobachteten Pflanzenwachstum führt. Die Methodik detektiert 18 % mehr bewässerte Flächen als offiziell an die FAO gemeldet werden und deckt damit eine Wissenslücke in der aktuellen Forschung auf. Dies zeigt, dass Handlungsempfehlungen, die auf den offiziell gemeldeten Daten beruhen, nur bedingt praxistauglich sind. Darauf aufbauend vertieft die Arbeit die Frage nach den Unsicherheiten und möglichen Fehlerquellen des entwickelten Datensatzes. Hierbei wird systematisch für drei verschiedene Regionen der Einfluss der räumlichen Auflösung des Sensors an Bord des Satelliten analysiert. Der entwickelte Datensatz basierst auf dem Sensor SPOT-VGT mit einer räumlichen Auflösung von ca. 1 km. Um den Einfluss der räumlichen Auflösung systematisch zu quantifizieren, wurden hochaufgelöste Satellitendaten von Sentinel-2 von 10 m schrittweise auf 1 km skaliert und erneut die Bewässerung detektiert. Für die Durchführung des Experiments wurde, um Rechenzeit zu sparen, drei Regionen ausgewählt. Es konnte gezeigt werden, dass in zwei der Regionen (USA und Sudan) mit abnehmender räumlicher Auflösung auch eine Abnahme der detektierten bewässerten Flächen erfolgte. In China bleibt die detektierte Fläche konstant. Eine Analyse zeigt, dass je nach Lage und Verteilung der bewässerten Flächen, diese detektiert werden. Dichte, zusammenhängende Felder werden detektiert, lose im Raum verteilte Felder werden bei einer gröberen räumlichen Auflösung vernachlässigt. Dies konnte in der Studie mit Landschaftsmetriken erklärt werden, mit denen ein regional unabhängiger Zusammenhang zwischen dem Verlust von bewässerten Flächen bei gröberer Auflösung und dem „Landscape Shape Index“ (LSI) hergestellt werden konnte. Der Index ist ein Aggregationsindex und berechnet wie komplex eine Klasse (in diesem Fall „bewässerte Fläche“) gegenüber einer anderen Klasse in einer Landschaft (in diesem Fall „nicht bewässerte Fläche“) ist. Anhand dieser Erkenntnis können Regionen identifiziert werden, die anfällig für die Unterschätzung bewässerter Flächen sind und daraufhin mit feiner aufgelösten Satellitendaten korrigiert werden können.

Die räumliche Auflösung eines Sensors ist immer eine Abwägung zwischen technischer und finanzieller Umsetzbarkeit, Handhabung, Einsatzgebiet und Forschungsfragen. Bestehende Multi- und Hyperspektrale Satellitenmissionen mit Fokus auf Fragen über die Umwelt und Landwirtschaft weisen Sensor Auflösungen von 10 m (Sentinel-2) bis 30 m (EnMAP, LANDSAT) auf. Inwiefern sich diese Auflösungen für die Analysen landwirtschaftlicher Flächen eignen, wurde bisher noch nicht systematisch untersucht und ist Teil der vorliegenden Arbeit. Hierfür wurden Feldgrenzen der deutschen Bundesländer Bayern und Niedersachsen

und der Niederlande in eine Sentinel-2 Geometrie umgewandelt und in die Auflösungen von 5 m, 10 m, 20 m, 30 m und 50 m gebracht. Die Felder wurden dahingegen analysiert, bei welcher Auflösung diese noch von einem Satelliten abgebildet werden können und sich so für die Analyse landwirtschaftlicher Fragestellungen eignen. Zudem wurde analysiert wie viele Felder sich für Precision Farming Anwendungen eignen, um gezielt innerhalb des Felders zu bewässern oder zu düngen. Hierfür wurde ein Minimum von 50 Pixel pro Feld angenommen, welche notwendig sind, um Precision Farming Anwendungen einzusetzen. Die Analyse zeigt, dass bei einer Sentinel-2 Auflösung von 10 m 2-4 % der Felder nicht abgedeckt werden können und 20-50 % nicht für die Anwendung von Precision Farming zur Verfügung stehen. In die Analyse wurden zudem die Feldfruchtarten miteinbezogen, um besser zu verstehen, welche Fruchtarten für das Monitoring mit Satellitendaten zur Verfügung stehen werden. Die Arbeit stellt eine Grundlage zur Entscheidungsfindung zukünftiger Satellitenmissionen dar und hilft die Umsetzbarkeit von Anwendungen mit den aktuellen Satellitenmissionen einzuschätzen.

Insgesamt stellt die Arbeit die hohe Bedeutung von Informationen über globale Bewässerung in den Vordergrund und verdeutlicht die hohe Komplexität der Detektion bewässerter Flächen. Mit der Entwicklung eines neuen Datensatzes konnte die räumliche Auflösung verbessert werden und es wurde aufgezeigt, dass in vielen Regionen die bewässerte Fläche deutlich unterschätzt wird. Zudem wurde der Einfluss der räumlichen Auflösung analysiert und es konnte aufgezeigt werden, welche Sensor Auflösung zukünftiger Satellitenmissionen landwirtschaftliche Felder in Europa am besten abbilden können.

SUMMARY

Irrigated agricultural area is of high importance for global food production. Approximately 20 % of global agricultural area is irrigated, but 40 % of the world's harvested food is produced on these irrigated area. Global agriculture is the largest consumer of freshwater (69 %) and due to a changing climate, irrigated area is expected to increase. Increased water consumption by agriculture would lead to conflicts of interest between sectors such as energy, industry, and households. Therefore, a more efficient use of water by agriculture becomes necessary. Current irrigation techniques mostly consist of surface or sprinkler irrigation. Both techniques use the resource water only very inefficiently, since a high proportion of the water evaporates from the surface into the atmosphere. In order to maintain the agricultural production of these areas in the case of a scarcity of the resource water due to a changing climate and the accompanying landscape changes, such as the melting of the glaciers, an increase in the water use efficiency becomes necessary. In order to model water flows and to analyze future changes for recommendations for policy decisions, information on irrigated area and irrigation techniques, at a high spatial resolution, is needed. Existing data set differ in the extent of global irrigated area. Reasons are the different definition ("irrigated" or "equipped for irrigation"), the investigated time period, and the different methodologies and input data. In the present work, a new methodology is developed that combines different input data and distinguishes irrigated areas from non-irrigated areas. National and sub-national statistics reported by countries to the Food and Agriculture Organization (FAO) are one input. This information is spatially distributed on agricultural area at a spatial resolution of 0.008333 degrees (approximately 1 km at the equator), the only available dataset with a spatial resolution of 1 km. In addition to the statistics, satellite data were used to examine plant growth globally and compare it to agricultural suitability derived from climate and soil data. If the vegetation development on agricultural area does not correspond to the plant growth expected from climate and soil data, it is assumed, that agricultural management, like irrigation, leads to the observed plant growth. The methodology detects 18 % more irrigated areas than officially reported to FAO, revealing a knowledge gap in current research and showing that recommendations for action based on officially reported data are limited. Based on these issues, this thesis delves into the question of uncertainties and possible sources of error in the dataset. The influence of the spatial resolution of the sensor is analyzed systematically for three different regions. The developed data set is based on the SPOT-VGT sensor with a spatial resolution of about 1 km. To systematically quantify the influence of spatial resolution, high-resolution satellite data from Sentinel-2 were scaled from 10 m to 1 km stepwise and irrigation was detected. To save computational time, three regions were

selected for the conduction of the experiment. It was shown that in two of the regions (USA and Sudan), decreasing spatial resolution leads to decreasing of detected irrigated area. In China the detected area remains constantly. An analysis of the spatial distribution of the irrigated area shows that the mapping result depends on the spatial arrangement and distribution of the irrigated area. Dense, contiguous fields are detected, loosely distributed fields are neglected at a coarser spatial resolution. The study demonstrated, that the negative areal change can be explained by landscape metrics. The application of landscape metrics showed a regionally independent relationship between the loss of irrigated areas at coarser resolution and the "Landscape Shape Index" (LSI). The index is an aggregation index and calculates how complex one class (in this case "irrigated area") is compared to another class in a landscape (in this case "non-irrigated area"). This finding can be used to identify regions that are prone to underestimating irrigated area, for further analysis using high resolution satellite data.

The spatial resolution of a sensor is always a trade-off between technical and financial feasibility, handling, scope of application, and research questions. Existing multi- and hyperspectral satellite missions focused on environment and agriculture have sensor resolutions ranging from 10 m (Sentinel-2) to 30 m (EnMAP, LANDSAT). The suitability of these resolutions for the analysis of agricultural areas has not yet been systematically investigated and is part of this thesis. Field boundaries of the German states Bavaria and Lower Saxony and the Netherlands were converted into a Sentinel-2 geometry and rescaled to the resolutions of 5 m, 10 m, 20 m, 30 m, and 50 m. The fields are analyzed regarding at which resolution the fields can be recorded completely by a satellite and are thus suitable for the analysis of agricultural questions. In addition, it was analyzed how many fields are suitable for precision farming applications in order to establish an in-field management monitored by satellites. Therefore, a minimum of 50 pixels per field was assumed, which are necessary to use precision farming applications. The analysis shows that at a Sentinel-2 resolution of 10 m, 2-4 % of the fields cannot be covered and 20-50 % are not available for precision farming applications. Field crop types were also included in the analysis for a better understanding which crop types will be available for a satellite-based monitoring. This thesis provides a basis for decision making for future satellite missions and helps to assess the feasibility of applications with current satellite missions.

Overall, this thesis highlights the high importance of global irrigation information and the high complexity of methods detecting irrigated area. With the development of a new dataset, the spatial resolution could be improved and it was shown that in many regions the irrigated area is significantly underestimated. Furthermore, the influence of spatial resolution was

analyzed and it could be shown how the spatial resolution of current and future satellite missions affects the possibility of agricultural monitoring in Europe and the possibility of in-field management and precision farming applications.

ACKNOWLEDGEMENTS

Writing this thesis was a challenging journey with some unseen findings and developments. So close to the end, I am thinking of so many people who accompanied and support me during this exciting and interesting but also demanding and challenging time. First of all, I would like to thank and express my deepest gratitude to my Ph.D. supervisor, Prof. Dr. Wolfram Mauser, who gave me the opportunity to take my first steps in the scientific world and who always inspired me with his sharp and innovative ideas and his view over the edge. During this long journey, he stood always by my side and supported and encouraged me to take the next steps and finalize this thesis.

As important for this work was my second supervisor PD Dr. Florian Zabel, who was always able to place my work into the big picture and was a driving force behind the ideas and implementations of the research. Also, for taking me out from time to time to free my mind and for reminding me on life beyond work. Thanks also to PD Dr. Tobias Hank for inspiring discussions and for all his unconditional support in different projects.

I also want to thank my former Ph.D. colleagues Matthias Wocher and Tom Jaksztat for all the challenging discussions, warm exchange of thoughts and the daily adventurous walks down Augusten Street for finding some lunch. Special thanks go to Dr. Franziska Koch, my long-term roommate at the LMU, for cheering me up in hard times and for her honest exchange of views.

Further, I would like to thank all my other LMU colleagues, not mentioned by name, for the vibrant working environment, the balcony beers and the activities beyond. Besides my colleagues from the LMU, I also want to thank my colleagues from the DLR for supporting and encouraging me in the final phase of this thesis.

Finally, I want to thank my family for making this possible, all my friends for being the best friends I can have and particularly Marie and my two kids Mathilda and Janosch, thank you for making this life as beautiful as it is.

CONTENTS

1 Introduction

1.1 Sustainable intensification of global agriculture as key to address the Sustainable Development Goals

Global agriculture plays a crucial role in addressing the two major challenges of the 21st century: food security and climate change. The transition of global agriculture towards a more sustainable use of resources is critical to both of these goals. Separate by sector, agriculture is with 69 % the largest consumer of fresh water (FAO, 2014) and with 17 % one of the largest producers of greenhouse gases (FAO, 2021). Therefore, changes are needed especially in the use of natural resources such as fresh water for irrigation or fertilizers and pesticides. To secure today's and future global food supplies in a sustainable way, agriculture has to increase the efficiency of the used resources (Foley *et al.*, 2011). Therefore, new agricultural farming practices, which use resources in a more sustainable way are needed (Mueller *et al.*, 2012). Considering a rising world population, a changing diet towards more meat consumption and an increase use of biofuel and bio-based materials lead to estimations that global agricultural production will have to double by 2050 (FAO, 2012, Godfray *et al.*, 2010, Tilman *et al.*, 2011). An expansion of cropland does not solve the problem of overusing natural resources and leads to a decline of biodiversity (Zabel *et al.*, 2019). Therefore, new agricultural farming practices, which use resources in a more sustainable way are needed. A crucial role for global food security plays the irrigated agricultural area. 40 % of the global yields are harvested on irrigated area, which currently constitutes 20 % of the harvested area globally (FAO, 2016). The extent of irrigated area almost doubled over the last 50 years and a future expansion and a related increase in water consumption is expected (FAO, 2016, Neumann *et al.*, 2011).

Depending on the region, climate change decreases agricultural water availability (Strzepek *et al.*, 2010). The low irrigation efficiency of the common irrigation techniques such as sprinkler and flood irrigation (Evans *et al.*, 2008), the unsustainable usage of limited sources like groundwater (Wada *et al.*, 2014), the changing river regimes (Döll *et al.*, 2012) and the changing supply by snowmelt (Mankin *et al.*, 2015, Prasch *et al.*, 2013) underline the need for a transition towards more sustainable and efficient use of water. The UN Sustainable Development Goals clearly reflect this need to achieve food security and the sustainable development of land use (United Nations, 2015). For better inventorying and investigation of global and regional water cycles and as input for crop models, detailed global information on irrigated areas at high resolution are needed.

Agriculture will not be the only sector with an increasing demand for fresh water, which leads to conflicts between different groups of interest like hydropower, industry and private houses (Mostafa *et al.*, 2021, Wu *et al.*, 2022). Further, the withdrawal of water has an impact on surrounding ecosystems and on downstream riparian. This could lead not only to conflicts between sectors but between states (Swain, 2011). Therefore, transnational rules are important to avoid resource conflicts (Petersen-Perlman *et al.*, 2017). Developing international rules must rely on current and reliable data on agricultural land and its management – in this case, irrigation practices, while these data are scarcely available.

1.2 LAND COVER AND LAND USE DATA, NATIONAL AGRICULTURAL STATISTICS AND THE QUESTION OF ACCURACY

Information about land use and management are available in different aggregation levels depending on the region. Well known are the country-wide statistics of the Food and Agriculture Organization (FAO) about cropland, yields and management practices. The FAO is part of the UN and successor of the International Institute of Agriculture (IIA) founded in 1905 (Phillips, 1981). To prevent exploitation and cartelization of the agriculture sector the IIA published a yearly report including information and statistics about the extent of cropland and indicators for production. In 1930 the IIA was the largest international organization representing the agricultural sector in 75 countries (Phillips, 1981). After the second World War, the UN and FAO was founded and the IIA merges into the FAO. The FAO sees itself in the tradition of the IIA, but sets other priorities and goals, such as raising the nutritional and living standards of its members, improving the production and distribution of food, and improving the living conditions of rural populations. The ultimate goal remains to produce and distribute enough food for all people. To achieve these goals, not only data and statistics are collected, but also research and application of alternative farming methods are carried out and global development projects towards sustainable agriculture are offered. The verification of these implemented new methods and the creation of a comprehensive monitoring will continue to be statistics and data of the member states as spatially accurate as possible requested and reported (FAO, 2015). The problem that already at the beginning of the IIA showed that by missing independent controls the data provided by the members are made consciously wrong to cover up wrong developments or to use it as an instrument to assert political interests (FAO, 2015, Vörösmarty, 2002). Nevertheless, the data are the only available data for global agriculture, even besides the described deficiencies and their spatial limitation since the

reports consist mostly of country-wide statistics. Surveys about agricultural management practices are always limited to a region and are costly and time-consuming to conduct. In addition, data about farming practices and yields are often sensitive data and are highly protected. In case of agricultural subsidies, like the Common Agriculture Policy (CAP) in Europe, farmers are reporting the extent and cultivated crops to the European Commission (European Commission, 2022). Data on the spatial location of the fields including their crops are available but are subject to strict data protection regulations and mostly not available to the public.

Methods that do not rely on surveys or official statistics and reports have been developed to identify agriculture area, their management and other land cover classes (García-Álvarez *et al.*, 2022). Even before the introduction of remote sensing tools, some land use and land cover (LULC) information were available but with the introduction of aerial and especially satellite imagery starts of systematic land use and land cover maps at different spatial scale. LULC maps in times before aerial and satellite imagery were based on ground-based data acquisition, a very time-consuming, laborious process (García-Álvarez et al., 2022). Using aerial photography and later satellite data LULC mapping became easier and cheaper (Fuller *et al.*, 1994). Especially the start of the Landsat program in 1972 is a turning point for the LULC mapping community, as the first multi spectral scanner (MSS) on board of a satellite. The first regional study about vegetation monitoring using the Normalized Difference Vegetation Index (NDVI) was based on Landsat 1 imagery (Rouse *et al.*, 1973). The constricted data access and the limited computational power leads to a more local and regional use for LULC mapping (Belward *et al.*, 2015). During the 1980ies first global LULC data set were produced with a strong thematic focus on vegetation by combining existing maps, field data and interpretation of aerial and satellite information from multiple spectral sensors like AVHRR sensor aboard the NOAA and EUMETSAT weather satellite (Giri, 2005). In 1994 the first systematically classified LULC was published by Defries *et al.* (1994) using AVHRR data at a very coarse spatial resolution of 1 degree (~111km at the equator). The development of medium resolution sensors like SPOT and MODIS opened a new chapter in LULC mapping at a high spatial resolution of 30 arc seconds (~1km at the equator) and the increasing computational power allows researcher to perform LULC mapping for different time periods like GlobeCover (Arino *et al.*, 2012), GLC250 (Wang *et al.*, 2015) or MCD12Q1 (Friedl, 2022). Improvements in LULC mapping methods and an increase in computational power takes place parallel to the launch of new satellite missions like the Copernicus program of the European Space Agency (ESA, 2022). This results in yearly updated LULC products at 300 m back to 1992 (ESA, 2017) and

since the operational use of Sentinel-2 data, LULC data are available at a spatial resolution of 10 m (Zanaga, 2021).

The methods deriving the LULC maps and the research objectives differ. Therefore, a cross-data analysis is not recommended, since even the classification scheme varies depending on the initial research objectives. Thematic LULC maps focus on a specific land use or land cover like water (Klein *et al.*, 2017, Pekel *et al.*, 2016), artificial land cover (Schneider *et al.*, 2008), ice, sown and glaciers (GLIMS Consortium, 2005) or regional focus e.g. Amazonas basin (Cherif *et al.*, 2022) or arctic shield (A'Campo *et al.*, 2021). A focus on vegetation is one of the most popular research objectives of LULC as it combines a wide range of different disciplines like mapping the extent and changes of forests (Holzwarth *et al.*, 2020, Thonfeld *et al.*, 2022), grassland (Reinermann *et al.*, 2020) or the classification of regional vegetation types (Borges *et al.*, 2020, Sano *et al.*, 2010). Agriculture as part of the vegetation and one of the predominant land use, plays an important role in LULC products. The land use class of agriculture ranges from rice fields to crops such as corn and wheat to specialty crops like vegetables and grapes. Agriculture area is also characterized by different agriculture management. Derived management practices are tilling (Porwollik *et al.*, 2019), fertilization (Ludemann *et al.*, 2022), harvesting (Kavats *et al.*, 2019) or irrigation (Meier *et al.*, 2018).

1.3 STATE OF THE ART IN GLOBAL IRRIGATION MAPPING

One part of this thesis is the development of a new method to derive irrigated area on a global scale. Previous studies showed the potential of earth observation (EO) data to detect irrigated areas for small- and medium-scale analyses. Several studies have shown the feasibility of mapping irrigated area using EO data from local to regional scale (Abuzar *et al.*, 2015, Ambika *et al.*, 2016, Jin *et al.*, 2016, Ozdogan *et al.*, 2008). The methods combine different data to exclude rain-fed and irrigated land by strong indicators like evapotranspiration (Cammalleri *et al.*, 2014), climatic conditions (Salmon *et al.*, 2015), thermal variations over an irrigated field (Abuzar et al., 2015) or soil moisture (Lawston *et al.*, 2017). Only few studies identify irrigated area on a global scale (Meier et al., 2018, Salmon et al., 2015, Siebert *et al.*, 2005, Thenkabail *et al.*, 2009). General LULC data often neglect irrigated area, some classify irrigated area as a separate class, without a focus on irrigated area (ESA, 2015).

The existing global irrigation maps are combining multiple data sources to derive irrigated area. A common approach distributes official reported irrigated area from national or sub-national statistics on agriculture area from existing LULC (Siebert et al., 2005). The resulting Global Map of Irrigation Areas (GMIA) is restricted to the official numbers and is hard to verify,

since statistics may include errors and the quality of the data depends on the willingness of the member countries. Around the year 2000 the official FAO statistics about irrigated area engendered criticism after comparing national statistics with remote sensed based data (Vorosmarty *et al.*, 2000). The discrepancies between those data were explained by the politicized nature of the FAO data reports and different definitions of irrigated area (Vörösmarty, 2002). The first remote sensing based global irrigation map is the study of Thenkabail et al. (2009). The study combines meteorological data, LULC maps and remote sensing data from multiple sensors and identified 43 % more irrigated area than reported in FAO statistics. Salmon et al. (2015) combine statistics, climate -and remote sensing data. The study also shows an underestimation by the national -and sub-national statistics – although a smaller one than the study of Thenkabail et al. (2009) – and showed, that merging remote sensing data and ancillary data is suitable for irrigation mapping. Thenkabail et al. (2009) concludes that 'both remote sensing and national statistical approaches require further refinement'.

The differences in the extent of irrigated area are well known and discussed controversy in the scientific community (Puy *et al.*, 2022a, Puy *et al.*, 2022b). The differences are caused by several reasons: the approaches differ, the studies are applied at different time periods and the EO data are not always from the same satellite/source. The sensor resolution of satellites varies depending on their initial research objectives and technological requirements. The influence of the sensor resolution on the accuracy of LULC mapping is analyzed with a focus on high spatial resolution between 1 m and 30 m (Fisher *et al.*, 2018, Yu *et al.*, 2020) but coarser resolution of global data are neglected. Even the source of error outgoing from sensor resolution of global irrigation map is very obvious but there is no study which analyze the influence of spatial resolution on irrigation mapping methods. From a global perspective, large contiguous irrigated area like the Nile delta, Central Valley in California, irrigated area at the Indus and Ganges or in South-East Asia are well known and are part of the global irrigation data set. In many regions irrigation is part of very small subsidence agriculture and is not part of any reports. For instance in some countries in Western Africa the informal irrigated areas in urban and peri-urban areas are twice the size of the officially reported irrigated areas for the whole country (Drechsel, 2006). Even with a high-resolution sensor the spatial resolution of the sensor always limits the analysis of small scaled agriculture.

1.4 SCOPE OF THE THESIS

Based on the state of the art in global irrigation mapping, this thesis is focusing on the development of a new approach to derive irrigated area, the comparison of the mapping result to existing products and the investigation of potential source of errors. One source of error lies in the choice of the spatial resolution. Therefore, a systematic analysis of the influence of the sensor resolution on the result of the irrigation mapping was conducted. The influence of the spatial resolution of a sensor on the mapping result has not been evaluated systematically yet. Velpuri *et al.* (2009) compared data from different satellites on an irrigation mapping method for a local study but did not transfer their findings to other regions. Applying the developed irrigation mapping approach on Sentinel-2 data downscaled stepwise from 10 m to 1000 m showed different results depending on the arrangement and size of the fields. The findings are important for the interpretation of existing irrigation maps since it shows, that the areal change with coarser resolution is caused by the spatial arrangement of the fields and this varies regionally. The spatial resolution of a sensor always limits the analysis of small scaled agriculture. To obtain meaningful information about agricultural management on field level, the spatial resolution of the sensor must correspond to the size of the fields. To evaluate the coverage of current and future satellite missions, this work analyzed the extent to which agricultural monitoring is possible with a common resolution of 5 m to 50 m. Agricultural fields are heterogeneous, depending on the soil properties and location. An in-field monitoring can assist farmers with detailed information about plant conditions for a precise application of fertilizer or water and can use resources more efficiently. The choice of spatial resolution of the satellite sensor is always a trade-off between several system parameters. Among those are the spatial resolution of the optical system, the sensor and the electronics, the onboard storage capacity and/or the transmission bandwidth in combination with the chosen orbit and revisit time. This study supports the design of future satellite missions in terms of how many fields are available for agriculture monitoring and site-specific management information e.g. precision farming which promises large commercial and environmental benefits through a more efficient use of resources.

2 Framework of the thesis and overview of the publications

1. Meier, J.; Zabel, F.; Mauser, W. (2018): A global approach to estimate irrigated areas – a comparison between different data and statistics. *Hydrol. Earth Syst. Sci.*, *22*, 1119-1133, https://doi.org/10.5194/hess-22-1119-2018.

2. Meier, J.; Mauser, W. (2023): Irrigation mapping at different spatial scales: Areal change with resolution explained by landscape metrics. *Remote Sensing*, 15, 315. https://doi.org/10.3390/rs15020315.

3. Meier, J.; Mauser, W.; Hank, T.; Bach, H. (2020): Assessments on the impact of high-resolution-sensor pixel sizes for common agricultural policy and smart farming services in European regions. *Computers and Electronics in Agriculture*, *169*, 105205, https://doi.org/10.1016/j.compag.2019.105205.

The first publication is focusing on global information about irrigated area. The paper outlines the possibilities of surveying data about irrigated area and summarizes the state of the art and approaches of the existing data set about global irrigated area. Outgoing from the state-of-the-art data set of Siebert et al. (2005) the study evolves a new data set of global irrigated area in combining existing data set and until now unknown irrigated area. First, the approach is downscaling the irrigation map of Siebert et al. from 5 arc minutes to 30 arc seconds, this increases the spatial resolution from approx. 10 km² to 1 km² (at the equator).

The approach investigates the development of the plant growth on agriculture area, known from global land use and land cover data set. The crop development is then compared to an agricultural suitability analysis considering soil and climate data (Zabel *et al.*, 2014). In case of observed plant growth at a low agricultural suitability, it is assumed that artificial irrigation has been applied. The agricultural suitability also provides the possibility of multiple cropping in one year. This information can be compared with the annual course of the multi temporal NDVI data. If the NDVI course shows two or more cropping seasons in one year while the agriculture suitability shows a limitation to fewer cropping cycles, the area is assumed as irrigated. The combination of the reported irrigated area and newly detected irrigated area results in a new global irrigation map. The new irrigation map is compared to existing global irrigation maps and the differences are discussed. The new global irrigation map is freely

available and serves as a basis and/or benchmark for many recent studies since the data set is downloaded 337 times and was cited 115 times in scientific publications.

One reason for the differences in mapping results is the sensor resolution of the used satellite. The scope of the second paper is to quantify the mapping result at different spatial resolutions. Therefore, data from Sentinel-2 at 10 m resolution are artificially downscaled to 20 m, 40 m, 60 m, 100 m 300 m, 600 m and 1000 m and the mapping approach presented in the first paper is applied. The study is conducted in three regions in USA, China and Sudan to cover a broad range of farming systems. The results show that in general the mapped area decreased but not to the same extent. The mapped irrigated area in USA (-48%) and Sudan (-29%) decreased tremendously while the mapped area in China remains at all spatial resolution. The study showed that the decrease in mapped irrigated area is caused by the spatial formation and arrangement of the irrigated area. A high distribution of the irrigated area is more affected by the downscaling to a lower resolution than irrigated area in a dense cluster. The negative change of mapped irrigated area can be explained by landscape metrics, a concept well known from biodiversity and habitat analysis. The applied Landscape Shape Index (LSI) showed in all three regions a strong correlation with the negative changes of mapped irrigated area with spatial resolution ($r>0.9$). The relations show that the concept is regionally independent and transferable to other regions.

The choice of the sensor resolution directly affects the mapping result. High resolution sensors like Sentinel-2 allows the analysis of agricultural management on field scale. From a global perspective, field scale differ regionally and depend on different parameters like the level of mechanization and on the economic, cultural and geographic background. Depending on the spatial resolution of the sensor and the field scale the derivation of information about agricultural management on field scale is possible. Coarser spatial resolution sensors lead to a spectral mix of different fields or land uses. Considering a field as a homogeneous unit the margins might overlap with other land uses in the recording path of the satellite. The question of the requirements for the spatial resolution of a sensor is the topic of the third paper. Which spatial sensor resolution is needed to cover agricultural area and how many fields are not part of the current satellite missions? To evaluate the agricultural coverage of current satellite missions, data on real field boundaries are essential. Information about agriculture field boundaries are available for some regions. The European Commission is using data about agricultural plots collected in the Land Parcel Identification System (LPIS) to monitor the Common Agricultural Policy (CAP), mainly known from agricultural subsidies, but the public availability of the data differs and is often subject to data protection law. Therefore, three regions are selected, where access to the LPIS data portal was possible: Bavaria and Lower

Saxony in Germany and the Netherlands. The field boundaries, available as polygons, are rasterized at 5 m, 10 m, 20 m, 30 m and 50 m using the Sentinel-2 pixel location and geometry. To avoid spectral mix pixel at the field margins, only the pure pixel inside the field boundaries were considered to ensure the correct application of algorithms for deriving agricultural management like irrigation. The study also evaluated the possibility of site-specific agriculture management (smart farming), which promises major economic and environmental benefits as resources such as water, pesticides, and fertilizers can be applied more efficiently and minimize environmental impacts. Therefore, we assume 50 pure pixel inside a field is a critical number of pixel for site-specific farming, fields with less than 50 pure pixel are not considered as available for smart farming applications. The information on the crop types remains during the analysis and shows which crops are covered by current or potential future satellite missions.

The abstracts of the three publications summarize the manuscripts and the results obtained.

2.1 A GLOBAL APPROACH TO ESTIMATE IRRIGATED AREAS – A COMPARISON BETWEEN DIFFERENT DATA AND STATISTICS. (PAPER 1)

Agriculture is the largest global consumer of water. Irrigated areas constitute 40 % of the total area used for agricultural production. Information on their spatial distribution is highly relevant for regional water management and food security. Spatial information on irrigation is highly important for policy and decision makers, who are facing the transition towards more efficient sustainable agriculture. However, the mapping of irrigated areas still represents a challenge for land use classifications, and existing global data set differ strongly in their results. The following study tests an existing irrigation map based on statistics and extends the irrigated area using ancillary data. The approach processes and analyzes multi-temporal normalized difference vegetation index (NDVI) SPOT-VGT data and agricultural suitability data – both at a spatial resolution of 30 arcsec – incrementally in a multiple decision tree. It covers the period from 1999 to 2012. The results globally show a 18 % larger irrigated area than existing approaches based on statistical data. The largest differences compared to the official national statistics are found in Asia and particularly in China and India. The additional areas are mainly identified within already known irrigated regions where irrigation is more dense than previously estimated. The validation with global and regional products shows the large divergence of existing data set with respect to size and distribution of irrigated areas caused by spatial resolution, the considered time period and the input data and assumption made.

2.2 IRRIGATION MAPPING AT DIFFERENT SPATIAL SCALES: AREAL CHANGE WITH RESOLUTION EXPLAINED BY LANDSCAPE METRICS (PAPER 2)

Monitoring of irrigated area still represents a complex and laborious challenge in land use classification. Extent and location of irrigated area vary with both methodology and scale. One major reason for discrepancies is the choice of spatial resolution. This study evaluates the influence of the spatial resolution on the mapped extent and spatial patterns of irrigation using an NDVI-threshold approach with Sentinel-2 and operational PROBA-V data. The influence of resolution on the irrigation mapping was analyzed in the USA, China and Sudan to cover a broad range of agricultural systems by comparing results from original 10 m Sentinel-2 data with mapped coarser results at 20 m, 40 m, 60 m, 100 m, 300 m, 600 m and 1000 m and with results from PROBA-V. While the mapped irrigated area in China is independent of resolution, it decreases in Sudan (-29%) and the USA (-48%). The differences in the mapping result can largely be explained by the spatial arrangement of the irrigated pixels at the fine resolution. The calculation of landscape metrics in the three regions shows that the Landscape Shape Index (LSI) can explain the loss of irrigated area from 10 m to 300 m ($r>0.9$)

2.3 ASSESSMENTS ON THE IMPACT OF HIGH-RESOLUTION-SENSOR PIXEL SIZES FOR COMMON AGRICULTURAL POLICY AND SMART FARMING SERVICES IN EUROPEAN REGIONS (PAPER 3)

High-resolution (5–50 m) remote sensing satellite sensors provide a reliable, free and open data infrastructure for public and private agriculture and land use services. The further market penetration of these services critically depends on the fraction of agricultural fields and area that the services can cover. EU's Common Agricultural Policy (CAP) and smart farming services require a minimum of spectrally pure measurements per agricultural field. The impact of pixel size on the coverage of agriculture is studied in this paper considering present free and open optical sensors (Sentinel-2 and LANDSAT). It further studies the implications of the selection of spatial resolution of planned extensions of these sensors, i.e. the next generation of Sentinel-2, as well as Copernicus's hyperspectral CHIME and thermal LSTM future candidate missions. The paper analyzes the 2018 vector boundaries and crop types of 3.6 million agricultural fields in the German States of Bavaria and Lower Saxony and the Netherlands. The fields were rasterized using Sentinel-2 flight geometry and a pixel spacing of 5, 10, 20, 30 and 50 m. The study specifically considered: (1) fields with no pure pixel inside where no CAP services can be provided and (2) fields with less than 50 pure pixels inside, which is estimated to be the critical number for site-specific smart farming. The percentage of agricultural fields

and agricultural area was determined for the main crop types. It shows, that with 10 m pixel spacing 2–4 % and 20 m pixel spacing 12–22 % of the agricultural fields in the study area do not contain a single pure spectral sample (Sentinel-2 case). This fraction decreases to 1–3 % at 5 m spacing and increases to 25–40 % for 30 m (LANDSAT and CHIME) and 50–70 % for 50 m (LSTM) spacing. The percentage of fields with less than 50 pure pixels is 20–50 % at 10 m and 70–85 % at 20 m spacing (Sentinel-2). This fraction decreases to 5–12 % for 5 m spacing and reaches the level of 92–97 % for 30 m (LANDSAT) and 99 % for 50 m spacing (LSTM). Our analysis shows, that with a pixel spacing of 5 m the Sentinel-2-based site-specific smart farming services could increase their potential customer base from ~50 % to ~90 % of the agricultural fields and could potentially cover 99 % of the regions' agricultural area. A 20 m pixel spacing would increase the agriculture area from 23 % to 56 % in the Central and Western European study regions on which the Copernicus hyperspectral candidate mission CHIME is capable to measure pure and full spectra for highly advanced future site-specific management services. LSTM would also profit from a spatial resolution of 30 m, which would raise coverage of the agricultural area in Central Europe with pure thermal measurements from 3 % at 50 m to 23 % at 30 m.

3 Conclusion and Outlook

The aim of the thesis was the development of a new global irrigation map. The complex approach, the influence of sensor resolution on the mapped extent of irrigated area and the question of how the sensor resolution should be designed to meet the requirements for agriculture monitoring and precision farming were the key issues addressed in the three publications.

Mapping irrigated area still represents a challenge in land use classification. Until now, there is no existing approach to detect irrigated area globally without ancillary data. This thesis pointed out that irrigation mapping in arid area is possible but is limited in humid area where farmers mostly use supplementary irrigation. That means, from a climatological point of view it is possible to farm in this area but due to economical or traditional reasons farmers are irrigating their fields. This is the case in the Po Valley in Italy, where a large amount of paddy rice is traditionally grown in a climate where rainfed agriculture would be possible. Therefore, additional data from official statistics are included. The developed global irrigation map extends the area officially reported by the FAO by 18 % and confirms findings from other independent information on global irrigated area, that official numbers are underestimating the current extent of irrigated area. The until now unknown or unreported irrigated area are located in regions already characterized by large irrigated area like in India and China but are not reported to the FAO. This shows the need of independent information about land use and agriculture management. Independent information on global irrigated area differs and are discussed in this thesis. The influence of spatial resolution on irrigation mapping is analyzed systematically in three different regions and showed that the mapped extent of irrigated area is affected differently depending on the spatial distribution and arrangement of the irrigated fields. This thesis could show that landscape metrics, well known from biodiversity and habitats analysis, can explain the negative areal change in irrigation mapping at different spatial resolutions. The relation between lost mapped irrigated area and the Landscape Shape Index (LSI) was found in all three analyzed regions which shows the correlation is regionally independent and thus transferable to other regions. Analyzing existing irrigation maps using the LSI can detect regions that tends to underestimate the mapped irrigated area in the existing products, which are mainly derived by wide swath medium-resolution sensors like VEGETATION, MODIS and AVHRR. Further, this thesis showed, that high spatial resolution sensors like Sentinel-2 satellite mission can open a new chapter of global irrigation mapping. This also relates to the temporal dynamic which is neglected in the existing products since the mapping is limited to one year or to a defined time period. Ambika et al. (2016) showed in a

regional study in India a high temporal dynamic regarding irrigation practices since the application of water is mainly done when water is available or access to infrastructures, like irrigation equipment or electric power, is provided. High resolution sensors like the Sentinel-2 satellite mission and increasing computational power enables a more precise detection of irrigated area. Information on irrigated area are highly needed in climate models, as the land surface influences the atmosphere and land surface models, like hydrological and crop growth models, to improve the knowledge regarding water flows. The combination and comparison of spatially distributed crop growth models with time series of multi spectral remote sensing observations over the whole vegetation period will allow the traceability of the irrigation management like the used irrigation water by the crops, irrigation water loss through interception or soil evaporation and overall water use efficiency. A remote sensing-based monitoring system of the described kind is the prerequisite for the improvement of irrigation management towards a less wasteful use of the precious water resources by the farmers and can be a strong instrument in negotiations regarding upstream-downstream water conflicts in large watersheds.

The next step should be the development of an automatically updated irrigation monitoring system that supplies the user's up-to-date information about the state of irrigation in terms of location, area and type. This allows in-field management and a direct application of water or fertilizers and pesticides to plants affected by water stress or diseases. Smart farming or precision farming with in-field management based on space-born information has the potential to increase the efficiency of used resources in agriculture in a sustainable way. The basic requirement for the use of smart farming applications is that the resolution of the sensor corresponds to the size of the fields and beyond. The evaluation of current satellite missions and their suitability for smart farming applications in Europe showed that future satellite missions should be designed in at least the Sentinel-2 resolution of 10 m. Due to the small scaled agriculture in parts of Europe, in-field management as a comprehensive solution would need an even higher spatial resolution of the sensor. The findings of this thesis can provide a basis for decision-makers in planning future satellite missions.

REFERENCES

A'Campo, W.; Bartsch, A.; Roth, A.; Wendleder, A.; Martin, V.S.; Durstewitz, L.; Lodi, R.; Wagner, J.; Hugelius, G. (2021): Arctic Tundra Land Cover Classification on the Beaufort Coast Using the Kennaugh Element Framework on Dual-Polarimetric TerraSAR-X Imagery. *Remote Sensing*, *13*, 4780.

Abuzar, M.; McAllister, A.; Whitfield, D. (2015): Mapping Irrigated Farmlands Using Vegetation and Thermal Thresholds Derived from Landsat and ASTER Data in an Irrigation District of Australia. *Photogrammetric Engineering & Remote Sensing*, *81*, 229-238.

Ambika, A.K.; Wardlow, B.; Mishra, V. (2016): Remotely sensed high resolution irrigated area mapping in India for 2000 to 2015. *Sci Data*, *3*, 160118.

Arino, O.; Ramos Perez, J.J.; Kalogirou, V.; Bontemps, S.; Defourny, P.; Van Bogaert, E. (2012): Global Land Cover Map for 2009 (GlobCover 2009). European Space Agency (ESA) & Université catholique de Louvain (UCL), PANGAEA.

Belward, A.S.; Skøien, J.O. (2015): Who launched what, when and why; trends in global land-cover observation capacity from civilian earth observation satellites. *ISPRS Journal of Photogrammetry and Remote Sensing*, *103*, 115-128.

Borges, J.; Higginbottom, T.P.; Symeonakis, E.; Jones, M. (2020): Sentinel-1 and Sentinel-2 Data for Savannah Land Cover Mapping: Optimising the Combination of Sensors and Seasons. *Remote Sensing*, *12*, 3862.

Cammalleri, C.; Anderson, M.C.; Gao, F.; Hain, C.R.; Kustas, W.P. (2014): Mapping daily evapotranspiration at field scales over rainfed and irrigated agricultural areas using remote sensing data fusion. *Agricultural and Forest Meteorology*, *186*, 1-11.

Cherif, E.; Hell, M.; Brandmeier, M. (2022): DeepForest: Novel Deep Learning Models for Land Use and Land Cover Classification Using Multi-Temporal and -Modal Sentinel Data of the Amazon Basin. *Remote Sensing*, *14*, 5000.

Defries, R.S.; Townshend, J.R.G. (1994): NDVI-derived land cover classifications at a global scale. *International Journal of Remote Sensing*, *15*, 3567-3586.

Döll, P.; Schmied, H.M. (2012): How is the impact of climate change on river flow regimes related to the impact on mean annual runoff? A global-scale analysis. *Environmental Research Letters*, *7*, 014037.

Drechsel, P., Graefe, S., Sonou, M., Cofie, O. O. (2006): Informal Irrigation In Urban West Africa: An Overview; International Water Management Institute: Colombo, Sri Lanka.

ESA (2022): Copernicus. Available online: https://www.esa.int/Applications/Observing_the_Earth/Copernicus (accessed on 25.10.2022).

ESA (2015): ESA CCI Land Cover. Available online: http://maps.elie.ucl.ac.be/CCI/viewer/index.php (accessed on 22.10.2022).

ESA (2017) Land Cover CCI Product User Guide Version 2. Tech. Rep. (2017). Available online: maps.elie.ucl.ac.be/CCI/viewer/download/ESACCI-LC-Ph2-PUGv2_2.0.pdf (accessed on 22.10.2022)

European Commission (2022) Agricultural monitoring. Available online: https://joint-research-centre.ec.europa.eu/scientific-activities-z/agricultural-monitoring_en (accessed on 25.10.2022).

Evans, R.G.; Sadler, E.J. (2008): Methods and technologies to improve efficiency of water use. *Water Resources Research*, *44*.

FAO (2015): 70 Years of FAO (1945-2015), Rome, Italy.

FAO (2021): Emissions due to agriculture, Rome, Italy.

FAO (2016): FAOSTAT statistical database. Available online: https://www.fao.org/faostat/en/#data (accessed on 14.06.2016).

FAO (2014): Total Withdrawal by Sector. Available online: http://www.fao.org/nr/water/aquastat/tables/WorldData-Withdrawal_eng.pdf (accessed on 24.11.2016).

FAO (2012): World agriculture towards 2030/2050: the 2012 revision, FAO Agricultural Development Economics Division: Rome, Italy.

Fisher, J.R.B.; Acosta, E.A.; Dennedy-Frank, P.J.; Kroeger, T.; Boucher, T.M. (2018): Impact of satellite imagery spatial resolution on land use classification accuracy and modeled water quality. *Remote Sensing in Ecology and Conservation*, *4*, 137-149.

Foley, J.A.; Ramankutty, N.; Brauman, K.A.; Cassidy, E.S.; Gerber, J.S.; Johnston, M.; Mueller, N.D.; O'Connell, C.; Ray, D.K.; West, P.C.; Balzer, C.; Bennet, E.M.; Carpenter, S.R.; Hill, J.; Monfreda, C.; Polasky, S.; Rockström, J.; Sheehan, J.; Siebert, S.; Zacks, D.P.M. (2011): Solutions for a cultivated planet. *Nature*, *478*, 337-342.

Friedl, M., Sulla-Menashe, D. (2022): MODIS/Terra+Aqua Land Cover Type Yearly L3 Global 500m SIN Grid V061 [Data set]. NASA EOSDIS Land Processes DAAC.

Fuller, R.M.; Groom, G.B.; Jones, A.R. (1994): The Land Cover Map of Great Britain: An Automated Classification of Landsat Thematic Mapper Data. *Photogramm Eng Remote Sensing*, *60*, 553-562.

García-Álvarez, D.; Nanu, S.F. (2022): Land Use Cover Datasets: A Review. In *Land Use Cover Datasets and Validation Tools: Validation Practices with QGIS*, García-Álvarez, D., Camacho Olmedo, M.T., Paegelow, M., Mas, J.F., Eds.; Springer International Publishing: Cham, pp. 47-66.

Giri, C. (2005): Global Land Cover Mapping and Characterization: Present Situation and Future Research Priorities. *Geocarto International*, *20*, 35-42.

GLIMS Consortium (2005): GLIMS Glacier Database, Version 1 [Data Set]. Boulder, Colorado USA. NASA National Snow and Ice Data Center Distributed Active Archive Center.

Godfray, H.C.J.; Beddington, J.R.; Crute, I.R.; Haddad, L.; Lawrence, D.; Muir, J.F.; Pretty, J.; Robinson, S.; Thomas, S.M.; Toulmin, C. (2010): Food Security: The Challenge of Feeding 9 Billion People. *Science*, *327*, 812-818.

Holzwarth, S.; Thonfeld, F.; Abdullahi, S.; Asam, S.; Da Ponte Canova, E.; Gessner, U.; Huth, J.; Kraus, T.; Leutner, B.; Kuenzer, C. (2020): Earth Observation Based Monitoring of Forests in Germany: A Review. *Remote Sensing*, *12*, 3570.

Jin, N.; Tao, B.; Ren, W.; Feng, M.; Sun, R.; He, L.; Zhuang, W.; Yu, Q. (2016): Mapping Irrigated and Rainfed Wheat Areas Using Multi-Temporal Satellite Data. *Remote Sensing*, *8*, 207.

Kavats, O.; Khramov, D.; Sergieieva, K.; Vasyliev, V. (2019): Monitoring Harvesting by Time Series of Sentinel-1 SAR Data. *Remote Sensing*, *11*, 2496.

Klein, I.; Gessner, U.; Dietz, A.J.; Kuenzer, C. (2017): Global WaterPack – A 250m resolution dataset revealing the daily dynamics of global inland water bodies. *Remote Sensing of Environment*, *198*, 345-362.

Lawston, P.M.; Santanello, J.A.; Kumar, S.V. (2017): Irrigation Signals Detected From SMAP Soil Moisture Retrievals. *Geophysical Research Letters*, *44*, 11,860-811,867.

Ludemann, C.I.; Gruere, A.; Heffer, P.; Dobermann, A. (2022): Global data on fertilizer use by crop and by country. *Scientific Data*, *9*, 501.

Mankin, J.S.; Viviroli, D.; Singh, D.; Hoekstra, A.Y.; Diffenbaugh, N.S. (2015): The potential for snow to supply human water demand in the present and future. *Environmental Research Letters*, *10*, 114016.

Meier, J.; Zabel, F.; Mauser, W. (2018): A global approach to estimate irrigated areas – a comparison between different data and statistics. *Hydrol. Earth Syst. Sci.*, *22*, 1119-1133.

Mostafa, S.M.; Wahed, O.; El-Nashar, W.Y.; El-Marsafawy, S.M.; Zeleňáková, M.; Abd-Elhamid, H.F. (2021): Potential Climate Change Impacts on Water Resources in Egypt. *Water*, *13*, 1715.

Mueller, N.D.; Gerber, J.S.; Johnston, M.; Ray, D.K.; Ramankutty, N.; Foley, J.A. (2012): Closing yield gaps through nutrient and water management. *Nature*, *490*, 254-257.

Neumann, K.; Stehfest, E.; Verburg, P.H.; Siebert, S.; Müller, C.; Veldkamp, T. (2011): Exploring global irrigation patterns: A multilevel modelling approach. *Agricultural Systems*, *104*, 703-713.

Ozdogan, M.; Gutman, G. A new methodology to map irrigated areas using multi-temporal MODIS and ancillary data: An application example in the continental US. (2008): *Remote Sensing of Environment*, *112*, 3520-3537.

Pekel, J.F.; Cottam, A.; Gorelick, N.; Belward, A.S. (2016): High-resolution mapping of global surface water and its long-term changes. *Nature*, *540*, 418-422.

Petersen-Perlman, J.D.; Veilleux, J.C.; Wolf, A.T. (2017): International water conflict and cooperation: challenges and opportunities. *Water International*, *42*, 105-120.

Phillips, R. (1981): FAO: its origins, formation and evolution 1945-1981; FAO: Rome, Italy.

Porwollik, V.; Rolinski, S.; Heinke, J.; Müller, C. (2019): Generating a rule-based global gridded tillage dataset. *Earth Syst. Sci. Data*, *11*, 823-843.

Prasch, M.; Mauser, W.; Weber, M. (2013): Quantifying present and future glacier melt-water contribution to runoff in a central Himalayan river basin. *The Cryosphere*, *7*, 889-904.

Puy, A.; Lankford, B.; Meier, J.; van der Kooij, S.; Saltelli, A. (2022a): Large variations in global irrigation withdrawals caused by uncertain irrigation efficiencies. *Environmental Research Letters*, *17*.

Puy, A.; Sheikholeslami, R.; Gupta, H.V.; Hall, J.W.; Lankford, B.; Lo Piano, S.; Meier, J.; Pappenberger, F.; Porporato, A.; Vico, G.; Saltelli, A. (2022b): The delusive accuracy of global irrigation water withdrawal estimates. *Nature Communications*, *13*, 3183.

Reinermann, S.; Asam, S.; Kuenzer, C. (2020): Remote Sensing of Grassland Production and Management—A Review. *Remote Sensing*, *12*, 1949.

Rouse, J.W.; Haas, R.H.; Schell, J.A.; Deering, D.W. (1973): Monitoring vegetation systems in the great plains with ETRS. *Environmental Science*, 309-317.

Salmon, J.M.; Friedl, M.A.; Frolking, S.; Wisser, D.; Douglas, E.M. (2015): Global rain-fed, irrigated, and paddy croplands: A new high resolution map derived from remote sensing, crop inventories and climate data. *International Journal of Applied Earth Observation and Geoinformation*, *38*, 321-334.

Sano, E.E.; Rosa, R.; Brito, J.L.; Ferreira, L.G. (2010): Land cover mapping of the tropical savanna region in Brazil. *Environ Monit Assess*, *166*, 113-124.

Schneider, A.; Friedl, M.A.; Potere, D. (2008): Monitoring the Extent and Intensity of Urban Areas Globally using the Fusion of MODIS 500m Resolution Satellite Imagery and Ancillary Data

Sources. In Proceedings of the IEEE International Geoscience and Remote Sensing Symposium, 7-11 July 2008.

Siebert, S.; Döll, P.; Hoogeveen, J.; Faures, J.M.; Frenken, K.; Feick, S. (2005): Development and validation of the global map of irrigation areas. *Hydrology and Earth System Sciences*, *9*, 535-547.

Strzepek, K.; Boehlert, B.(2010): Competition for water for the food system. *Philosophical transactions of the Royal Society of London. Series B, Biological sciences*, *365*, 2927-2940.

Swain, A. (2011): Challenges for water sharing in the Nile basin: changing geo-politics and changing climate. *Hydrological Sciences Journal*, *56*, 687-702.

Thenkabail, P.S.; Biradar, C.M.; Noojipady, P.; Dheeravath, V.; Li, Y.; Velpuri, M.; Gumma, M.; Gangalakunta, O.R.P.; Turral, H.; Cai, X.; Vithanage, J.; Schull, M.A.; Dutta, R. (2009): Global irrigated area map (GIAM), derived from remote sensing, for the end of the last millennium. *International Journal of Remote Sensing*, *30*, 3679-3733.

Thonfeld, F.; Gessner, U.; Holzwarth, S.; Kriese, J.; da Ponte, E.; Huth, J.; Kuenzer, C. (2022): A First Assessment of Canopy Cover Loss in Germany’s Forests after the 2018–2020 Drought Years. *Remote Sensing*, *14*, 562.

Tilman, D.; Balzer, C.; Hill, J.; Befort, B.L. (2011): Global food demand and the sustainable intensification of agriculture. *Proceedings of the National Academy of Sciences*, *108*, 20260-20264.

United Nations (2015): Transforming our World: The 2030 Agenda for Sustainable Development. Available online: https://documents-dds-ny.un.org/doc/UNDOC/GEN/N15/291/89/PDF/N1529189.pdf?OpenElement (accessed on 20.10.2022).

Velpuri, N.M.; Thenkabail, P.S.; Gumma, M.K.; Biradar, C.; Dheeravath, V.; Noojipady, P.; Yuanjie, L. (2009): Influence of Resolution in Irrigated Area Mapping and Area Estimation. *Photogrammetric Engineering & Remote Sensing*, *75*, 1383-1395.

Vörösmarty, C.J. (2002): Global water assessment and potential contributions from Earth Systems Science. *Aquatic Sciences*, *64*, 328-351.

Vorosmarty, C.J.; Sahagian, D. (2000): Anthropogenic disturbance of the terrestrial water cycle. *Bioscience*, *50*, 753-765.

Wada, Y.; Wisser, D.; Bierkens, M.F.P. (2014): Global modeling of withdrawal, allocation and consumptive use of surface water and groundwater resources. *Earth Syst. Dynam.*, *5*, 15-40.

Wang, J.; Zhao, Y.; Li, C.; Yu, L.; Liu, D.; Gong, P. (2015): Mapping global land cover in 2001 and 2010 with spatial-temporal consistency at 250m resolution. *ISPRS Journal of Photogrammetry and Remote Sensing*, *103*, 38-47.

Wu, L.; Elshorbagy, A.; Alam, M.S. (2022): Dynamics of water-energy-food nexus interactions with climate change and policy options. *Environmental Research Communications*, *4*, 015009.

Yu, X.; Lu, D.; Jiang, X.; Li, G.; Chen, Y.; Li, D.; Chen, E. (2020): Examining the Roles of Spectral, Spatial, and Topographic Features in Improving Land-Cover and Forest Classifications in a Subtropical Region. *Remote Sensing*, *12*, 2907.

Zabel, F.; Delzeit, R.; Schneider, J.M.; Seppelt, R.; Mauser, W.; Václavík, T. (2019): Global impacts of future cropland expansion and intensification on agricultural markets and biodiversity. *Nature Communications*, *10*, 2844.

Zabel, F.; Putzenlechner, B.; Mauser, W. (2014): Global agricultural land resources--a high resolution suitability evaluation and its perspectives until 2100 under climate change conditions. *PloS one*, *9*, e107522.

Zanaga, D.V.D.K., Ruben; De Keersmaecker, Wanda; Souverijns, Niels; Brockmann, Carsten; Quast, Ralf; Wevers, Jan; Grosu, Alex; Paccini, Audrey; Vergnaud, Sylvain; Cartus, Oliver; Santoro, Maurizio; Fritz, Steffen; Georgieva, Ivelina; Lesiv, Myroslava; Carter, Sarah; Herold, Martin; Li, Linlin; Tsendbazar, Nandin-Erdene; Ramoino, Fabrizio; Arino, Olivier. (2021): ESA WorldCover 10 m 2020 v100 (Version v100) [Data set]. Zenodo.

Appendix I

Appendix I consists of the three consecutive peer-reviewed publications that comprise this thesis.

PUBLICATION 1

Meier, J.; Zabel, F.; Mauser, W. A global approach to estimate irrigated areas – a comparison between different data and statistics (2018): *Hydrol. Earth Syst. Sci.*, *22*, 1119-1133, https://doi.org/10.5194/hess-22-1119-2018

Hydrol. Earth Syst. Sci., 22, 1119–1133, 2018
https://doi.org/10.5194/hess-22-1119-2018

Hydrology and Earth System Sciences
Open Access
EGU

A global approach to estimate irrigated areas – a comparison between different data and statistics

Jonas Meier, Florian Zabel, and Wolfram Mauser

Department of Geography, Ludwig Maximilians University, 80333 Munich, Germany

Correspondence: Jonas Meier (jonas.meier@lmu.de)

Received: 17 March 2017 – Discussion started: 5 April 2017
Revised: 7 January 2018 – Accepted: 8 January 2018 – Published: 9 February 2018

Abstract. Agriculture is the largest global consumer of water. Irrigated areas constitute 40 % of the total area used for agricultural production (FAO, 2014a) Information on their spatial distribution is highly relevant for regional water management and food security. Spatial information on irrigation is highly important for policy and decision makers, who are facing the transition towards more efficient sustainable agriculture. However, the mapping of irrigated areas still represents a challenge for land use classifications, and existing global data sets differ strongly in their results. The following study tests an existing irrigation map based on statistics and extends the irrigated area using ancillary data. The approach processes and analyzes multi-temporal normalized difference vegetation index (NDVI) SPOT-VGT data and agricultural suitability data – both at a spatial resolution of 30 arcsec – incrementally in a multiple decision tree. It covers the period from 1999 to 2012. The results globally show a 18 % larger irrigated area than existing approaches based on statistical data. The largest differences compared to the official national statistics are found in Asia and particularly in China and India. The additional areas are mainly identified within already known irrigated regions where irrigation is more dense than previously estimated. The validation with global and regional products shows the large divergence of existing data sets with respect to size and distribution of irrigated areas caused by spatial resolution, the considered time period and the input data and assumption made.

1 Introduction

One of the major challenges of the 21st century will be feeding the world's growing population (Foley et al., 2011). Considering increasing meat consumption and additionally the increased use of biofuel and bio-based materials leads to estimations that global agricultural production will have to double by 2050 (Alexandratos and Bruinsma, 2012; Godfray et al., 2010; Tilman et al., 2011). Separated by sector, agriculture is the largest consumer of water. 69 % of the global water withdrawal from rivers, lakes and groundwater (blue water) is used for agriculture, in some regions the share can be over 90 % like in Southern Asia or in the Middle East (FAO, 2014b; please note that regional designations are based on UN Geographical Regions in UN, 2013). The regional limitation of fresh water availability plays a crucial role in global agricultural production, considering that 40 % of the global yields are harvested on irrigated fields (FAO, 2014a). Irrigated areas almost doubled over the last 50 years and currently constitute 20 % of the harvested areas globally (FAO, 2016b). Future expansion of irrigated areas and a related increase in water consumption is expected (Neumann et al., 2011). Due to climate change in some areas agricultural water availability is expected to decrease (Strzepek and Boehlert, 2010). The low irrigation efficiency of the common irrigation techniques such as sprinkler and flood irrigation (Evans and Sadler, 2008), the unsustainable usages of limited sources like groundwater (Wada et al., 2014), the changing river regimes (Döll and Schmied, 2012) and the changing supply by snowmelt (Mankin et al., 2015; Prasch et al., 2013) underline the need for a transition towards more sustainable and efficient use of water. The UN Sustainable Development Goals clearly reflect this need to achieve food security and the sustainable development of land use (UN, 2016). For better inventorying and investigation of global and regional water cycles and as input for crop models, detailed global information on irrigated areas at high resolution is needed.

Methods that do not rely on surveys and that are independent of statistics have been developed to identify irrigated areas (Ozdogan et al., 2010). Remote sensing can be an alternative approach for mapping irrigated areas. Previous studies showed that remote sensing data can be used to detect irrigated areas for small- and medium-scale analyses (Abuzar et al., 2015; Ambika et al., 2016; Jin et al., 2016; Ozdogan and Gutman, 2008). Vegetation indices (Ozdogan and Gutman, 2008) and climate elements, such as evapotranspiration (Abuzar et al., 2015) derived from satellite information and combined with meteorological data, have been used to determine irrigated area. Ozdogan et al. (2010) summarized different approaches for mapping irrigated areas from local to global scale.

There are only a few studies which identify irrigated areas globally (Salmon et al., 2015; Siebert et al., 2005; Thenkabail et al., 2009a). Land use classification data sets often neglect irrigated area. Some classify irrigated area as a separate class (ESA, 2015; USGS, 2000) but do not make it a focus.

A common approach to the specific mapping of irrigated area, such as provided by the Global Map of Irrigation Areas (GMIA; Siebert et al., 2005), distributes statistical data of national and subnational agricultural surveys like AQUASTAT (FAO, 2016a) to the agricultural and "other" land use classifications. However, approaches that are restricted to statistics alone are hard to verify, since statistics may include errors and multi-scale statistics hardly exist globally. For instance in some countries in Western Africa the informal irrigated areas in urban and peri-urban areas are twice the size of the official irrigated areas for the whole country (Drechsel et al., 2006). Irrigation may increase due to economic growth and a dietary shift from staple crops towards more vegetables and fruits (Molden, 2007). In fact, even 15 years ago official FAO statistics were criticized after comparing national statistics with remote-sensing-based data (Vörösmarty and Sahagian, 2000). The study of Thenkabail et al. (2009a) globally identified 43 % more irrigated areas than reported in official FAO statistics. The discrepancies between those data were explained by the politicized nature of the FAO data reports and different definitions of irrigated area (Vörösmarty, 2002). The global irrigated area mapping (GIAM) undertaken by Thenkabail et al. (2009a) is a combination of meteorological data, land use classification information (forest) and remote sensing data from multiple satellite sensors. It is validated using ground truth data and Google Earth images. Thenkabail et al. (2009a) showed that the global irrigated areas might be underestimated by the official statistics. Another approach to map global irrigated areas was developed by Salmon et al. (2015). They combine statistics, climate and remote sensing data. The study also shows, although small, an underestimation by the national and subnational statistics. Salmon et al. (2015) showed that merging remote sensing data and ancillary data is suitable for irrigation mapping. Thenkabail et al. (2009b) conclude that "both remote sensing and national statistical approaches require further refinement".

The aim of this study is to test an existing statistics-based medium-resolution irrigation map (Siebert et al., 2013) with high-resolution data from satellite observations which have since become available. We study, through extraction of likely irrigated areas from the high spatial resolution data, to what extent and where formally undetected irrigated areas show up. At first we downscale the Siebert et al. (2005) statistically based irrigation map using high-resolution remote sensing information. In the second step we derive irrigated land from agricultural suitability data combined with remote sensing information consisting of multi-temporal normalized difference vegetation index (NDVI) profiles at high spatial resolution. By following a decision tree we identify irrigated areas as showing active vegetation growth in agricultural unsuitable regions. If these irrigated areas are not reported by the official statistics they are added in the new irrigation map. Hence, the new irrigation map is not restricted to irrigated areas recognized in official reports and allows for extending these predetermined areas. Finally, we compare our results with existing global approaches as well as with regional analyses (USA, India, China) and investigate the differences with the official national and subnational statistics.

2 Data and methods

The basic idea of our approach is to combine different data sets providing different kind of information. The applied data sets are available at different spatial resolutions (Table 1). As a first step, the data sets are homogenized to the same spatial resolution. We decided on the high spatial resolution of 30 arcsec (approx. 1 km^2 at the Equator), since the demand for high-resolution global data is increasing in different applications (Deryng et al., 2016; Jägermeyr et al., 2015; Liu et al., 2007; Mauser et al., 2015; Rosenzweig et al., 2014) and the pixel size of approximately 1 km^2 is already close to the size of large fields (depending on the region) or an agglomeration of smaller irrigated fields. For Africa and Asia, the field size of 1 km^2 might be too large (Fritz et al., 2015), but usually, irrigated fields can be much bigger in size, since irrigation is often applied by large-scale farms. Small fields are agglomerated since irrigation is usually not practiced on a single field, due to high investment and installation costs of irrigation systems. The resulting data at 30 arcsec only distinguishes between irrigated and rain-fed and does not contain percentage shares.

The decision tree in Fig. 1 shows how the data sets are analyzed and formerly undetected irrigated areas are identified. As we mentioned above, the basic idea is to increase the spatial resolution of an existing global irrigation map to 30 arcsec and to extend the data set with additional identified irrigated areas. The lower grey box in Fig. 1 shows the principal of the downscaling process, where we assign the percentage values of Siebert et al. (2005) to the high-resolution pixels within a medium-resolution pixel showing the highest

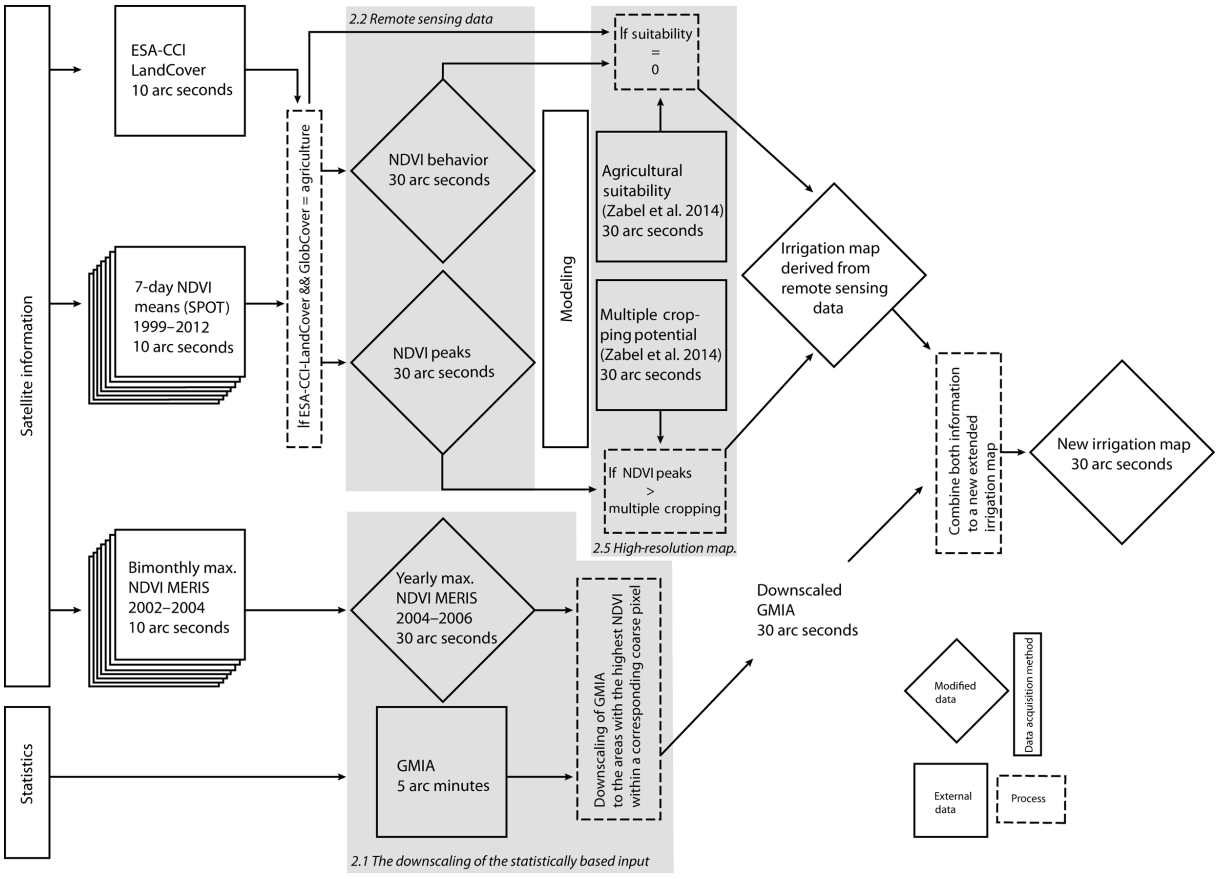

Figure 1. The scheme used for processing and analyzing the different spatial data and the multiple decision tree to determine irrigated area. The grey boxes show the described Sects. 2.1, 2.2 and 2.5.

NDVI values (see Sect. 2.1). The assigned irrigation percentages of the high-resolution pixels form the basis of our new irrigation map. The upper grey box in Fig. 1 shows the processing of the NDVI data, which is only done on agricultural areas (see Sect. 2.2 and 2.3). The processed NDVI data are compared to a global high-resolution data set of agricultural suitability (see Sect. 2.5 and the right grey box in Fig. 1). The combination of the downscaling and the comparison of NDVI and agricultural suitability results in a global high-resolution irrigation map. The development of the map is described more in detail in the following section.

2.1 The downscaling of the statistically based data set

Siebert et al. (2005) distribute statistical data to the Global Map of Irrigated Areas (GMIA). The data set has a resolution of 5 arcmin and is available in several versions – we applied the version 5.0 (Siebert et al., 2013). To combine the different data sets to a final irrigation map at a resolution of 30 arcsec, the resolution of GMIA has to increase. For the downscaling process, shown in the lower grey box in Fig. 1, we use global bimonthly (computed once every 2 months) maximum MERIS NDVI data (ESA, 2007) at a spatial resolution of 10 arcsec and calculate the yearly maximum NDVI (Fig. 2). The bimonthly maximum NDVI data cover the period November 2004–June 2006 and represent more or less the center of the covered time period of the applied GMIA version. After upscaling the yearly maximum NDVI to 30 arcsec using a majority algorithm, the GMIA data are distributed to the areas with the highest NDVI within a corresponding coarse pixel. To avoid distributions to dense woodlands (closed tree cover $> 40\,\%$), cities and open water, these areas are excluded from the distribution, based on the ESA Climate Change Initiative Land Cover (CCI-LC) data set (ESA, 2015). Pixels with a share of irrigated area below $1\,\%$ are not considered. The downscaled data set of Siebert et al. (2013) shows the irrigated area at a high spatial resolution of 30 arcsec and will in the next steps be extended by irrigated area, which are not part of the statistics yet. In the following, the downscaled data set of Siebert et al. (2013) is referred to as "downscaled GMIA".

2.2 Remote sensing data

This part of the decision tree is shown in the upper left grey box in Fig. 1. For the detection of the actual active vegeta-

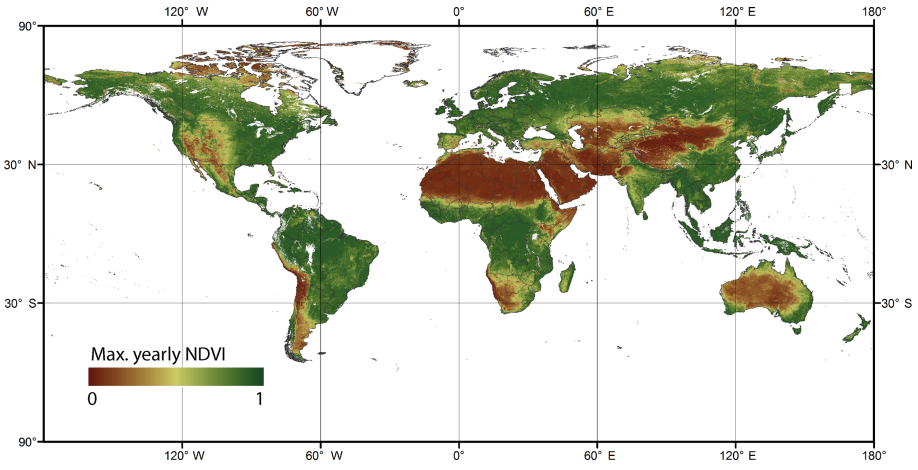

Figure 2. Yearly maximum NDVI derived from maximum bimonthly NDVI data of the EnviSAT MERIS instrument.

Table 1. Applied global data sets.

Name	Description	Period	Resolution	Data source
Global Map of Irrigation Areas (GMIA) version 5.0	Areas equipped for irrigation in percent of the total pixel area.	2000–2008	5 arcmin	Siebert et al. (2013)
Agricultural suitability	Agricultural suitability, rain-fed and irrigated for the period 1980–2010	1981–2010	30 arcsec	Zabel et al. (2014)
Multiple cropping	Numbers of crop cycles, rain-fed and irrigated	1981–2010	30 arcsec	Zabel et al. (2014)
Maximum NDVI	Maximum of global bimonthly NDVI maxima from the ENVISAT MERIS instrument	2004–2006	10 arcsec	ESA (2007)
7-day mean NDVI	7-day mean NDVI data SPOT-VGT	1999–2012	30 arcsec	ESA (2015)
ESA-CCI-LC (v. 1.6.1)	Land classification product	2008–2012	10 arcsec	ESA (2015)
GlobCover	Land classification product	2009	10 arcsec	ESA (2010)
WorldClim precipitation	Yearly reanalysis precipitation data	1961–1990	30 arcsec	Hijmans et al. (2005)

tion we used the NDVI product of ESA-CCI (ESA, 2015). The data provide 7-day NDVI means and covers the time period from 1999 to 2012. From these data, we calculated the annual course of NDVI, averaged over the whole time period, from which we derived the number of annual NDVI peaks. In order to increase the precision of detecting active vegetation, each pixel is analyzed according to an NDVI threshold approach (Ambika et al., 2016; Shahriar Pervez et al., 2014). The chosen thresholds are a result of a comparison of different studies (Ambika et al., 2016; Shahriar Pervez et al., 2014) and the comparison of NDVI values of known irrigated and rain-fed areas. The following criteria need to be fulfilled and are shown in Fig. 3:

– The minimum NDVI has to be below 0.4, while the maximum NDVI has to be over 0.4. Since the NDVI product is a 7-day mean over 14 years, it is very likely that fields lie fallow within the time period, resulting in lower mean values. Therefore, an NDVI of 0.4 turned out to be a suitable lower threshold. This guarantees clear distinction between non-vegetated and vegetated pixels and eliminates evergreen vegetation, such as

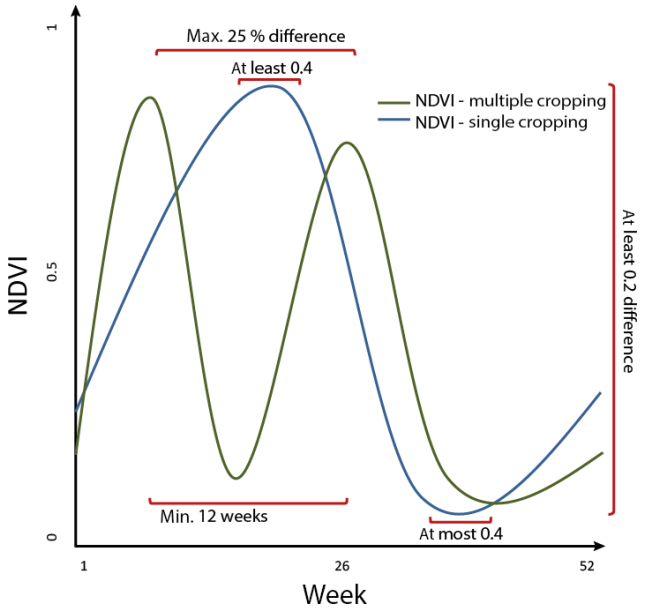

Figure 3. Idealized NDVI course of single and multi-cropping and the conditions which must be fulfilled.

forests and pasture. Thresholds like minimum and maximum NDVI used in this study have a strong effect on the result. For a global study it is difficult to find universal, transferable thresholds that can be applied globally.

- Minimum and maximum NDVI must at least differ by 0.2 to identify only pixels with a dynamic annual course that is assumed for agricultural areas.

- NDVI peaks must be at least 12 weeks apart to assign a peak to a specific growing period, assuming that the growing period length is at least 12 weeks (Sys et al., 1993). Additionally, this allows for separating multiple growing periods within a year. Often, a slight greening right after harvest was observed. This can be explained by the seeding of legumes for soil treatment, or the development of natural vegetation after harvest, which results in an increase in NDVI.

- In order to avoid classifying multiple peaks as a regular harvest, it turned out that two sequenced peaks must not differ by more than 25 %.

The described criteria of minimum, maximum and yearly course of NDVI and the length of growing period turned out to be robust for determining the number of crop cycles globally. The chosen criteria are suitable regarding the fact that we used 7-day NDVI means averaged over 14 years.

2.3 Land use classification products

The extension of irrigation is restricted to agricultural areas. The information on cropland is taken from the ESA-CCI-LC product (cropland rain-fed, cropland irrigated, mosaic cropland> 50 %; ESA, 2015) and from the predecessor GlobCover (ESA, 2010; post-flooding or irrigated croplands, rain-fed croplands, mosaic cropland; 50–70 %). According to the authors, the "accuracy associated with the cropland and forest classes" is high "and therefore a quite good result" (ESA, 2015). The user's accuracies of both data sets are shown in Table 2. The classification of cropland depends on the definition of cropland. In both data sets pasture is neither a separate class nor part of the class "grassland" or "cropland". False classification of cropland can therefore lead to false classification of irrigated areas. The combination of both data sets increases the chance of classifying irrigated areas only on cropland. Pixels that are classified as mosaic cropland in the underlying land use data sets are weighted by the averaged amount of cropland fraction for the corresponding class. All other cropland pixels are assumed to be 100 % cropland.

Table 2. User accuracy of the applied land use data sets.

	ESA-CCI-LC	GlobCover
Cropland rain-fed	88 %	82 %
Cropland irrigated	92 %	83 %
Mosaic cropland > 50 %	59 %	97 %

Table 3. List of all considered crops.

Crop name
Barley (*Hordeum vulgare*)
Cassava (*Manihot esculenta*)
Peanut (*Arachis hypogaea*)
Maize (*Zea mays*)
Millet (*Pennisetum americanum*)
Oil palm (*Elaeis guineensis*)
Potato (*Solanum tuberosum*)
Rapeseed (*Brassica napus*)
Paddy rice (*Oryza sativa*)
Rye (*Secale cereale*)
Sorghum (*Sorghum bicolor*)
Soy (*Glycine max*)
Sugarcane (*Saccharum officinarum*)
Sunflower (*Helianthus annuus*)
Summer wheat (*Triticum aestivum*)
Winter wheat (*Triticum aestivum*)

2.4 Agricultural suitability data

Agricultural suitability data are taken from Zabel et al. (2014). The data describe the suitability for 16 staple, energy and forage crops (Table 3) according to climate, soil and topography conditions at a spatial resolution of 30 arcsec. It determines suitability for crop cultivation and the potential number of crop cycles per year, under the climate for 1981–

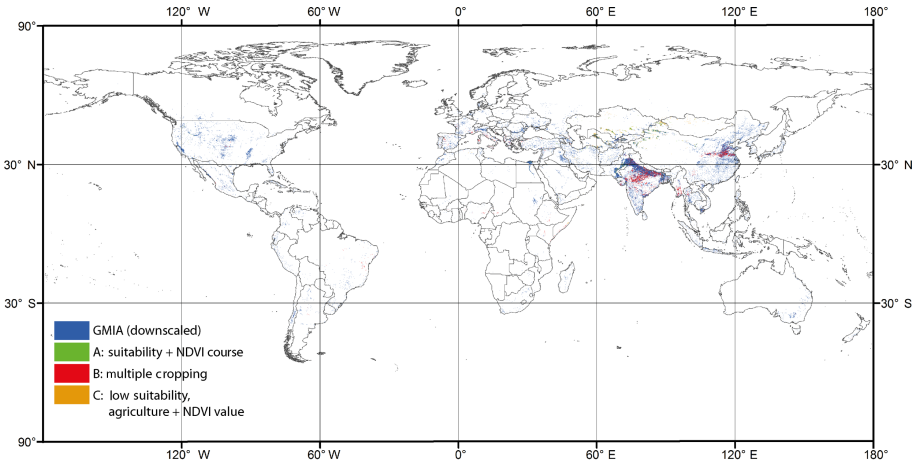

Figure 4. Irrigated areas identified by different approaches.

2010 (Zabel et al., 2014). Soil properties are not considered in this approach, because human activities may alter soil properties, for example through fertilizer and manure application or soil tillage. The data are available for past and future climate periods as well as for rain-fed and irrigated conditions separately. The data set used in this study represents for each pixel the highest suitability value over all selected crops as well as the annual course of the growing period and the potential number of crop cycles per year.

2.5 High-resolution mapping of irrigated areas

The downscaled GMIA data serve as a basis, providing a proven global distribution of irrigated areas. The irrigated areas which are already part of the statistics are extended with additional, previously undetected irrigated areas. The identification of the additional irrigated areas in the new irrigation map is accomplished using the criteria described above and relationships of the annual temporal NDVI profiles to the agricultural suitability. The general criterion for the identification of unknown irrigated areas is that the land use is already cropland according to ESA-CCI-LC and GlobCover. The restriction to cropland avoids the classification of irrigated areas in other land use or cover types in dry areas with high NDVI values due to lichen or weeds, since a low agricultural suitability does not exclude plant growth at all. The upper right grey box in Fig. 1 shows the assumption for irrigated areas using the NDVI and agricultural suitability data:

A. the annual NDVI course clearly suggests dynamic vegetation growth while the agricultural suitability shows a low value;

B. the number of NDVI peaks is higher than the potential number of crop cycles per year under rain-fed conditions;

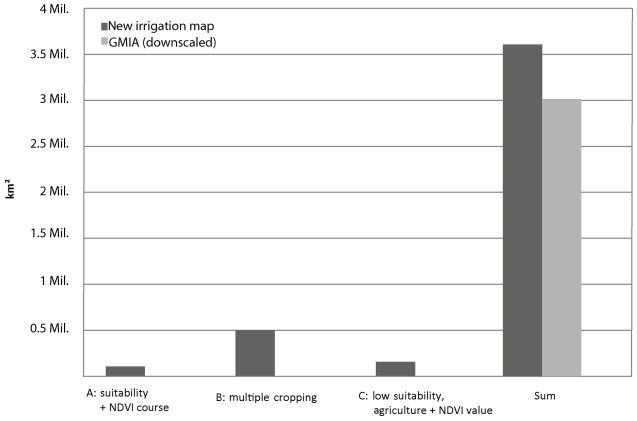

Figure 5. Results of the new irrigation map compared the downscaled GMIA.

C. land is not suitable but classified as cropland, while at the same time NDVI values and yearly courses indicate vegetation.

If one of the criteria is true, we assume the full area of the 30 arcsec pixel as being irrigated. As a result, the combination of A, B and C identify the irrigated pixels that were not assigned to irrigation areas in the downscaled GMIA irrigation map.

3 Results

3.1 Global analysis

The new global irrigation map shows 18 % more irrigated areas than the downscaled GMIA (Fig. 4). Overall, 3 674 478 km^2 of irrigated areas have been identified, which is an increase of 659 605 km^2 compared to the downscaled GMIA (Fig. 5). The global result confirms the underestima-

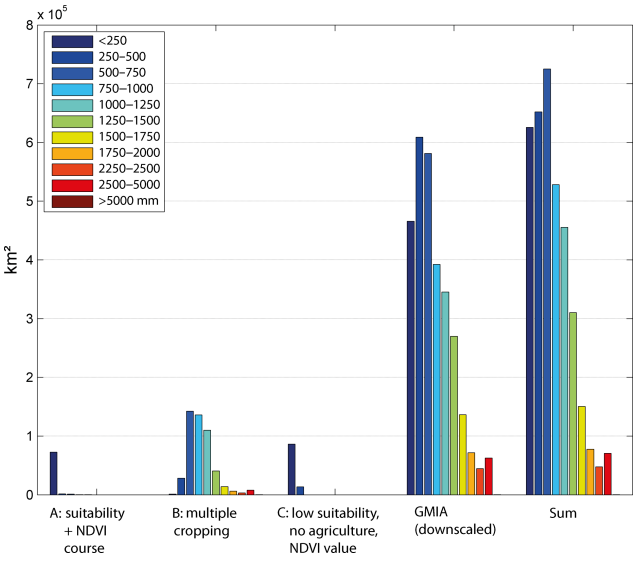

Figure 6. Yearly precipitation within the irrigated areas. Criteria A and C are suitable in dry regions, while criterion B identifies in humid regions as well. Further, irrigation decreases with increasing precipitation, but is also used in regions with high yearly precipitation.

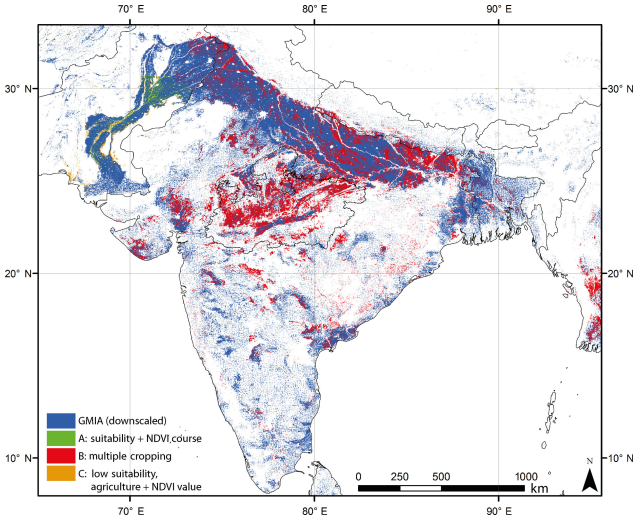

Figure 7. The Indian subcontinent and its identified irrigated areas. The blue areas are the information of the downscaled GMIA. Irrigation is more dense than expected in already irrigated regions and new areas appear in the state Madhya Pradesh.

tion of irrigated areas of Thenkabail et al. (2009a), who globally identified 3 985 270 km^2 of irrigated area using a remote-sensing-based approach, which is significantly higher than the results of Salmon et al. (2015) with 3 141 000 km^2 and the global estimates of the FAO or of Siebert et al. (2005).

Figure 5 shows the global irrigated area additionally allocated through each of the criteria A, B and C of Sect. 2.5. The largest amount of additional irrigated area is identified by considering multiple cropping (B). In this case, 493 123 km^2 is not part of the downscaled GMIA. These areas are mainly found in Asia (Fig. 4), where according to our results, irrigation is often required for multiple cropping. An area of 100 069 km^2 is additionally identified because it is not suitable for crop cultivation but is classified as cropland (criterion C). By the use of criterion A, 76 054 km^2 is additionally allocated.

3.2 Regional analysis

The criteria A, B and C show different amounts of additional irrigated area for different regions. Criteria A and C identified irrigated areas mostly in arid and semi-arid regions, by comparing low or no suitability versus high NDVI. Figure 6 shows that additional irrigated areas by using A and C are mainly found in regions with annual precipitation < 500 mm, according to the WorldClim data set for 1961–1990 (Hijmans et al., 2005).

In humid regions, criteria A and C are not sensitive, because agricultural suitability values in humid regions are high since precipitation is not limiting. We found that B extends irrigated areas in regions with low as well as high annual precipitation (Fig. 6), where irrigation is often used to allow for a second harvest. In total, Fig. 6 demonstrates that irrigation decreases with increasing precipitation, but irrigation does not only take place in dry regions. The largest amounts of new areas are in countries where irrigation plays an important role in agriculture. Irrigated areas seem to be denser in already irrigated regions.

3.2.1 Asia

The newly identified irrigated areas are mainly found in Asia, particularly in Central and Southeastern Asia. The countries with the largest amounts of additional area are India (+267 283 km^2) and China (+149 871 km^2). In these countries, irrigation plays a dominant role in agriculture, where 40 % (India) and 57 % (China) of the total cropland is irrigated according to statistics (FAO, 2016b). Nevertheless, statistics seem to largely underestimate irrigated areas, particularly in India. Here, we found on the one hand considerable additional irrigated areas compared to GMIA within regions that are sparsely irrigated, such as the state of Madhya Pradesh (Fig. 7). On the other hand, irrigated areas are additionally identified within regions that already show a high irrigation density, such as Uttar Pradesh along the foothills of the Himalaya, where even the density of irrigated areas increases in our results (Fig. 7). In these regions in particular, the irrigated areas were detected by comparing the potential vegetation cycles to the actual yearly NDVI course. Due to its seasonality, precipitation only allows for one harvest – a second harvest requires irrigation. Even legumes, which serve as nitrogen fertilizers, have to be irrigated.

Within Asia, the developed method unveils large previously unknown irrigated areas in Kazakhstan (+30 661 km^2), Pakistan (+26 667 km^2), Myanmar (+25 212 km^2), Uzbekistan (+17 454 km^2) and Turkmenistan (+13 483). In Central Asia the irrigated areas along the rivers are particularly larger than previously reported. The Asian countries with the largest percentage difference compared to FAOSTAT (FAO, 2016b) statistical data (averaged from 1999 to 2012) are Mongolia (+815 %), Kazakhstan (+183 %), Myanmar (+119 %) and Yemen (+103 %).

3.2.2 Africa

Irrigation plays a minor role in the tropical regions of Africa, while there are contiguous irrigated regions along the Nile in Egypt and Sudan, some smaller irrigated areas within the Mediterranean countries and some irrigated areas within Southern Africa. The countries with the largest amount of additional irrigated areas are found in Somalia (+6427 km^2), Egypt (3867 km^2) and Ethiopia (+3536 km^2). The irrigated regions along the Nile Delta are denser and result in an increase in irrigated area of 12 % in Egypt. The African continent shows the highest percentage discrepancy when compared to FAOSTAT (averaged from 1999 to 2012; Table 4). Countries with the highest percentage differences compared to the statistics are Chad (+500 %), Somalia (315 %), Kenya (311 %) and Cameroon (+243 %).

3.2.3 Europe

The discrepancy between the downscaled GMIA and the new irrigation map in Europe is smaller than in the regions mentioned above. The largest differences exist in Italy (+11 059 km^2), Spain (+5270 km^2) and Greece (+3922 km^2). While the Po Valley, the largest contiguous irrigated region within Europe, does not show significant differences between the downscaled GMIA and our high-resolution irrigation map, many additional areas on Sardinia and Sicily are detected. In Spain, the known irrigated areas near the Pyrenees are well captured by GMIA, but the intensely used agricultural area around Valladolid in the northwest of Spain in particular shows additional irrigated areas according to our results. The highest percentage difference compared to FAOSTAT is found for Bosnia and Herzegovina (+500 %), Croatia (+220 %), Montenegro (+207 %) and some other countries in Eastern Europe. The comparison of FAOSTAT to GMIA in these regions results in similar high differences, since the FAOSTAT data were obviously not used in the GMIA data. The highest percentage differences in Western Europe to FAOSTAT are found in Portugal (+41 %), Great Britain (+28 %), France (+27 %) and Italy (+26 %).

3.2.4 America

The position and extent of the large irrigated areas in North America in Fig. 4 are very consistent with the distributed statistics of the downscaled GMIA. Only in the northwestern USA do our results show significantly more irrigated areas than GMIA. It is notable that additional identified irrigated areas are found next to already detected irrigated areas in California, northwest and midwest of the USA. Thus, density increases within irrigated agglomeration regions. The percentage differences compared to FAOSTAT are relatively low compared to the other continents (Table 4). The highest percentage difference is found in Chile (+71 %), Canada (+41 %), Mexico (+12 %) and Brazil (+8 %).

To demonstrate the effect of the high spatial resolution of the results, Fig. 8 shows the results for a particular area in the northwest USA (Oregon). The comparison of the new irrigation map at 30 arcsec resolution with the GMIA at 5 arcmin resolution demonstrates the improvement of the data (Fig. 8). The higher resolution allows for more precise identification of irrigated fields. Further, the additionally recognized irrigated areas that are not included in the GMIA data set match well with the underlying true-color satellite image. In this case it also shows that the resolution of 30 arcsec degree is suitable for field-scale irrigation mapping in this region.

Table 4. The results of the new irrigation map compared to the downscaled GMIA and FAOSTAT (FAO, 2016b). The countries are grouped according to UN Geographical Regions (UN, 2013).

Region	New irrigation map (km^2)	GMIA downscaled (km^2)	FAOSTAT 1999–2012 (km^2)
Africa	163 783	136 826	137 817
Eastern Africa	38 232	25 194	24 589
Middle Africa	3820	1685	1692
Northern Africa	89 870	82 853	83 969
Southern Africa	15 844	15 828	15 956
Western Africa	16 018	11 267	11 611
Americas	520 446	500 106	494 988
Caribbean	13 267	13 248	13 346
Central America	76 072	73 226	70 638
South America	133 743	122 695	135 183
North America	297 365	290 938	275 822
Asia	2 675 125	2 094 375	2 147 293
Central Asia	165 668	102 861	99 412
Eastern Asia	799 187	642 388	664 684
Southern Asia	1 284 744	976 866	1 018 484
Southeastern Asia	252 997	216 052	213 601
Western Asia	172 528	156 209	151 112
Europe	269 190	238 939	262 372
Eastern Europe	83 967	81 799	109 648
Northern Europe	10 227	10 227	10 015
Southern Europe	130 460	106 134	104 132
Western Europe	44 536	40 780	38 578
Oceania	41 844	41 266	30 673
Australia and New Zealand	41 821	41 242	30 525
Melanesia	24	24	134
Micronesia	0	0	3
Polynesia	0	0	10
World	3 670 390	3 011 512	3 073 142

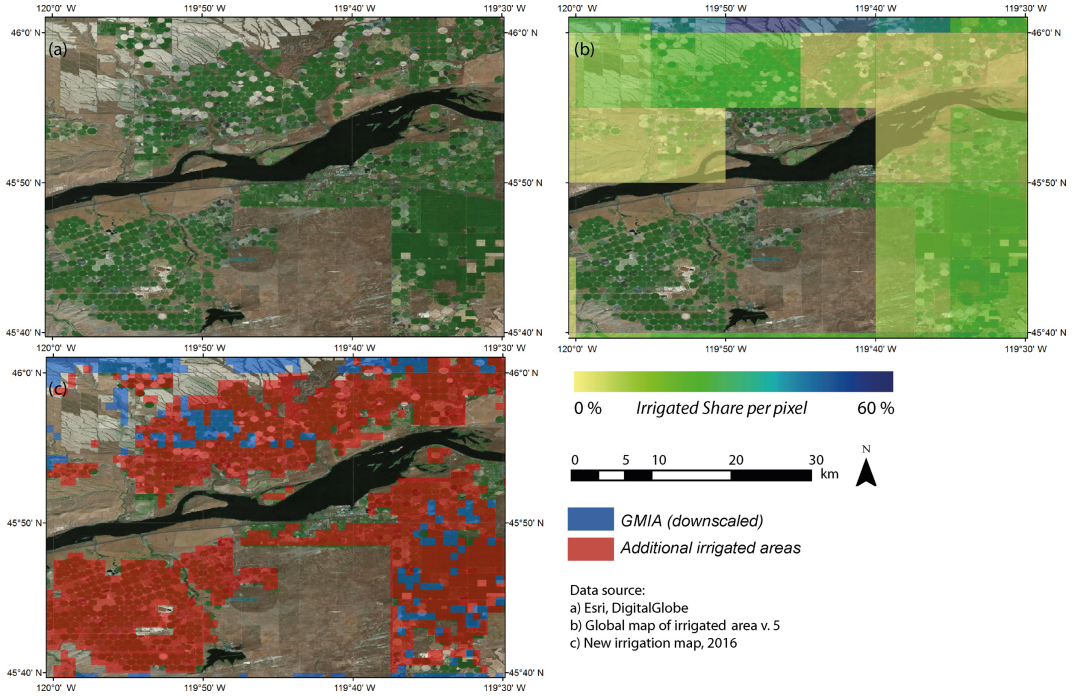

Figure 8. Small-scale analysis of the new irrigation map **(c)** and GMIA **(b)** in the USA compared to the raw satellite image **(a)**.

3.3 Differences between the downscaled GMIA and the original GMIA

The downscaling process leads to differences between the downscaled and the original GMIA data. Since fractions of irrigated areas < 1 % are not allocated to the finer resolution, they are neglected within the downscaling process. This leads to a global loss of irrigated area of 46 329 km^2. If there are no pixels available for distribution, e.g., due to excluded land such as forests, water bodies or urban areas, the irrigated area may not be allocated, which results in a global reduction of 19 780 km^2. Since we can only distribute integer values we additionally lose 2442 km^2 through rounding the floating point numbers of the percentage share of the irrigated areas. Overall, we do not distribute 68 551 km^2 of irrigated areas, which is 2.28 % of the GMIA data set at its original resolution. This small difference in percentages allows us to spatially compare the new irrigation map with the downscaled GMIA at the same spatial resolution, which is a result of the procedure described above.

4 Validation

The new irrigation map partially shows significant differences compared to the statistics and the resulting GIAM data set. No final truth exists on the amount and location of global irrigated area. Nevertheless, in order to validate the new high-resolution irrigation map we compare our results to existing global and also regional studies. The comparison of ground truth data with the new irrigation map can also be a way to outline the differences between the new map and ground truth data. There are ground truth data available (European Environment Agency, 2014), providing point-specific land use information for specific regions, but they are rare and not always tagged with needed land use information like irrigation. Further, there are always scaling issues, concerning the spatial resolution, in comparing point information with spatial information. For the validation we decided to compare our map with the existing global data set IWMI-GIAM (Thenkabail et al., 2009a) and GRIPC (Salmon et al., 2015). Additionally we compare our results with regional studies in the USA (Ozdogan et al., 2010), China (Zhu et al., 2014) and India (Ambika et al., 2016), where we map the highest absolute differences compared to the statistical data and where irrigation is an important agricultural practice. Regional studies are able to develop approaches which consider local characteristics, while global studies have to transfer their methods to regions with completely different conditions. The global comparison is done on country level and the regional comparison on the level of states or provinces. For each country/state the irrigated area is calculated and compared to other studies.

4.1 Global validation

The resulting global irrigated area of 3.67 million km^2 lies between the GRIPC results of 3.14 million km^2 (Salmon et al., 2015) and IWMI-GIAM results of 3.98 million km^2 (Thenkabail et al., 2009a). All three data sets show a larger

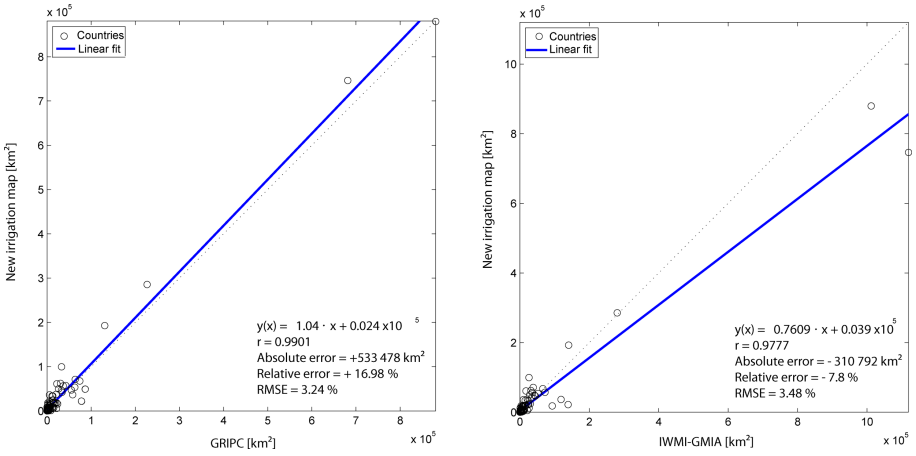

Figure 9. Regression plots of the two compared global data sets. The blue line is the linear fit and the dotted black line the linear equation.

irrigated area than reported by the statistics. Despite the absolute difference our new high-resolution map shows strong correlation with both data sets (IWMI-GIAM $r = 0.97$; GRIPC $r = 0.99$; Fig. 9) when correlating country values. The irrigated area is weighted by the size of the country. Thus, the deviations of the countries are comparable with each other. The slope shows a small overestimation of our results compared to GRIPC (1.04) and a larger underestimation of IWMI-GIAM (0.76). The regression plots also show the range of deviation (Fig. 9). The linear fit is strongly influenced by the high values and shows the underestimation of our results compared to IWMI-GIAM and overestimation compared to GRIPC (Fig. 9). The average difference per country is expressed in RMSE. The RMSEs of IWMI-GIAM (3.48 %) and GRIPC (3.24 %) are quite similar. The results of GRIPC (3.14 million km^2) are very close to the official statistics (3.07 million km^2). GRIPC uses a regionally based field size factor which weights the size of the pixels. Without the field size factor the results show remarkably more irrigation (3.76 million km^2 instead of 3.14 million km^2). If we apply the GRIPC field size factor to our results, it changes the amount of irrigated area to 3.05 million km^2. The use of field size factors can be a way to adjust regions characterized by small holder farms and heterogeneous landscapes. On the other hand it needs to be appropriately determined and validated, and it may create other sources of uncertainty.

4.2 Regional validation

The regional data suggest a strong linear correlation between our results and the regional studies described by the correlation coefficient: $r = 0.94$ (USA), 0.84 (China) and $r = 0.92$ (India; Fig. 10). The slope shows overestimation of our results compared to all other data sets. The RMSE was weighted by the size of the compared state and shows a small overestimation of our data set compared to the regional studies.

The difference between our results and the irrigated area in the USA given by Ozdogan et al. (2010) can be explained by the statistical areas used to derive our irrigation map. They are 25 % larger than the corresponding areas of Ozdogan et al. (2010). Our map extends this area and results in 28.7 % more irrigated area than given by Ozdogan et al. (2010). The regions where our analysis shows more irrigated areas are in the dry regions in the western USA and in the south (Table S1 in the Supplement). The largest irrigated areas in the USA are found in California, where we estimate 41 816 km^2 of irrigated areas. Ozdogan et al. (2010) calculate 26 808 km^2 of irrigated areas, while the United States Geological Survey (USGS) reports 42 087 km^2 of irrigated areas for the year 2010 (USGS, 2014). California is a good example of the different information about irrigated areas and the problems of validating irrigation maps. Even the official statistics for the year 2010 show two different values: the USGS states an irrigated area in California of 42 087 km^2, while the California Department of Water Resources (2010) reports 38 033 km^2. The example of California shows that the available statistics differ remarkably, which leads to strong impacts on the validation results. The water rights complaints in California regarding "Unauthorized Diversion" prove the existence of illegal irrigation activities (California Environmental Protection Agency, 2017), which are not part of the official statistics and are not only an issue of smallholder farmers or of watering lawns (Bauer et al., 2015). The comparison of our irrigation map with a study of irrigated areas in India shows a smaller relative error compared to the irrigation map of the USA. Overall the results are 138 172 km^2 higher than the results for India of Ambika et al. (2016). The differences could be caused by the different spatial resolution. The data of Ambika et al. (2016) are applied at a spatial resolution of $\sim$ 250 m, which fits better to the small fields and the heterogeneous landscape of smallholder farms as they occur in India.

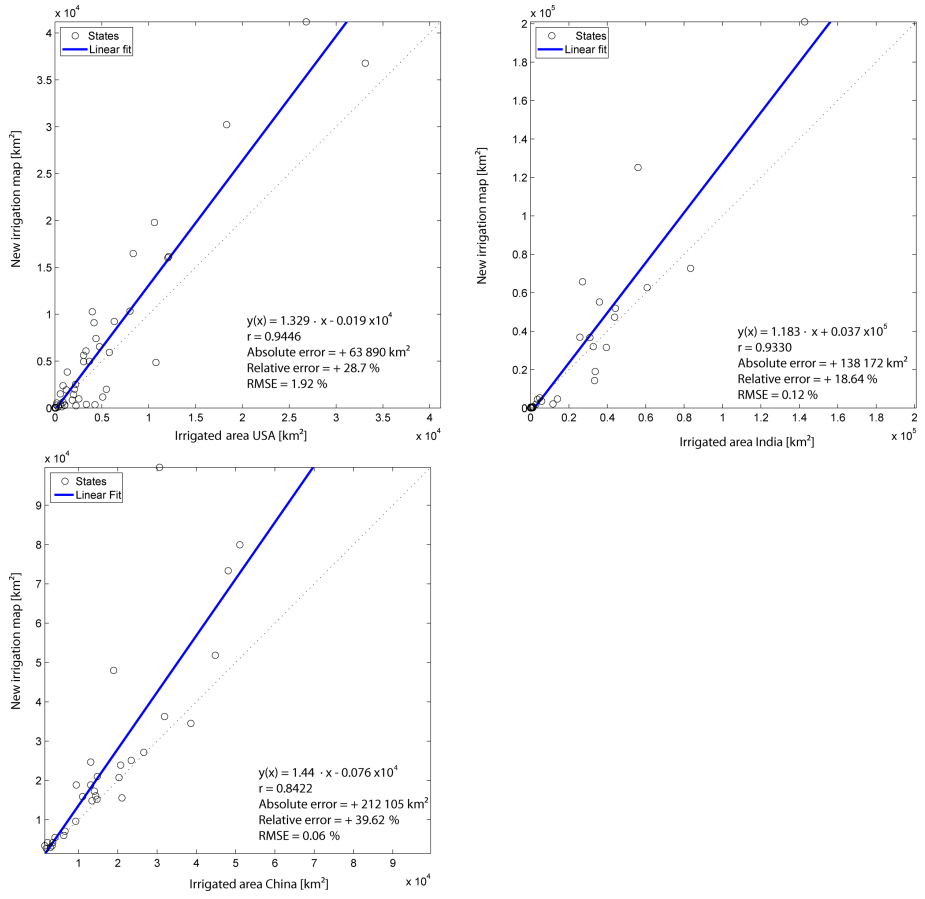

Figure 10. Regression plots of the compared our irrigation map compared to regional data sets of the USA (Ozdogan et al., 2010), India (Ambika et al., 2016) and China (Zhu et al., 2014). The blue line is the linear fit and the dotted black line the linear equation.

Zhu et al. (2014) developed an irrigation map of China that shows official statistics downscaled by using NDVI data. The differences compared to the new irrigation map are high and expectable, due to the restriction to the statistics. The highest differences are found in the province of Xinjiang (percentage and absolute) in the northwestern part of China. Xinjiang is characterized by a very dry continental climate. Nearly 90 % of the area has less than 200 mm of precipitation per year (Hijmans et al., 2005). Therefore, agriculture is almost impossible without irrigation. Similar to the examples in the USA and in India, the distribution and the patterns of the irrigated areas fit the data of Zhu et al. (2014) but are denser. Irrigated areas seem to exceed the official numbers and confirm the results of previous studies on water allocation and water consumption in the Tarim Basin, where the water consumption exceeds the relevant water quotas (Thevs et al., 2015). The denser distribution of irrigated areas in the Tarim Basin shows the overuse of water despite the water quotas of the Chinese government and shows an underestimation of irrigated areas in the official reports.

5 Discussion and conclusion

This study focuses on the development of a new global irrigation map and its comparison with the most common irrigation maps on the global and regional scale. The results enable a high spatial resolution global view on the distribution of irrigated areas. The analysis indicates that the high-resolution view allows for the detection of additional irrigated areas, which were not covered by the existing data sets. This also increases the global estimate of irrigated land by 18 % compared to the reported statistics.

Differences between irrigation maps result from the quality and the spatial resolution of the input data, the assumptions made and from the different terms and definitions of irrigated areas. The large differences between our results and the statistics in Central Asia (Mongolia, Kazakhstan) may result from classification errors in the underlying input data. Despite the high accuracy of the applied land use data sets, the ESA-CCI-LC and GlobCover land use classification include uncertainties which lead to errors in mapping irrigated areas. For example grassland, pastures or meadows are sometimes classified as cropland. Especially in dry regions, such

as in Central Asia, this misinterpretation of cropland leads to a false classification of irrigated area. Further, since the collapse of the Soviet Union the cropping patterns of the independent countries of Central Asia has changed tremendously and fallow fields may influence the land use classification products through the present day.

The cropland area in the underlying land use data is not given as a proportional area of cropland within a pixel, which may also lead to an overestimation of cropland and thus also of irrigation.

The use of the agricultural suitability may lead to errors because it consists of 16 crops and may neglect, e.g., drought-resistant varieties or other species that are adapted to regional climatic conditions. Some typically irrigated crops are not considered in the crop suitability data, such as expensive (and therefore most likely irrigated) vegetables, olive trees, almond trees and irrigated pastures, which potentially leads to an underestimation of irrigated area. On a global scale, these areas are nevertheless assumed to be relatively small.

Errors in classifying irrigated areas could occur through high groundwater levels or the proximity to open water; plants could reach water sources through capillary rise or directly tap into the groundwater. This creates alternate water availability for the plants and can mimic irrigation in otherwise unsuitable locations.

A major reason for the differences between the irrigation maps lies in the different definitions of irrigated areas. While the FAO defines an irrigated area as an "area equipped for irrigation" (FAO, 2016b), the new irrigation map presented here classifies areas as irrigated if additional water (besides precipitation) is applied on a field. In some regions this may influence the result. For example in Bangladesh paddy fields are not considered as irrigated land as they cultivate mainly during the wet season and have no permanent irrigation infrastructure. The high differences in India may also result from the different definition, where 1999 only 47 % of the total harvested area for paddy rice utilized permanent irrigation infrastructure (Frenken, 2012). The precipitation is harvested and concentrated on the paddy fields and used for rice cultivation by flood water recession (Frenken, 2012). Non-equipped cultivated wetlands, an upgrade of rain-fed cropland using soil moisture conservation, supplemental irrigation through water harvesting, non-permanent dug wells or water concentration may also result in irrigated area in the presented irrigation map (Molden, 2007). Due to the definition of "area equipped for irrigation" these areas are not part of the FAO irrigation class and accordingly not part of FAO related irrigation maps. This may influence the results particular in semi-arid and arid regions and in regions with small-scale and non-permanent irrigation systems (Frenken, 2012).

Compared with statistics and existing studies, our results show differences in both directions: underestimation and overestimation – depending on the reference data. The example of information on irrigated areas in the USA illustrates that the large discrepancies between the studies can be explained by the input data and the references.

The highest discrepancies to the statistics are generally found in developing countries. Possible reasons are inadequate statistics that may often also be a result of political interests (Thenkabail et al., 2009b). General uncertainties or inadequacies of agricultural statistics are well known in many developing countries and discussed in, for example, Young (1999) and Thenkabail et al. (2009b). The results suggest that not all irrigated areas are correctly reported in the official statistics. This indicates the existence of illegal or unregistered irrigation activities. The results also go along with previous analyses that showed large underestimation of irrigated areas in statistical data, especially for India (Thenkabail et al., 2009b) and Western Africa (Drechsel et al., 2006). Even the FAO recommends a careful handling of their official reports for countries in Central, Southern and Eastern Asia since many countries make no distinctions between rain-fed and irrigated cropland (Frenken, 2012, 2013). Independent survey techniques are strongly needed to verify the official statistics and reports.

The huge differences between estimated and reported irrigated areas demonstrate the need for further research in the field of irrigation mapping to get a more realistic picture of water withdrawal. The recent progress in the availability of remote sensing instruments through the Copernicus system of the EU (European Commission, 2017), which delivers weekly global high-resolution (10–20 m) coverage, improves the data availability for land use classifications and crop status analysis and is very promising for irrigation mapping.

Irrigation is important for increasing agricultural production (Smith, 2012): it reduces vulnerability of crop failures and increases food security and income (Bhattarai et al., 2002; Mengistie and Kidane, 2016). At the same time, more irrigated areas require more water, which is mainly taken from surface runoff and groundwater storage. This may increase the pressure in existing water resources and lead to an overuse of regionally available water resources which may threaten future agricultural activities (Du et al., 2014). Therefore, an accurate and more detailed inventory of irrigated areas is required to better estimate and manage available water resources to avoid overuse of water.

Data availability. Data are available at https://doi.pangaea.de/10.1594/PANGAEA.884744.

Supplement. The supplement related to this article is available online at: https://doi.org/10.5194/hess-22-1119-2018-supplement.

Competing interests. The authors declare that they have no conflict of interest.

Acknowledgements. This research was carried out within the framework of the GLUES (Global Assessment of Land Use Dynamics, Greenhouse Gas Emissions and Ecosystem Services) Project, which is supported by the German Ministry of Education and Research (BMBF) programme on Sustainable Land Management.

Edited by: Micha Werner
Reviewed by: two anonymous referees

References

Abuzar, M., McAllister, A., and Whitfield, D.: Mapping Irrigated Farmlands Using Vegetation and Thermal Thresholds Derived from Landsat and ASTER Data in an Irrigation District of Australia, Photogram. Eng. Remote Sens., 81, 229–238, 2015.

Alexandratos, N. and Bruinsma, J.: World agriculture towards 2030/2050: the 2012 revision, ESA working paper no. 12-03, Global Perspective Studies Team, FAO Agricultural Development Economics Division, Rome, Italy, 2012.

Ambika, A. K., Wardlow, B., and Mishra, V.: Remotely sensed high resolution irrigated area mapping in India for 2000 to 2015, Sci Data, 3, 160118, https://doi.org/10.1038/sdata.2016.118, 2016.

Bauer, S., Olson, J., Cockrill, A., van Hattem, M., Miller, L., Tauzer, M., and Leppig, G.: Impacts of Surface Water Diversions for Marijuana Cultivation on Aquatic Habitat in Four Northwestern California Watersheds, PLoS ONE, 10, e0120016, https://doi.org/10.1371/journal.pone.0120016, 2015.

Bhattarai, M., Sakthivadivel, R., and Hussain, I.: Irrigation impacts on income inequality and poverty alleviation: Policy issues and options for improved management of irrigation systems, edited by: International Water Management Institute (IWMI), Colombo, 2002.

California Department of Water Resources: Agricultral Land and Water Estimates, http://www.water.ca.gov/landwateruse/anlwuest.cfm (last access: 6 August 2017), 2010.

California Environmental Protection Agency: Water Rights Enforcement, http://www.waterboards.ca.gov/waterrights/water_issues/programs/enforcement/complaints, last access: 6 August 2017.

Deryng, D., Elliott, J., Folberth, C., Muller, C., Pugh, T. A. M., Boote, K. J., Conway, D., Ruane, A. C., Gerten, D., Jones, J. W., Khabarov, N., Olin, S., Schaphoff, S., Schmid, E., Yang, H., and Rosenzweig, C.: Regional disparities in the beneficial effects of rising CO_2 concentrations on crop water productivity, Nat. Clim. Change, 6, 786, https://doi.org/10.1038/nclimate2995, 2016.

Döll, P. and Schmied, H. M.: How is the impact of climate change on river flow regimes related to the impact on mean annual runoff? A global-scale analysis, Environ. Res. Lett., 7, 014037, https://doi.org/10.1088/1748-9326/7/1/014037, 2012.

Drechsel, P., Graefe, S., Sonou, M., and Cofie, O. O.: Informal Irrigation In Urban West Africa: An Overview, International Water Management Institute, Colombo, Sri Lanka, 2006.

Du, T., Kang, S., Zhang, X., and Zhang, J.: China's food security is threatened by the unsustainable use of water resources in North and Northwest China, Food Energy Secur., 3, 7–18, 2014.

European Commission: Copernicus – Europe's eyes on Earth, http://www.copernicus.eu, last access: 3 February 2017.

European Environment Agency: Coordination of Information on the Environment (CORINE), http://land.copernicus.eu/pan-european/corine-land-cover/clc-2012/view (last access: 2 February 2017), 2014.

ESA – European Space Agency: Bimonthly MERIS FR Composites – NDVI, https://www.esa.int/SPECIALS/Eduspace_Global_EN/SEMQHINW91H_0.html (last access: 24 November 2016), 2007.

ESA – European Space Agency: GlobCover 2009, http://due.esrin.esa.int/page_globcover.php (last access: 24 November 2016), 2010.

ESA – European Space Agency: ESA CCI Land Cover, http://maps.elie.ucl.ac.be/CCI/viewer/index.php (last access: 24 November 2016), 2015.

Evans, R. G. and Sadler, E. J.: Methods and technologies to improve efficiency of water use, Water Resour. Res., 44, W00E04, https://doi.org/10.1029/2007WR006200, 2008.

FAO – Food and Agriculture Organization of the United Nations: Did you know ...? Facts and figures about, http://www.fao.org/nr/water/aquastat/didyouknow/index3.stm (last access: 24 November 2016), 2014a.

FAO – Food and Agriculture Organization of the United Nations: Total Withdrawal by Sector, http://www.fao.org/nr/water/aquastat/tables/WorldData-Withdrawal_eng.pdf (last access: 24 November 2016), 2014b.

FAO – Food and Agriculture Organization of the United Nations: AQUASTAT, http://www.fao.org/nr/water/aquastat/data/query/ (last access: 14 June 2016), 2016a.

FAO – Food and Agriculture Organization of the United Nations: FAOSTAT, http://faostat3.fao.org/download/Q/QC/E (last access: 14 June 2016), 2016b.

Foley, J. A., Ramankutty, N., Brauman, K. A., Cassidy, E. S., Gerber, J. S., Johnston, M., Mueller, N. D., O'Connell, C., Ray, D. K., West, P. C., Balzer, C., Bennett, E. M., Carpenter, S. R., Hill, J., Monfreda, C., Polasky, S., Rockstrom, J., Sheehan, J., Siebert, S., Tilman, D., and Zaks, D. P.: Solutions for a cultivated planet, Nature, 478, 337–342, 2011.

Frenken, K.: Irrigation in Southern and Eastern Asia in figures, edited by: AQUASTAT, Food and Agriculture Organization of the United Nations, Rome, 2012.

Frenken, K.: Irrigation in Central Asia in figures, edited by: AQUASTAT, Food and Agriculture Organization of the United Nations, Rome, 2013.

Fritz, S., See, L., McCallum, I., You, L., Bun, A., Moltchanova, E., Duerauer, M., Albrecht, F., Schill, C., Perger, C., Havlik, P., Mosnier, A., Thornton, P., Wood-Sichra, U., Herrero, M., Becker-Reshef, I., Justice, C., Hansen, M., Gong, P., Abdel Aziz, S., Cipriani, A., Cumani, R., Cecchi, G., Conchedda, G., Ferreira, S., Gomez, A., Haffani, M., Kayitakire, F., Malanding, J., Mueller, R., Newby, T., Nonguierma, A., Olusegun, A., Ortner, S., Rajak, D. R., Rocha, J., Schepaschenko, D., Schepaschenko, M., Terekhov, A., Tiangwa, A., Vancutsem, C., Vintrou, E., Wenbin, W., van der Velde, M., Dunwoody, A., Kraxner, F., and Obersteiner, M.: Mapping global cropland and field size, Global Change Biol., 21, 1980–1992, 2015.

Godfray, H. C., Beddington, J. R., Crute, I. R., Haddad, L., Lawrence, D., Muir, J. F., Pretty, J., Robinson, S., Thomas, S. M., and Toulmin, C.: Food security: the challenge of feeding 9 billion people, Science, 327, 812–818, 2010.

Hijmans, R. J., Cameron, S. E., Parra, J. L., Jones, P. G., and Jarvis, A.: Very high resolution interpolated climate surfaces for global land areas, Int. J. Climatol., 25, 1965–1978, 2005.

Jägermeyr, J., Gerten, D., Heinke, J., Schaphoff, S., Kummu, M., and Lucht, W.: Water savings potentials of irrigation systems: global simulation of processes and linkages, Hydrol. Earth Syst. Sci., 19, 3073–3091, https://doi.org/10.5194/hess-19-3073-2015, 2015.

Jin, N., Tao, B., Ren, W., Feng, M., Sun, R., He, L., Zhuang, W., and Yu, Q.: Mapping Irrigated and Rainfed Wheat Areas Using Multi-Temporal Satellite Data, Remote Sensing, 8, 207, 2016.

Liu, J., Williams, J. R., Zehnder, A. J. B., and Yang, H.: GEPIC – modelling wheat yield and crop water productivity with high resolution on a global scale, Agricult. Syst., 94, 478–493, 2007.

Mankin, J. S., Viviroli, D. J., Singh, D., Hoekstra, A. Y., and Diffenbaugh, N. S.: The potential for snow to supply human water demand in the present and future, Environ. Res. Lett., 10, 114016, https://doi.org/10.1088/1748-9326/10/11/114016, 2015.

Mauser, W., Klepper, G., Zabel, F., Delzeit, R., Hank, T., Putzenlechner, B., and Calzadilla, A.: Global biomass production potentials exceed expected future demand without the need for cropland expansion, Nat. Commun., 6, 8946, https://doi.org/10.1038/ncomms9946, 2015.

Mengistie, D. and Kidane, D.: Assessment of the Impact of Small-Scale Irrigation on Household Livelihood Improvement at Gubalafto District, North Wollo, Ethiopia, Agriculture, 6, 1–22, 2016.

Molden, D.: Water for Food Water for Life: A Comprehensive Assessment of Water Management in Agriculture, Earthscan, London, Washington, D.C., 2007.

Neumann, K., Stehfest, E., Verburg, P. H., Siebert, S., Müller, C., and Veldkamp, T.: Exploring global irrigation patterns: A multilevel modelling approach, Agricult. Syst., 104, 703–713, 2011.

Ozdogan, M. and Gutman, G.: A new methodology to map irrigated areas using multi-temporal MODIS and ancillary data: An application example in the continental US, Remote Sens. Environ., 112, 3520–3537, 2008.

Ozdogan, M., Yang, Y., Allez, G., and Cervantes, C.: Remote Sensing of Irrigated Agriculture: Opportunities and Challenges, Remote Sensing, 2, 2274–2304, 2010.

Prasch, M., Mauser, W., and Weber, M.: Quantifying present and future glacier melt-water contribution to runoff in a central Himalayan river basin, The Cryosphere, 7, 889–904, https://doi.org/10.5194/tc-7-889-2013, 2013.

Rosenzweig, C., Elliott, J., Deryng, D., Ruane, A. C., Muller, C., Arneth, A., Boote, K. J., Folberth, C., Glotter, M., Khabarov, N., Neumann, K., Piontek, F., Pugh, T. A., Schmid, E., Stehfest, E., Yang, H., and Jones, J. W.: Assessing agricultural risks of climate change in the 21st century in a global gridded crop model intercomparison, P. Natl. Acad. Sci. USA, 111, 3268–3273, 2014.

Salmon, J. M., Friedl, M. A., Frolking, S., Wisser, D., and Douglas, E. M.: Global rain-fed, irrigated, and paddy croplands: A new high resolution map derived from remote sensing, crop inventories and climate data, Int. J. Appl. Earth Obs. Geoinf., 38, 321–334, 2015.

Shahriar Pervez, M., Budde, M., and Rowland, J.: Mapping irrigated areas in Afghanistan over the past decade using MODIS NDVI, Remote Sens. Environ., 149, 155–165, 2014.

Siebert, S., Döll, P., Hoogeveen, J., Faures, J.-M., Frenken, K., and Feick, S.: Development and validation of the global map of irrigation areas, Hydrol. Earth Syst. Sci., 9, 535–547, https://doi.org/10.5194/hess-9-535-2005, 2005.

Siebert, S., Henrich, V., Frenken, K., and Burke, J.: Update Of The Digital Global Map Of Irrigation Areas to Version 5, Rheinische Friedrich-Wilhelms-University, Bonn, Germany/Food and Agriculture Organization of the United Nations, Rome, Italy, 2013.

Smith, M.: Yield response to water: the original FAO water production function, in: Crop yield response to water, edited by: Steduto, P., Hsiao, T. C., Fereres, E., and Raes, D., Food and Agriculture Organization of the United Nations, Rome, 2012.

Strzepek, K. and Boehlert, B.: Competition for water for the food system, Philos. T. Roy. Soc. Lond. B, 365, 2927–2940, 2010.

Sys, C. O., van Ranst, E., Debaveye, J., and Beernaert, F.: Land Evalutation: Part III Crop Requirements, Agricultural Publications, General Administration for Development Cooperation, Brussels, 1993.

Thenkabail, P. S., Biradar, C. M., Noojipady, P., Dheeravath, V., Li, Y., Velpuri, M., Gumma, M., Gangalakunta, O. R. P., Turral, H., Cai, X., Vithanage, J., Schull, M. A., and Dutta, R.: Global irrigated area map (GIAM), derived from remote sensing, for the end of the last millennium, Int. J. Remote Sens., 30, 3679–3733, 2009a.

Thenkabail, P. S., Dheeravath, V., Biradar, C. M., Gangalakunta, O. R. P., Noojipady, P., Gurappa, C., Velpuri, M., Gumma, M., and Li, Y.: Irrigated Area Maps and Statistics of India Using Remote Sensing and National Statistics, Remote Sensing, 1, 50–67, 2009b.

Thevs, N., Peng, H., Rozi, A., Zerbe, S., and Abdusalih, N.: Water allocation and water consumption of irrigated agriculture and natural vegetation in the Aksu-Tarim river basin, Xinjiang, China, J. Arid Environ., 112, 87–97, 2015.

Tilman, D., Balzer, C., Hill, J., and Befort, B. L.: Global food demand and the sustainable intensification of agriculture, P. Natl. Acad. Sci. USA, 108, 20260–20264, 2011.

UN – United Nations Statistics Divisions: Composition of macro geographical (continental) regions, geographical sub-regions, and selected economic and other groupings, http://unstats.un.org/unsd/methods/m49/m49regin.htm (last access: 24 November 2016), 2013.

UN – United Nations: Sustainable Development Goals, https://sustainabledevelopment.un.org/sdgs, last access: 24 November 2016.

USGS – US Geological Survey: Global Land Cover Characteristics Data Base Version 2.0, https://lta.cr.usgs.gov/glcc/globdoc2_0 (last access: 26 November 2016), 2000.

USGS – US Geological Survey: Estimate Use of Water in the United States in 2010, https://pubs.usgs.gov/circ/1405/ (last access: 2 September 2017), 2014.

Vörösmarty, C. J.: Global water assessment and potential contributions from Earth Systems Science, Aquat. Sci., 64, 328–351, 2002.

Vörösmarty, C. J. and Sahagian, D.: Anthropogenic disturbance of the terrestrial water cycle, Bioscience, 50, 753–765, 2000.

Wada, Y., Wisser, D., and Bierkens, M. F. P.: Global modeling of withdrawal, allocation and consumptive use of surface water and groundwater resources, Earth Syst. Dynam., 5, 15–40, https://doi.org/10.5194/esd-5-15-2014, 2014.

Young, A.: Is there Really Spare Land? A Critique of Estimates of Available Cultivable Land in Developing Countries, Environ. Dev. Sustain., 1, 3–18, 1999.

Zabel, F., Putzenlechner, B., and Mauser, W.: Global agricultural land resources – a high resolution suitability evaluation and its perspectives until 2100 under climate change conditions, PLoS One, 9, e107522, https://doi.org/10.1371/journal.pone.0107522, 2014.

Zhu, X., Zhu, W., Zhang, J., and Pan, Y.: Mapping Irrigated Areas in China From Remote Sensing and Statistical Data, IEEE J. Select. Top. Appl. Earth Obs. Rem. Sens., 7, 4490–4504, 2014.

PUBLICATION 2

Meier, J.; Mauser, W. Irrigation mapping at different spatial scales: Areal change with resolution explained by landscape metrics (2023): *Remote Sensing.*, 15, 315. https://doi.org/10.3390/rs15020315

remote sensing

MDPI

Technical Note

Irrigation Mapping at Different Spatial Scales: Areal Change with Resolution Explained by Landscape Metrics

Jonas Meier [1,*] and Wolfram Mauser [2]

[1] German Remote Sensing Data Center (DFD), German Aerospace Center (DLR), Muenchener Str. 20, 82234 Wessling, Germany
[2] Department of Geography, Ludwig-Maximilians-University Munich, Luisenstr. 37, 80333 Munich, Germany
* Correspondence: jonas.meier@dlr.de

Abstract: The monitoring of irrigated areas still represents a complex and laborious challenge in land use classification. The extent and location of irrigated areas vary in both methodology and scale. One major reason for discrepancies is the choice of spatial resolution. This study evaluates the influence of spatial resolution on the mapped extent and spatial patterns of irrigation using an NDVI threshold approach with Sentinel-2 and operational PROBA-V data. The influence of resolution on irrigation mapping was analyzed in the USA, China and Sudan to cover a broad range of agricultural systems by comparing results from original 10 m Sentinel-2 data with mapped coarser results at 20 m, 40 m, 60 m, 100 m, 300 m, 600 m and 1000 m and with results from PROBA-V. While the mapped irrigated area in China is constant independent of resolution, it decreases in Sudan (−29%) and the USA (−48%). The differences in the mapping result can largely be explained by the spatial arrangement of the irrigated pixels at a fine resolution. The calculation of landscape metrics in the three regions shows that the Landscape Shape Index (LSI) can explain the loss of irrigated area from 10 m to 300 m ($r > 0.9$).

Keywords: irrigation mapping; land use classification; Sentinel-2; NDVI; rescaling technique; spatial resolution; scaling relation; land monitoring; sensor resolution; landscape metrics

Citation: Meier, J.; Mauser, W. Irrigation Mapping at Different Spatial Scales: Areal Change with Resolution Explained by Landscape Metrics. *Remote Sens.* **2023**, *15*, 315. https://doi.org/10.3390/rs15020315

Academic Editors: Georgios Mallinis and Won-Ho Nam

Received: 7 November 2022
Revised: 23 December 2022
Accepted: 27 December 2022
Published: 5 January 2023

1. Introduction

Remote sensing has proven to be a suitable instrument for land use classification and land surface monitoring. The time series of remote sensing data allow for detecting land use change and changes in agricultural patterns and management practices. Agriculture uses vast amounts of natural resources such as fresh water for irrigation in an often-non-sustainable way [1]. To secure current and future global food supplies in a sustainable way, agriculture has to increase the efficiency of the water it uses, which is expressed in the principle of "more crop per drop" [2]. Developing and finally establishing monitoring capabilities for agricultural irrigation and its efficiency therefore constitutes a major prerequisite towards improving the efficiency, effectiveness and sustainability of agricultural water use.

Remote sensing is the central data source for a quantitative global, regional and local monitoring of areal extent, timing and technique of irrigation. The Copernicus Sentinel missions provide, on an operational basis, high spatial and temporal resolution data. Together with increasing computing capacities, they extend our Earth observation capacities to develop and deploy the monitoring systems necessary to achieve the necessary efficiency gains in irrigation.

Since approx. 20% of the total cropland is irrigated and approx. 40% of the world food is produced on this cropland, irrigation plays a crucial role in global food production [3]. Irrigated cropland consumes 69% of the global water withdrawal from surface and groundwater [4]. Global irrigated area doubled in the last 50 years [3] and future expansion is expected [5,6]. Over 50% of the irrigated areas are located in regions characterized by annual precipitation smaller than 750 mm, which is considered the limit below which diverse

demands for water may lead to allocation conflicts [7,8]. Additionally, the impact of climate change may regionally influence precipitation and snowmelt patterns and, consequently, river flows and groundwater recharge, and may thus reduce the availability of fresh water, aggravate water scarcity and amplify water-related conflicts [8].

The high demand for irrigation water strains the regional hydrological cycle mainly through withdrawal from local and regional rivers and aquifers. Irrigation water is diverted into the atmosphere and, as a result, lost for further downstream uses. Dramatic reductions in run-off and aquifer levels caused by irrigation with adverse effects for the regional environment and for the downstream population are documented worldwide [9–12]. It is, therefore, crucial to monitor, with high accuracy, the location and extent of irrigated area.

Mapping of irrigated areas still represents a challenge for remote sensing. Several studies have shown the feasibility of mapping irrigated areas using remote sensing data from the local to global scale [13–18]. Existing irrigation mapping methods combine different data to exclude rain-fed and irrigated land by strong indicators such as evapotranspiration [19], climatic conditions [17], thermal variations over an irrigated field [20] or soil moisture [21]. The few existing global studies about irrigated areas show large differences in its extent and spatial pattern and are subject to controversial discussions in the scientific community [22,23]. The differences are caused by different assumptions and definitions, different time periods and data from different satellite missions with different spatial resolution and spectral coverage. This study focusses on the influence of spatial resolution of remote sensing data on the resulting location and extent of derived irrigated areas. Velpuri et al. [24] already showed, in a case study, that finer spatial resolution can result in an increase in classified irrigated area. They conclude that current operational irrigation monitoring systems, which are based on coarser resolution imagery from, e.g., AVHRR, MODIS or PROBA-V, neglect relevant parts of the global irrigated area [24]. Nevertheless, they do not address the transferability of their findings to other regions. On the other hand, coarser resolution has convincing advantages for global monitoring systems of the temporal development of global irrigation, such as daily global coverage and low data rates.

The existing long time series of medium-resolution LANDSAT data and the new medium spatial and high-temporal-resolution Sentinel-2 data have successfully been used in regional and local studies to determine the extent of irrigated areas with high precision [25–27]. In principle, they would be the data source of choice for a more complete, global, operational irrigation mapping. Sentinel-2 now allows, in principle, to precisely and operationally resolve, with high spatial resolution, the temporal NDVI-developments on which current approaches to distinguish irrigated areas from non-irrigated areas rely. Improved global irrigation monitoring therefore seems possible but not feasible considering the massive computational resources necessary to analyze frequent time series of large areas with high spatial resolution. This may be one reason why, despite the anticipated added precision, to our knowledge, operational irrigation monitoring on a global scale using Sentinel-2-time series is not available yet.

On the other hand, Sentinel-2 time series could potentially be used to augment existing global low-resolution approaches to map irrigated areas, given that the local scaling laws, which govern the change in detected irrigated areas with decreased spatial resolution, are well understood. The hypothesis of our paper, therefore, is that the change in detected irrigated areas with decreasing spatial resolution inherent in the current approaches follows a regional independent scaling relation. We consider the resulting scaling relations as a property of the plot size, the spatial arrangement and the complexity of the shape of the irrigated fields. The complexity of the spatial structure of the irrigated areas can be described by landscape metrics, well known from biodiversity and habitat analysis [28,29]. The Landscape Shape Index (LSI) was identified to be suitable for explaining the negative changes in the mapping results [30–32]. A proven correlating functional relation between the differences in the mapping results caused by resolution and the LSI can be used for estimating the accuracy of global low-resolution irrigation monitoring. In order to investigate the scaling properties, we use a proven approach to globally monitor irrigated areas

using NDVI time series, which have been widely used with wide-swath low-resolution sensors such as MERIS and PROBA-V [7]. For the first time, we systematically analyze the impact of spatial resolution from 10 m to 1 km on the pattern and extent of irrigated areas in three selected global regions. We consider different geographical conditions with respect to climate and farming systems by selecting as case studies regions in Sudan, China and the USA.

2. Materials and Methods

2.1. Multi-Resolution Analysis

We applied the method described in Meier, Zabel and Mauser [7] to determine irrigated area. It does not explicitly use spatial resolution as a parameter. The basis of the mapping method is annual NDVI time series. They are used together with parameters such as land suitability for agriculture, a land use classification, NDVI data and official national statistics to determine global irrigated area. The annual course of NDVI is analyzed, interpreted and compared with agricultural suitability evaluations [7,33]. The method analyzes the NDVI time series using parameters such as amplitude of the NDVI, position of NDVI peaks and shape of the NDVI annual temporal course. If the course of NDVI suggests active vegetation growth with typical characteristics of agriculture and, simultaneously, the agricultural suitability is low due to a rainfall deficit, we assume a high likeliness of irrigation. In our case, the original mapping-method [7] is modified in two points to be applicable to the finer spatial resolutions: (1) the information about irrigated area derived from the official statistics are not used to avoid a biased result and (2) the restriction of the approach to only process the land-use cropland is lifted because using an external (coarser resolution) land use classification at this fine spatial resolution would lead to a predetermination of the result. The result of the threshold mapping method is a map containing Boolean information of the status of the field: irrigated or not irrigated.

We derive scaling relation of irrigation extent vs. spatial resolution in three different regions: central Sudan around Khartoum, in northwestern China in the Uighur province Xinjiang and in Colorado, southeast of Denver (Figure 1). These three regions were selected based on the following criteria:

- The region's agricultural suitability is low due to rainfall deficit to avoid both confusion between irrigated and rain-fed areas and high cloud cover.
- The region should be dominated by irrigated agriculture.
- The selected regions should cover a broad range of agricultural systems—from subsistence to high-intensity agriculture.

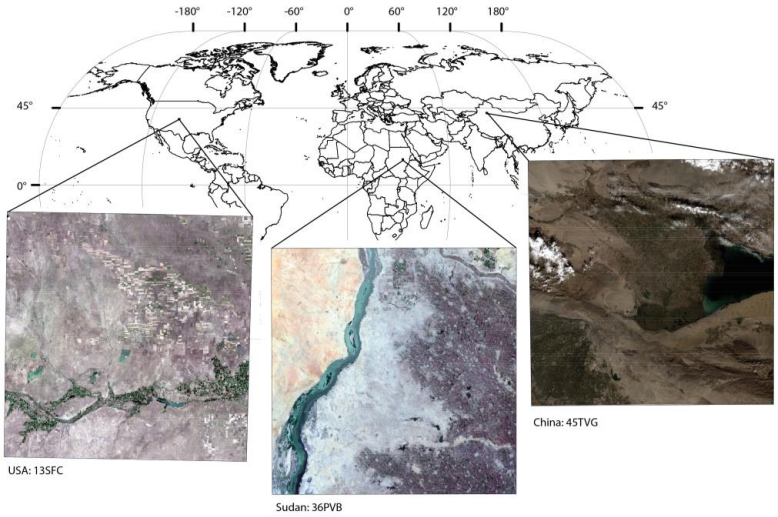

Figure 1. Global overview of the selected regions including the Sentinel−2 tile name.

All three regions are characterized by low annual precipitation values. The region in the USA (303 mm/year) is the wettest, followed by Sudan (202 mm/year) and China (173 mm/year), based on the ERA5 data of the year 2016 [34]. Each study area covers one Sentinel-2 tile of approx. 100 × 100 km.

According to Fritz et al. [35], the field sizes in the three tiles ranges from "very small" to "very large". The field sizes in the USA are categorized as "large", in China as "medium" and in Sudan from "very small" to "small". A visual pre-analysis shows that the sizes and shapes of the fields in China and Sudan vary strongly whereas the fields in the USA are homogeneous and only differ in shape: squared or the typical circular fields shaped by center pivot irrigation. The cultivated crops range from alfalfa and cereals to groundnut and fruits. The area in the USA is characterized by alfalfa (66%) and maize (31%); the remaining agricultural areas are used mainly for fruits and vegetables [36]. The agricultural areas in Sudan are mainly used for the cultivation of groundnut (71%), cotton (8%) and millet (6%). The remaining area of 15% is used for the cultivation of crop types such as maize, cassava, beans, dates and fruits. In the selected China tile, mainly cotton (37%) and maize (32%) are cultivated. Permanent crops such as grapes (4%) and apple trees (3%) are also cultivated, as well as vegetables and fruits.

The study of the scaling relations is carried out for the year 2016. In this study, we apply the modified mapping method described above to the selected Sentinel-2 tiles at a spatial resolution of 10 m, 20 m, 40 m, 60 m, 100 m, 300 m, 600 m and 1000 m to systematically evaluate the impact of spatial resolution on the identified irrigated area. In order to investigate how the Sentinel-2 and PROBA-Vegetation (PROBA-V) spectral coverage compares when using the selected irrigation mapping approach and in order to link the results of the varying-resolution Sentinel-2 mapping with the operational PROBA-V (300 m) mapping of irrigated area, the same irrigation mapping method is also applied to the available PROBA-V data sets of the same period and regions. PROBA-V was developed as successor of SPOT5 to ensure the continuation of low-resolution vegetation products and was successfully launched in 2013. The spectral range is similar to SPOT5 and provides 4 bands (BLUE, RED, NIR, SWIR) in a spatial resolution from 100 to 300 m [37,38]. The Sentinel-2 and PROBA-V results are compared at a spatial resolution of 300 m.

Sentinel-2 is a multi-spectral satellite and is part of the EU's Copernicus program. The spatial resolution depends on the spectral band. The bands (band 8 (NIR) and band 4 (RED)) used in this study are available at a resolution of 10 m. We use the Top-Of-Atmosphere reflectance (TOA) Sentinel-2 data that are corrected for atmospheric effects to Top-Of-Canopy (TOC) reflectance data at 10 m using an inverse radiative transfer approach based on MODTRAN radiative transfer simulations [39]. During the atmospheric correction process, a cloud and snow mask is automatically derived from the images. All available unmasked data of all available dates of 2016 for the selected tiles are used for our analysis. Figure 2 shows the average number of valid observations per pixel for each month.

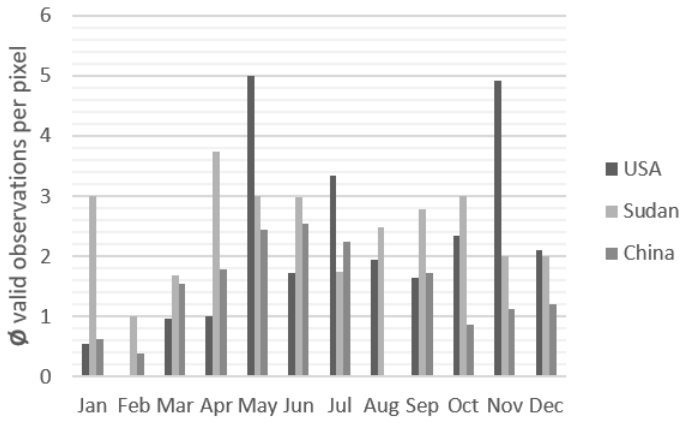

Figure 2. The average number of valid Sentinel-2 observations per pixel for each month in the study regions.

The Normalized Difference Vegetation Index (NDVI) is calculated from the available Sentinel data where RED is TOC reflectance in band 4 and NIR is TOC reflectance in band 8 as:

$$\begin{aligned} \text{NDVI} &= \frac{\text{NIR(band8)} - \text{RED(band4)}}{\text{NIR(band8)} + \text{RED(band4)}} \\ \text{RED} &= \text{TOC reflectance in band 4} \\ \text{NIR} &= \text{TOC reflectance in band 8} \end{aligned} \tag{1}$$

This results in a spatially distributed multi-temporal 10 m-resolution temporal course of NDVI covering the year 2016. To calculate multi-temporal NDVI data at 20 m, 40 m, 60 m, 100 m, 300 m, 600 m and 1000 m, the TOC reflectance values of the spectral bands RED and NIR are separately rescaled using a moving window which averages the reflectance of the pixel within the respective area of the coarser resolution. The upscaled reflection value is then used to calculate the NDVI according to Formula 1. For each spatial resolution data set, irrigation maps are created using the identical adapted threshold method to map irrigated areas [7].

2.2. Scaling Relation at Different Spatial Resolution

The irrigation mapping results differ depending on the spatial resolution. Whereas a perfectly homogeneous image does not show differences in NDVI with changing resolution, the averaging of heterogeneous (with reference to the considered resolution) reflectances in the higher resolution images results in a tendency to homogenize the NDVI values in the coarser resolution images. Since the irrigation detection algorithm is non-linear with NDVI, this changes the amount of detected irrigation, with NDVIs averaged over heterogeneous areas. Therefore, we assume a relationship between the heterogeneity of the spatial position and formation of the irrigated area as it is shown in the fine resolution and the area changes when moving up to coarser resolutions. To measure the heterogeneity or homogeneity of the irrigation pattern, we use landscape metrics, a measure for the complexity of a landscape. To quantify the relation between landscape metrics and the areal change with resolution of the mapped irrigated area, we calculate landscape metrics for the three regions. To increase the number of samples, we split each region in 36 tiles to generate more stable statistics. A pre-analysis showed that at and above 6 by 6 pixels, the results remained constant. For the 36 tiles, the areal change between 300 m and 10 m is calculated as follows:

$$\text{areal change}[\%] = \text{irrigated area 300 m } [\%] - \text{irrigated area 10 m } [\%] \tag{2}$$

While the pixel at 300 m gives Boolean information (irrigated or not irrigated), the result at 10 m gives more precise information about the irrigated area at the corresponding 300 m pixel. This information is used to determine the difference between the mapping result at 300 m and 10 m. Depending on the position and spatial arrangement of the irrigated area, the change in spatial resolution from 10 m to 300 m can result in positive or negative areal change of irrigated area detected by the algorithm. Negative changes occur in case of a high heterogeneity of the considered area. Positives changes occur when the majority of the considered area is classified as irrigated, and the spectral reflectance is hardly affected by the upscaling process. Positive changes are rather theoretical and hardly ever occur. Therefore, this study will focus solely on the negative changes.

To quantify the relation between landscape metrics and the areal change with resolution of the mapped irrigated area, we calculate landscape metrics on the same 36 tiles of the three regions using the R-package of Hesselbarth et al. [40]. We assume that the position, the shape and the spatial arrangement are reasons for the areal change of the mapping results. To explain the negative changes of irrigated area with decreasing resolution, we calculate the Landscape Shape Index (LSI, see Equation (3)), which describes the ratio of the total edge length of a class, in our case, irrigated area, to the minimum edge length. LSI

measures the complexity of a selected class (irrigated) compared to the other classes (not irrigated) of a landscape.

$$\begin{aligned} \text{LSI} &= \frac{\text{E}}{\min(\text{E})} \\ \text{E} &= \text{total edge length of the class} \end{aligned} \tag{3}$$

Thus, as a ratio between the actual class edge length and the minimum class edge length, the LSI is an 'aggregation metric'. In case of only one class in the landscape, the minimum length equals the edge length. The higher the ratio, the more complex the pattern of the irrigated area. The result is a high expected loss of mapped irrigated area at the coarser spatial resolution. The LSI is calculated for the 36 tiles of the irrigation mapping at 300 m and is correlated with the negative areal change for the mapping result between 300 m and 10 m.

3. Results

3.1. Extent of Irrigated Area

The mapped irrigated area as a function of spatial resolutions is compared in Figure 3 for the three selected study sites. Generally, it shows a decrease in irrigated area with decreasing spatial resolution. Nevertheless, there are large differences in the relationship between resolution and area between the selected regions. This can be seen in Figure 3 in China, where the scaling effect is rather small, whereas Sudan and USA show a pronounced scaling effect.

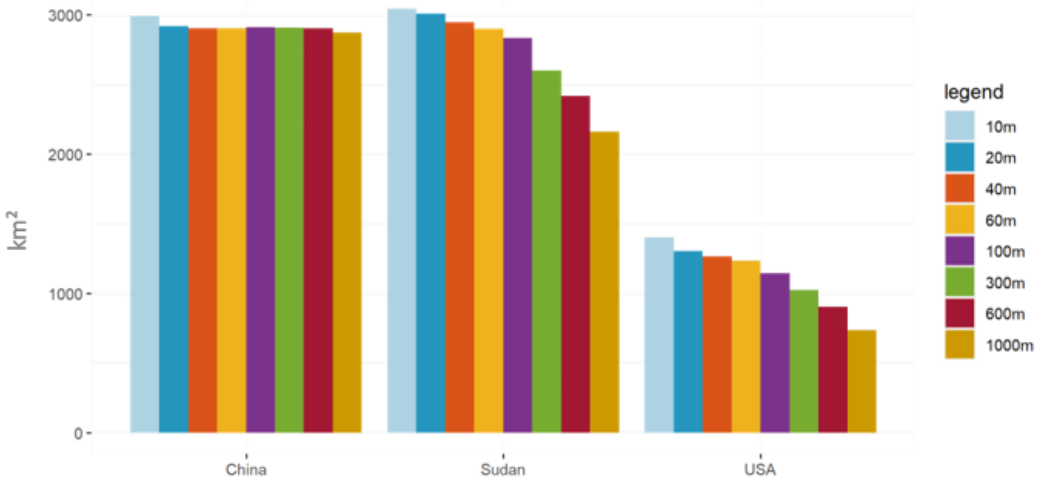

Figure 3. Mapped irrigated area in the selected Sentinel-2 tiles in China, Sudan and USA at different spatial resolutions. In Sudan and USA, the mapped irrigated area decreases with decreasing spatial resolution while the mapped irrigated area in China is almost independent of resolution.

Table 1 shows the absolute values of the mapped irrigated area in the three study sites in km^2 for the selected spatial resolutions.

Table 1. Resulting irrigated area in the three different regions.

Spatial Resolution	China [km^2]	Sudan [km^2]	USA [km^2]
1000 m	2872.95	2159.24	734.21
600 m	2904.48	2416.68	903.24
300 m	2908.71	2599.83	1021.41
100 m	2910.75	2832.09	1144.47
60 m	2905.35	2901.15	1233.78
40 m	2905.28	2945.68	1262.84
20 m	2919.77	3009.17	1305.00
10 m	2992.01	3044.93	1401.12

Figure 3 and Table 1 show that the mapping result in China is hardly affected by the upscaling resolution from 10–1000 m. Reasons are the structure of the irrigated area in this region which consists of very large-scale cohesive irrigated plots. In this case, NDVI does not change significantly by averaging towards lower resolutions and a mix of different NDVI values hardly occurs in the high-resolution ensemble underlying the low-resolution pixels.

Figure 4 shows the spatial distribution of the mapped irrigated area in the three selected Sentinel-2 tiles for a spatial resolution of 10 m, 300 m and 1000 m. Visually, the spatial irrigation patterns largely differ in the three regions: while irrigation in Sudan and USA is scattered, the irrigated area in China is more clumped in two large contiguous irrigation clusters. At the coarser spatial resolutions, the small and scattered irrigated areas in Sudan and USA disappear while the irrigated agglomerations in China prevail.

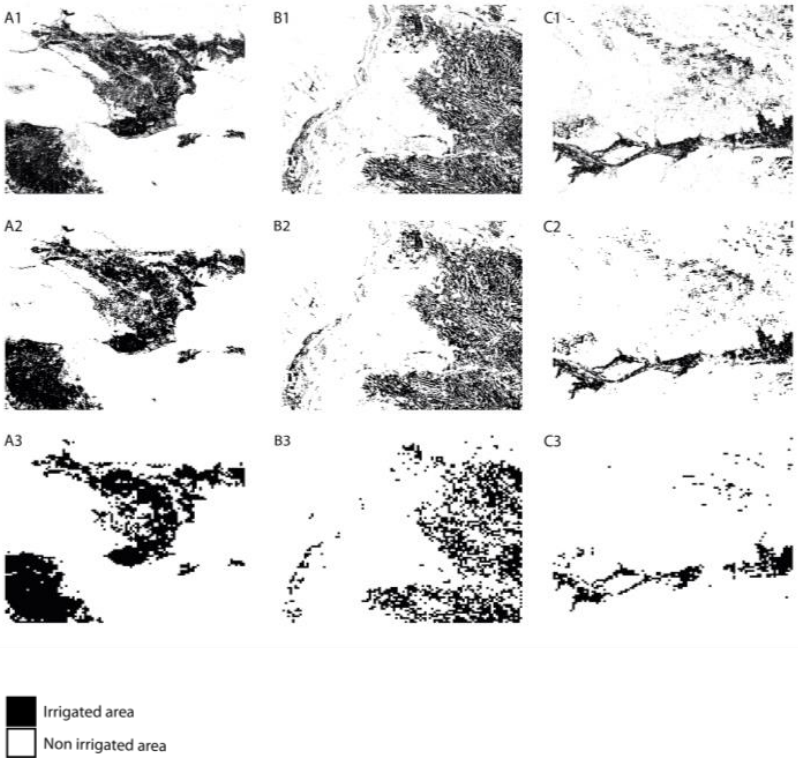

Figure 4. Mapped irrigated area as a function of spatial resolution in the three different study sites: **A** = China, **B** = Sudan, **C** = USA. **1** = 10 m, **2** = 300 m, **3** = 1000 m.

3.1.1. Sudan

The identified irrigated area in Sudan clearly decreases with coarser spatial resolution. At a resolution of 100 m, the irrigated area decreases by 7% and continues to decrease to 29% at a resolution of 1000 m (Figure 3 and Table 1). At a coarser resolution of 300 m, single small-scale fields are no longer classified as irrigated, especially when they are surrounded by non-cultivated or abandoned fields or non-vegetated areas. This effect decreases the extent of irrigated areas. Figure 5 shows that contiguous clusters of fields are less affected by resolution decrease. At the finer resolutions (below 300 m), the fields are well defined and differentiation between fallow fields, possible artificial area and other irrigated fields is possible. At the coarser resolutions (from 300 m upwards), the areal extent decreases and the original patterns are hardly visible.

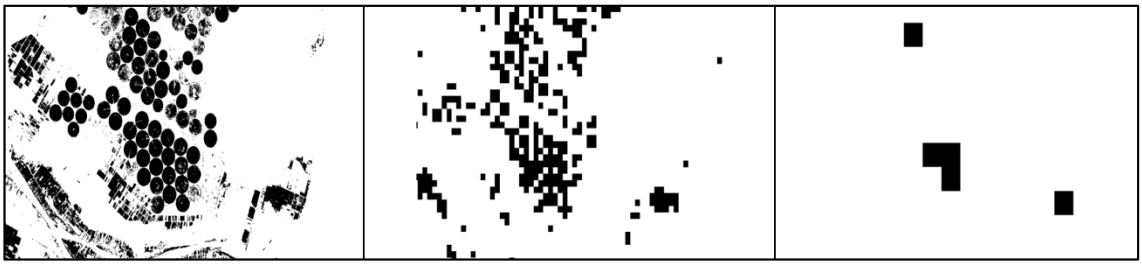

Figure 5. The decrease in irrigated area at coarser resolutions at the study site in Sudan. The left image shows the area classified as irrigated at the resolution of 10 m. The middle shows the same area at 300 m and at the right at 1000 m.

Figure 5 shows the center pivot fields in the northwestern part of the Sudan tile. This detail serves as a good example of the decrease in the irrigated area. At the finer resolutions, the center pivot fields can clearly be identified. At a resolution of 300 m, the center pivot fields dissolve and almost completely disappear at the resolution of 1000 m.

3.1.2. USA

In the USA, the irrigated area decreases by 27% at the resolution of 300 m and by 48% at the coarsest resolution of 1000 m (Figure 3 and Table 1). At the finest resolution, the irrigated area around the Arkansas River in the south of the scene is dense and, therefore, not affected by the coarser resolutions. In the northwestern part of the scene, some single fields and fields in small irrigation clusters exist. Small single irrigated fields or smaller irrigated clusters are scattered over the whole tile. By decreasing the spatial resolution, the small, irrigated fields disappear and the fields in the larger agglomerations prevail.

3.1.3. China

In contrast to the findings in Sudan and USA, the identified irrigated area in China almost remains constant across all spatial resolutions. The differences between the spatial resolutions are small (~1%). The tile shows two large agglomerations and two smaller agglomerations of irrigated area. The fields are more densely organized than in the USA and Sudan tiles and the irrigated area is affected differently by the decrease in resolution. Instead of decreasing the irrigated area, the small space between the fields is averaged out and also classified as irrigated and the original pattern of the agglomeration of the fields remains. This results in a smaller decrease in the irrigated area at resolutions up to 1000 m compared to the results in the USA and Sudan.

3.2. Comparison of the Sentinel-2 Irrigation Mapping to PROBA-V

The coarser spatial resolutions of the different data sets, which were used to investigate the scaling behavior, are generated by spatially averaging the reflectance values from Sentinel-2 data before further processing the data. This ensures that the spectral sensitivity with which the red and NIR bands reflectance is measured is the same for all resolutions and that resulting NDVIs are derived in a consistent manner.

Operational irrigation monitoring relies on coarse resolution sensors such as PROBA-V. It is, therefore, important from a monitoring point of view to investigate whether this downscaling approach leads to irrigated areas, which are comparable to those which are monitored operationally with PROBA-V. For one, the spatial resolution of 300 m of the downscaled Sentinel-2 data geometrically closely resembles that of VEGETATION on PROBA-V. Nevertheless, there are differences in the spectral characteristics of the red and NIR spectral bands, the time of overpass and, thereby, the illumination condition and related bi-directional reflectance effects during recording and the temporal coverage between the two sensors. To explore the influence of the different sensor systems on irrigation mapping, the results of the 300 m Sentinel-2 irrigation maps are compared to the results using the identical approach and NDVI time series derived from PROBA-V.

Figure 6 shows the irrigation map derived from PROBA-V NDVI data in 2016 with the same approach used for the Sentinel-2 series of spatial resolution data sets. The patterns shown in Figure 6 closely resemble those in Figure 3. Table 2 shows that the mapping results of approx. 300 m PROBA-V are very close to the results at the aggregated 300 m Sentinel-2 results in all three regions. PROBA-V overestimates the area in all three regions by approx. 6% in Sudan, 1.4% in China and 0.7% in the USA compared to Sentinel-2.

Figure 6. Irrigated area of 2016 derived from PROBA-V data at 10 arc seconds (approx. 300 m) for the regions of China (**left**), Sudan (**middle**) and USA (**right**).

Table 2. Comparison of the irrigation mapping results using PROBA-V and the degraded Sentinel-2 data at 300 m.

Satellite	Spatial Resolution	Sudan	USA	China
PROBA-V	~300 m	2671 km^2	1035 km^2	2940 km^2
Sentinel-2_{300}	300 m	2599 km^2	1021 km^2	2908 km^2

We thus conclude that our irrigation mapping method using annual NDVI courses is transferable between Sentinel-2 and PROBA-V data. On the other hand, our analysis of the mapping results at different spatial resolutions shows that Sentinel-2, at a resolution of 10m, is able to detect additional irrigated areas which are lost at the coarser resolution. On the other hand, the large data volume involved would be a large obstacle for an operational global irrigation monitoring system based on Sentinel-2. By possibly using scaling relations that would, depending on the geographical setting, allow us to correct for the lost irrigated area in the coarse resolution operational irrigation monitoring system, the use of 10m-resolution Sentinel-2 data would largely enhance the monitoring result. Here, we propose a framework which would allow global PROBA-V irrigation monitoring to profit from sample Sentinel-2 irrigation mapping by allying appropriate scaling relations.

3.3. Scaling Relation between Lost Irrigated Area and the Landscape Shape Index

In Section 2.2, we hypothesized a relationship between the Landscape Shape Index and the negative areal change of the irrigation mapping with spatial resolution. When applying the LSI to the 36 sub-tiles in each of the three selected Sentinel-2 tiles, the results in Figure 7 show a strong linear relationship between the LSI and the negative change of the mapped irrigation area at 300 m compared to at 10 m (Sudan: $r = -0.92$, USA: $r = -0.95$, China: $r = -0.96$). Figure 7 shows the result in the three regions and the different characterization of the areal change and the LSI.

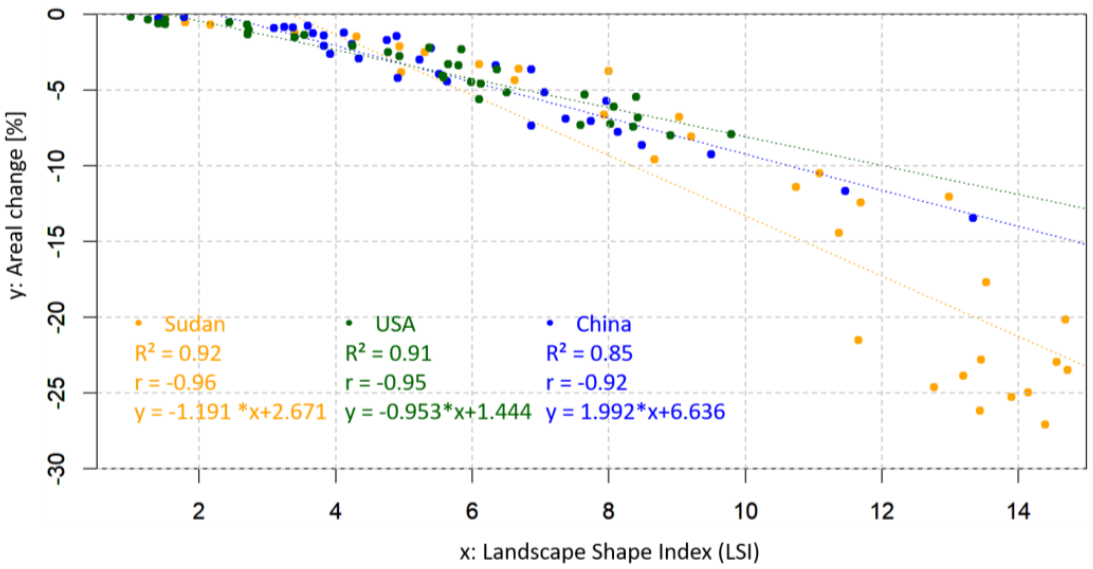

Figure 7. Loss of the mapped irrigated area from 10 m to 300 m spatial resolution as a function of the Landscape Shape Index (LSI) in the three regions: Sudan, USA and China.

At small values, the relationship in all three regions behave similarly. Higher LSI values are observed in Sudan and changes the linear equation compared to the equations in USA and China. This shows that the mapping result depends on the spatial formation and arrangement and the complexity of the shape of the irrigation network. These relations seem to be independent from the region and are based solely on the spatial arrangement and the complexity of the shapes of the mapped irrigated area.

4. Discussion

This study represents a systematical analysis of the influence of spatial resolution of the selected sensor on the mapped irrigated area. The study confirms the findings of Velpuri et al. [24], in that the mapped irrigated area generally decreases when moving to a coarser spatial resolution. The magnitude of change in the irrigated area with spatial resolution shows a strong linear relation with the LSI in all three regions and seems to be regionally independent.

However, many factors influence the scaling relation, with the characteristics of the regional farming system being the most obvious. These characteristic farming systems result in the spatial formation of the irrigated fields and were affected differently according to their shape and their spatial arrangement in the coarser spatial resolution. While the mapping result in China stayed constant, the analyzed regions in Sudan and USA showed large discrepancies in the mapped irrigated area at different spatial resolutions. This implies a high complexity of the irrigation patterns which affect the spectral upscaling to a coarser resolution, while the irrigated area in China is ordered mainly in irrigation agglomerations with a low complexity in shape. That means the determination of irrigated areas in regions of small and scattered fields is more affected when moving to coarser resolutions than in regions of larger, connected fields in areas which are completely used for agriculture. As soon as single fields are embedded in a non-irrigated surrounding of fallow fields or barren land, the identified irrigated area is highly sensitive to a decrease in resolutions.

The upscaling of the spectral information smooths the NDVI signal and influences the mapping method. This leads to a significant change of the average NDVI in case of a high NDVI variation at the underlying resolution. High NDVI variations are caused by different growth phase or by a mix of different land uses at one 300 m-resolution pixel. This effect is shown in the example of Sudan, where the landscape is characterized by a mix of small fields, meadows and settlements interrupted by streets and fallow land. At coarser

resolutions (>100 m), this leads to high variations in the NDVI within one coarse resolution pixel and, thereby, influences the mapping result (Figures 3 and 5).

The largest absolute changes in identified irrigated area with decreasing spatial resolutions were found in the USA. The differences may have several reasons: The annual precipitation in the region is 329 mm/a, which is the highest of the three compared regions. For rain-fed agricultural systems, this precipitation amount is very low, causing supplemental irrigation systems to be widely used in this area. Precipitation events might occur very locally and in summer as heavy thunderstorms, which have comparable effects to technical irrigation. The high-resolution images show small water ponds and water channels used for storage and transportation of water from wells or water bodies to the irrigated fields. The greening effect around the water storage and transportation bodies are part of the high-resolution images but are too small to be resolved in the coarser resolution images. Decreasing the resolution, therefore, affects the recognition of the areas around the water bodies and results in a smaller irrigated area. The most decisive reason is the structure and the complexity of shape of the agricultural fields in this area. The irrigated fields in the north of the scene are distributed spatially, separated by barren land, pastures or unmanaged land. This leads to low NDVI values at the coarser resolutions, which reduce the identified irrigated area. However, the NDVI is limited regarding the fast saturation in case of active vegetation and does not provide details about biomass or LAI [41]. The example in the USA shows the difficulties of greening along water-channels or the greening after small-scale precipitation events, which leads to higher NDVI-values and influences the irrigation mapping method. In contrast to the results in the USA and Sudan, the mapping results in China are very similar at all spatial resolutions. Large-scaled fields of similar sizes and a small share of fallow fields characterize the two large agricultural areas of the scene. They indicate that the farming system follows a central management scheme resulting in a low complexity of the shape of the fields. The regular pattern of the fields, the absence of fallow fields and the large size of the fields in combination result in constant NDVI values across the different spatial resolutions and, hence, scale-independent mapping results.

Besides the different behavior regarding the mapping result at a coarser spatial resolution in China compared to Sudan and the USA, the relation of the negative changes of mapped irrigated area and the LSI behaves in all three regions constantly. This means the negative areal change of irrigated area with resolution is explained by the LSI and shows that landscape metrics can also be used outside of the analysis of natural ecosystems in man-made patterns. The relations between negative areal change and LSI can be used as information about the considered region regarding an expected loss of mapped irrigated area at a coarser resolution derived by wide-swath medium-resolution satellites. A transferability is possible, since the study showed that the downscaled Sentinel-2 and original PROBA-V NDVI time series of the same spatial resolution and the same time period were practically identical despite the differences in sensor characteristics, measurement and sun angle. This demonstrates the stability of the overall approach and allows to link Sentinel-2- and PROBA-V-derived irrigation maps. The scaling relation builds a bridge between the medium-resolution sensors such as PROBA-V or the new Sentinel-3 mission and high-resolution sensors such as Sentinel-2.

The presented results identify three main driving forces on the extent of the irrigated area: (a) the spatial resolution, (b) the spatial distribution of the irrigated fields in the analyzed area and (c) the complexity of the shape of the connected irrigated fields. Changes in the spatial resolution influence the mapping results differently depending on the spatial distribution and the complexity of the shape of the irrigated fields in the analyzed area. Thus, the influence of the spatial resolution on the mapping results differs from landscape to landscape. The trend towards spatially and temporally high-resolution satellite data and high-performance computing offers opportunities to rethink existing methods of irrigation mapping considering local conditions such as the spatial distribution of fields and combine crop growth model results with derived information about the development of biomass and plant conditions.

5. Conclusions

Overall, it can be concluded that the mapping of irrigated area using an NDVI threshold approach highly depends on both the spatial distribution of irrigated fields and the spatial resolution of the observing sensor. The study demonstrates the potential of Sentinel-2 to open a new chapter of irrigation mapping by providing high-spatial-resolution NDVI time series with a temporal resolution of up to 2.5 days and can be applied as a transition from the historical irrigation mapping with wide-swath medium-resolution sensors such as VEGETATION, MODIS and AVHRR to an irrigation monitoring at a high temporal and spatial resolution. Further, the use of the landscape metrics shows the potential to estimate an expected accuracy of irrigation mapping derived by wide-swath medium-resolution satellites such as Sentinel-3. Landscape metrics can identify regions characterized by a high expected loss in irrigation mapping with coarser resolution. The information about the influence of spatial scale on irrigation mapping will increase the accuracy of the estimation of the actual amount of water that is withdrawn from the regional water resources and diverted regionally into the atmosphere by irrigation.

The next step should be the development of an automatically updated irrigation monitoring system which supplies the users up-to-date information about the state of irrigation in terms of location, area and type. Irrigation monitoring as input information in spatially distributed crop growth models will improve the model results regarding water flows. The comparison of the model results with time series of multispectral remote sensing observations, which document the development of the irrigated crops from seeding to harvest, will allow the traceability of irrigation management such as the used irrigation water by the crops, irrigation water loss through interception or soil evaporation and overall water use efficiency. A remote-sensing-based monitoring system of the described kind is the prerequisite for the improvement of irrigation management towards a less wasteful use of the precious water resources by the farmers and can be a strong instrument in negotiations regarding upstream–downstream water conflicts in large watersheds.

Author Contributions: Conceptualization, J.M. and W.M.; methodology, J.M. and W.M.; software, J.M.; formal analysis, J.M. and W.M.; data curation, J.M.; writing—original draft preparation, J.M.; writing—review and editing, J.M. and W.M.; visualization, J.M.; supervision, W.M. All authors have read and agreed to the published version of the manuscript.

Funding: This research was funded by the Bavarian Environment Agency (Landesamt für Umwelt, LfU) under the grant number 81-44214.9-89131/2017, 81-4421.9-89123/2017 and 81-4421.992819/2017, by the open access publication fund of the German Aerospace Center (DLR) and to a smaller part by AgRAIN, a project funded by the Federal Ministry of Education and Research (Bundesministerium für Bildung und Forschung, BMBF) under the grant number 01LZ1904A.

Data Availability Statement: The irrigation maps at different spatial scale produced in this study are available from the corresponding author upon reasonable request.

Acknowledgments: The authors would like to thank the Vista GmbH—Remote Sensing Applications in Geosciences for providing the processed Sentinel-2 data. We also gratefully acknowledge the anonymous reviewers and editors for constructive comments for improvement of the manuscript. The responsibility for the content of this publication lies with the authors.

Conflicts of Interest: The authors declare no conflict of interest. The funders had no role in the design of the study; in the collection, analyses or interpretation of data; in the writing of the manuscript, or in the decision to publish the results.

References

1. Mueller, N.D.; Gerber, J.S.; Johnston, M.; Ray, D.K.; Ramankutty, N.; Foley, J.A. Closing yield gaps through nutrient and water management. *Nature* **2012**, *490*, 254–257. [CrossRef]
2. Foley, J.A.; Ramankutty, N.; Brauman, K.A.; Cassidy, E.S.; Gerber, J.S.; Johnston, M.; Mueller, N.D.; O'Connell, C.; Ray, D.K.; West, P.C.; et al. Solutions for a cultivated planet. *Nature* **2011**, *478*, 337–342. [CrossRef]
3. FAO. *FAOSTAT*; Food and Agriculture Organization of the United Nations (FAO): Paris, France, 2016.
4. FAO. *Total Withdrawal by Sector*; Food and Agriculture Organization of the United Nations (FAO): Paris, France, 2014.

5. Neumann, K.; Stehfest, E.; Verburg, P.H.; Siebert, S.; Müller, C.; Veldkamp, T. Exploring global irrigation patterns: A multilevel modelling approach. *Agric. Syst.* **2011**, *104*, 703–713. [CrossRef]
6. Puy, A. Irrigated areas grow faster than the population. *Ecol. Appl.* **2018**, *28*, 1413–1419. [CrossRef] [PubMed]
7. Meier, J.; Zabel, F.; Mauser, W. A global approach to estimate irrigated areas—A comparison between different data and statistics. *Hydrol. Earth Syst. Sci.* **2018**, *22*, 1119–1133. [CrossRef]
8. Strzepek, K.; Boehlert, B. Competition for water for the food system. *Philos. Trans. R. Soc. London. Ser. B Biol. Sci.* **2010**, *365*, 2927–2940. [CrossRef] [PubMed]
9. Micklin, P. The Aral Sea Disaster. *Annu. Rev. Earth Planet. Sci.* **2007**, *35*, 47–72. [CrossRef]
10. Chen, L.; Ma, Z.-G.; Zhao, T.-B.; Li, Z.-H.; Li, Y.-P. Simulation of the regional climatic effect of irrigation over the Yellow River Basin. *Atmos. Ocean. Sci. Lett.* **2017**, *10*, 291–297. [CrossRef]
11. Udall, B.; Overpeck, J. The twenty-first century Colorado River hot drought and implications for the future. *Water Resour. Res.* **2017**, *53*, 2404–2418. [CrossRef]
12. Maupin, M.A.; Ivahnenko, T.; Bruce, B. Estimates of Water Use and Trends in the Colorado River Basin, Southwestern United States, 1985–2010. In *U.S. Geological Survey Scientific Investigations Report 2018-5049*; U.S. Geological Survey: Reston, VA, USA, 2018.
13. Ozdogan, M.; Yang, Y.; Allez, G.; Cervantes, C. Remote Sensing of Irrigated Agriculture: Opportunities and Challenges. *Remote Sens.* **2010**, *2*, 2274–2304. [CrossRef]
14. Ozdogan, M.; Gutman, G. A new methodology to map irrigated areas using multi-temporal MODIS and ancillary data: An application example in the continental US. *Remote Sens. Environ.* **2008**, *112*, 3520–3537. [CrossRef]
15. Ambika, A.K.; Wardlow, B.; Mishra, V. Remotely sensed high resolution irrigated area mapping in India for 2000 to 2015. *Sci. Data* **2016**, *3*, 160118. [CrossRef]
16. Jin, N.; Tao, B.; Ren, W.; Feng, M.; Sun, R.; He, L.; Zhuang, W.; Yu, Q. Mapping Irrigated and Rainfed Wheat Areas Using Multi-Temporal Satellite Data. *Remote Sens.* **2016**, *8*, 207. [CrossRef]
17. Salmon, J.M.; Friedl, M.A.; Frolking, S.; Wisser, D.; Douglas, E.M. Global rain-fed, irrigated, and paddy croplands: A new high resolution map derived from remote sensing, crop inventories and climate data. *Int. J. Appl. Earth Obs. Geoinf.* **2015**, *38*, 321–334. [CrossRef]
18. Thenkabail, P.S.; Biradar, C.M.; Noojipady, P.; Dheeravath, V.; Li, Y.; Velpuri, M.; Gumma, M.; Gangalakunta, O.R.P.; Turral, H.; Cai, X.; et al. Global irrigated area map (GIAM), derived from remote sensing, for the end of the last millennium. *Int. J. Remote Sens.* **2009**, *30*, 3679–3733. [CrossRef]
19. Cammalleri, C.; Anderson, M.C.; Gao, F.; Hain, C.R.; Kustas, W.P. Mapping daily evapotranspiration at field scales over rainfed and irrigated agricultural areas using remote sensing data fusion. *Agric. For. Meteorol.* **2014**, *186*, 1–11. [CrossRef]
20. Abuzar, M.; McAllister, A.; Whitfield, D. Mapping Irrigated Farmlands Using Vegetation and Thermal Thresholds Derived from Landsat and ASTER Data in an Irrigation District of Australia. *Photogramm. Eng. Remote Sens.* **2015**, *81*, 229–238.
21. Lawston, P.M.; Santanello, J.A.; Kumar, S.V. Irrigation Signals Detected From SMAP Soil Moisture Retrievals. *Geophys. Res. Lett.* **2017**, *44*, 860–867. [CrossRef]
22. Puy, A.; Sheikholeslami, R.; Gupta, H.V.; Hall, J.W.; Lankford, B.; Lo Piano, S.; Meier, J.; Pappenberger, F.; Porporato, A.; Vico, G.; et al. The delusive accuracy of global irrigation water withdrawal estimates. *Nat. Commun.* **2022**, *13*, 3183. [CrossRef]
23. Puy, A.; Lankford, B.; Meier, J.; van der Kooij, S.; Saltelli, A. Large variations in global irrigation withdrawals caused by uncertain irrigation efficiencies. *Environ. Res. Lett.* **2022**, *17*, 044014. [CrossRef]
24. Velpuri, N.M.; Thenkabail, P.S.; Gumma, M.K.; Biradar, C.; Dheeravath, V.; Noojipady, P.; Yuanjie, L. Influence of Resolution in Irrigated Area Mapping and Area Estimation. *Photogramm. Eng. Remote Sens.* **2009**, *75*, 1383–1395. [CrossRef]
25. Ferrant, S.; Selles, A.; Le Page, M.; Herrault, P.-A.; Pelletier, C.; Al-Bitar, A.; Mermoz, S.; Gascoin, S.; Bouvet, A.; Saqalli, M.; et al. Detection of Irrigated Crops from Sentinel-1 and Sentinel-2 Data to Estimate Seasonal Groundwater Use in South India. *Remote Sens.* **2017**, *9*, 1119. [CrossRef]
26. Sharma, A.K.; Hubert-Moy, L.; Buvaneshwari, S.; Sekhar, M.; Ruiz, L.; Bandyopadhyay, S.; Corgne, S. Irrigation History Estimation Using Multitemporal Landsat Satellite Images: Application to an Intensive Groundwater Irrigated Agricultural Watershed in India. *Remote Sens.* **2018**, *10*, 893. [CrossRef]
27. Demarez, V.; Helen, F.; Marais-Sicre, C.; Baup, F. In-Season Mapping of Irrigated Crops Using Landsat 8 and Sentinel-1 Time Series. *Remote Sens.* **2019**, *11*, 118. [CrossRef]
28. Patton, D.R. A Diversity Index for Quantifying Habitat "Edge". *Wildl. Soc. Bull.* **1975**, *3*, 171–173.
29. Hargis, C.D.; Bissonette, J.A.; David, J.L. The behavior of landscape metrics commonly used in the study of habitat fragmentation. *Landsc. Ecol.* **1998**, *13*, 167–186. [CrossRef]
30. Bogaert, J.; Van Hecke, P.; Salvador-Van Eysenrode, D.; Impens, I. Quantifying habitat edge for nature reserve design. *Coenoses* **1998**, *13*, 131–136.
31. Wang, X.; Blanchet, F.G.; Koper, N.; Tatem, A. Measuring habitat fragmentation: An evaluation of landscape pattern metrics. *Methods Ecol. Evol.* **2014**, *5*, 634–646. [CrossRef]
32. Nowosad, J.; Stepinski, T.F. Information theory as a consistent framework for quantification and classification of landscape patterns. *Landsc. Ecol.* **2019**, *34*, 2091–2101. [CrossRef]
33. Zabel, F.; Putzenlechner, B.; Mauser, W. Global agricultural land resources—A high resolution suitability evaluation and its perspectives until 2100 under climate change conditions. *PLoS ONE* **2014**, *9*, e107522. [CrossRef]

34. Hersbach, H.; Bell, B.; Berrisford, P.; Hirahara, S.; Horányi, A.; Muñoz-Sabater, J.; Nicolas, J.; Peubey, C.; Radu, R.; Schepers, D.; et al. The ERA5 global reanalysis. *Q. J. R. Meteorol. Soc.* **2020**, *146*, 1999–2049. [CrossRef]
35. Fritz, S.; See, L.; McCallum, I.; You, L.; Bun, A.; Moltchanova, E.; Duerauer, M.; Albrecht, F.; Schill, C.; Perger, C.; et al. Mapping global cropland and field size. *Glob. Chang. Biol.* **2015**, *21*, 1980–1992. [CrossRef] [PubMed]
36. Monfreda, C.; Ramankutty, N.; Foley, J. Farming the planet: 2. Geographic distribution of crop areas, yields, physiological types, and net primary production in the year 2000. *Glob. Biogeochem. Cycles* **2008**, *22*. [CrossRef]
37. Sterckx, S.; Benhadj, I.; Duhoux, G.; Livens, S.; Dierckx, W.; Goor, E.; Adriaensen, S.; Heyns, W.; Van Hoof, K.; Strackx, G.; et al. The PROBA-V mission: Image processing and calibration. *Int. J. Remote Sens.* **2014**, *35*, 2565–2588. [CrossRef]
38. Santandrea, S.; Mellab, K.; Vrancken, D.; Versluys, J. The PROBA-V mission: The space segment AU—Francois, Michael. *Int. J. Remote Sens.* **2014**, *35*, 2548–2564. [CrossRef]
39. Verhoef, W.; Bach, H. Simulation of hyperspectral and directional radiance images using coupled biophysical and atmospheric radiative transfer models. *Remote Sens. Environ.* **2003**, *87*, 23–41. [CrossRef]
40. Hesselbarth, M.H.K.; Sciaini, M.; With, K.A.; Wiegand, K.; Nowosad, J. landscapemetrics: An open-source R tool to calculate landscape metrics. *Ecography* **2019**, *42*, 1648–1657. [CrossRef]
41. Viña, A.; Gitelson, A.A.; Nguy-Robertson, A.L.; Peng, Y. Comparison of different vegetation indices for the remote assessment of green leaf area index of crops. *Remote Sens. Environ.* **2011**, *115*, 3468–3478. [CrossRef]

PUBLICATION 3

Meier, J.; Mauser, W.; Hank, T.; Bach, H. (2020): Assessments on the impact of high-resolution-sensor pixel sizes for common agricultural policy and smart farming services in European regions. *Computers and Electronics in Agriculture*, *169*, 105205, https://doi.org/10.1016/j.compag.2019.105205.

Computers and Electronics in Agriculture 169 (2020) 105205

Contents lists available at ScienceDirect

Computers and Electronics in Agriculture

journal homepage: www.elsevier.com/locate/compag

Assessments on the impact of high-resolution-sensor pixel sizes for common agricultural policy and smart farming services in European regions

Jonas Meier[a,*], Wolfram Mauser[a], Tobias Hank[a], Heike Bach[b]

[a] Dept. of Geography, Ludwig-Maximilians-Universität Munich, Germany
[b] VISTA GmbH – Remote Sensing Applications in Geosciences Munich, Germany

ARTICLE INFO

Keywords:
Smart farming
COPERNICUS
Sentinel-2
Spatial resolution
Field sizes

ABSTRACT

High-resolution (5–50 m) remote sensing satellite sensors provide a reliable, free and open data infrastructure for public and private agriculture and land use services. The further market penetration of these services critically depends on the fraction of agricultural fields and area that the services can cover. EU's Common Agricultural Policy (CAP) and smart farming services require a minimum of spectrally pure measurements per agricultural field. The impact of pixel size on the coverage of agriculture is studied in this paper considering present free and open optical sensors (Sentinel-2 and LANDSAT). It further studies the implications of the selection of spatial resolution of planned extensions of these sensors, i.e. the next generation of Sentinel-2, as well as Copernicus's hyperspectral CHIME and thermal LSTM future candidate missions.

The paper analyzes the 2018 vector boundaries and crop types of 3.6 million agricultural fields in the German States of Bavaria and Lower Saxony and the Netherlands. The fields were rasterized using Sentinel-2 flight geometry and a pixel spacing of 5, 10, 20, 30 and 50 m. The study specifically considered: (1) fields with no pure pixel inside where no CAP services can be provided and (2) fields with less than 50 pure pixels inside, which is estimated to be the critical number for site-specific smart farming. The percentage of agricultural fields and agricultural area was determined for the main crop types. It shows, that with 10 m pixel spacing 2–4% and 20 m pixel spacing 12–22% of the agricultural fields in the study area do not contain a single pure spectral sample (Sentinel-2 case). This fraction decreases to 1–3% at 5 m spacing and increases to 25–40% for 30 m (LANDSAT and CHIME) and 50–70% for 50 m (LSTM) spacing. The percentage of fields with less than 50 pure pixels is 20–50% at 10 m and 70–85% at 20 m spacing (Sentinel-2). This fraction decreases to 5–12% for 5 m spacing and reaches the level of 92–97% for 30 m (LANDSAT) and 99% for 50 m spacing (LSTM). Our analysis shows, that with a pixel spacing of 5 m the Sentinel-2-based site-specific smart farming services could increase their potential customer base from ~50% to ~90% of the agricultural fields and could potentially cover 99% of the regions' agricultural area. A 20 m pixel spacing would increase the agriculture area from 23% to 56% in the Central and Western European study regions on which the Copernicus hyperspectral candidate mission CHIME is capable to measure pure and full spectra for highly advanced future site-specific management services. LSTM would also profit from a spatial resolution of 30 m, which would raise coverage of the agricultural area in Central Europe with pure thermal measurements from 3% at 50 m to 23% at 30 m.

1. Introduction

Approximately 12% of the global land surface is managed farmland (grassland and cropland) and subject to high temporal dynamics through annual, inter-annual and perennial variations in crop type and areal extent (Faostat, 2019). Managed farmland, contrary to unmanaged nature, is spatially organized as fields. Field size varies considerably depending on the level of mechanization of agriculture and on the economic, cultural and geographic background (Lesiv et al., 2019; Fritz et al., 2015; Graesser and Ramankutty, 2017). In general, crop management actions like plowing, seeding, fertilizing and harvesting are practiced on an agricultural management unit, which we denote a field. A so-defined field is independent of a cadastral property unit. In Central and Western Europe each field in general carries one crop at a time and is managed by one farmer. Using the information contained in spectral measurements of agricultural fields e.g. through the Copernicus Sentinel-2 satellites, to improve farm management is among the most promising and economically as well as environmentally important

* Corresponding author.
E-mail address: jonas.meier@lmu.de (J. Meier).

https://doi.org/10.1016/j.compag.2019.105205
Received 29 October 2019; Received in revised form 19 December 2019; Accepted 29 December 2019
Available online 13 January 2020

applications of land surface remote sensing. Time series of satellite images at a spatial resolution, which enables to recover information of and within a field, allow monitoring important crop parameters like crop type, plant growth and health, phenology and yield formation. In-field, site-specific agricultural management in the context of smart farming promises large commercial and environmental benefits by improving resource efficiency and minimizing environmental impacts (Wolfert et al., 2017; Walter et al., 2017).

The practical usefulness on remotes sensing data for digital services for agriculture depends on its spatial, spectral and temporal resolution (Hank et al., 2018). This paper focuses on the assessment of the role of pixel spacing for the coverage of agricultural fields and area with special emphasis on high-resolution 5–50 m Earth observation sensors. We chose this resolution segment for our study in favor of the available ultra-high resolution of 0.5–5 m because it provides a reliable, free and open public data infrastructure, which will emerge into the future with candidate satellites for a hyperspectral and thermal coverage of the Earth surface. Pixel spacing of remote sensing data results from a trade-off between a number of system parameters. Among those are, most importantly, the spatial resolution of the instrument expressed by the modulation transfer function (MTF) of the optical system, the sensor (sensitivity, signal-to-noise ratio (SNR), spectral resolution) and the electronics, the on-board storage capacity and/or the transmission bandwidth in combination with the chosen orbit and revisit time. Pixel spacing can also be chosen during the processing of raw sensor data into the defined final data-products. Pixel spacing determines the data quality (SNR), the data volume and handling costs and the loss or gain of valuable information on agricultural fields and their spatial heterogeneity. Therefore, being aware of the difference of concepts of pixel spacing and spatial resolution, in the following text we assume that pixel spacing of a real world space borne sensor closely resembles its spatial resolution, which is also the well-introduced term in almost all documentations of Earth observation sensors. Therefore, we further use the term spatial resolution synonymously with pixel spacing. Decreasing spatial resolution increases the fraction of mixed pixels in a field and below a certain ratio of a field to pixel size, no pure pixel can be identified. At least one pure spectral measurement should be available to determine crop type, which is a monitoring requirement of the EU's Common Agricultural Policy (CAP) , from a time series of spectral measurements (Skogstad and Verdun, 2009; European Commission, 2019). The ability to resolve in-field heterogeneity of crop growth is the prerequisite for satellite-based remote sensing to contribute to site-specific field management in the context of smart farming. Site specific smart farming uses understanding of in-field spatial heterogeneity of crop growth conditions (e.g. soil fertility, ground water level, relief and its influence on erodability and climate) and their influence on crop growth and yield in combination with advanced farming machinery to optimize resource use (fertilizer, pesticides, irrigation water) and minimize cost and environmental impacts. Site specific smart farming usually divides a field into management zones for which different management options are chosen. Different strategies are available to optimize results. They range from gradually intensifying to extensifying the less fertile parts of a field depending on situation and aim. For the management options to be successful the spatial resolution should of the spectral samples should be at a fraction of the sizes of the considered agricultural field to be able to fully quantify the in-field heterogeneity.

Current generation Sentinel-2 delivers multispectral images in 13 bands with a spatial resolution of 10 m in the VIS/NIR bands, 20 m in the NIR/SWIR bands and 60 m in the atmosphere bands (ESA, 2015). For next-generation Sentinel-2 satellites, an increase in spatial resolution of the VIS to SWIR bands to 5–10 m is considered (European Commission, 2016). In addition, ESA currently conducts Phase A/B1 studies on the candidate Copernicus Hyperspectral Imaging Mission (CHIME) (Nieke and Rast, 2018) and the Land Surface Temperature Mission (LSTM) (Koetz et al., 2018). Here mission requirements regarding spatial resolution between 20 and 30 m for CHIME and between 30 and 50 m for LSTM are discussed.

Market penetration of Copernicus based remote sensing services in a region is limited by spatial resolution. Copernicus-based agricultural services are usually contracted on a field basis and paid per hectare. Empirical evidence on these real-world limits of different high-resolution sensors must therefore determine both all agricultural fields and the complete agricultural area affected by mixed pixels with varying spatial resolutions. This assessment is not straight forward. It has to take into account the field size distribution, the ratio of the field to pixel size as well as the shape of the fields. EU's "Land Parcel Identification System" (LPIS) as part of the "Integrated Administration- and Control System" (IACS) is the basis for EU-subsidies to farmers. Farmers annually report the crop type of all their subsidized agricultural fields. IACS-LPIS therefore contains all fields for which satellite-based services can potentially be offered to support CAP and site-specific smart farming. IACS-LPIS data of selected regions in Central and Western Europe is used in our study reported as agricultural parcels, containing field boundaries of single fields and their cultivated crops per year. We have chosen Central and Western Europe test regions because they are among the most productive agricultural areas on the globe, have a diverse agricultural structure and because their agricultural services, which depend on EU's Copernicus Sentinel data, dynamically emerge.

This paper evaluates the impact of spatial resolutions ranging from 5 m (possibly improved future Sentinel-2), 10 m (current Sentinel-2, VIS-NIR), 20 m (current Sentinel-2 NIR-SWIR and upper CHIME specification), 30 m (LANDSAT, lower CHIME and upper LSTM specification) and 50 m (lower LSTM specification) on the coverage of agricultural fields for digital agriculture services in Central and Western Europe. We use as indicators the fraction of fields and the affected area in the selected Central and Western European study areas, which at a selected spatial resolution (1) have to be excluded from any remote sensing based agricultural services and (2) have to be excluded from in-field heterogeneity analysis due to a lack of pure pixels. The study covers three European regions: The German Free State of Bavaria and State of Lower Saxony in Central Europe and the Netherlands in Western Europe. The three regions represent different cultivated landscapes from large agricultural operations to small family owned part-time farms and therefore covers a large portion of the variety of Central and Western Europe's agriculture. Rather than using simulated field boundaries, the use of real-world field boundaries is needed to obtain unbiased and objective assessment results because of the complexities in field shapes, proportions of various shapes and sizes, adjacent fields' neighboring topology, and disturbances in field regularities caused by land surface features such as streams (Graesser and Ramankutty, 2017; Yan and Roy, 2014; Schmidt et al., 2016).

To our knowledge, this is the first time that field-wise agricultural coverage by different spatial resolutions of remote sensing instruments is investigated on a complete set of real-world subsidized fields for application in EU's common agricultural policy (CAP) as well as in site-specific farming in three Central European regions. To create these new scientific results, the paper relies on state-of-art geo-statistical methods. The challenge of aggregating spatial data into defined boundaries is well known and discussed since years under the "modifiable areal unit problem" (Gehlke and Biehl, 1934; Openshaw and Tylor, 1979; Openshaw, 1984). The problem also affects satellite images when the spectral reflectance measured in a pixel is composed of objects with different spectral properties (mixed pixel) (Löw and Duveiller, 2014). Several studies addressed the influence of spatial resolution on land use classifications derived from remote sensing data (Fisher et al., 2018; Pax-Lenney and Woodcock, 1997) or on estimated biophysical parameters like leaf nitrogen concentration (Zhou et al., 2018) or leaf area indices (Sprintsin et al., 2007). To find the most suitable spatial resolution these studies suggest to consider the local conditions, the topic of the research or service question and costs when choosing the appropriate spatial resolution (Atkinson, 1997).

2. Materials and methods

The study is based on data from the EU's "Integrated Administration- and Control System" (IACS). One element of the IACS is called the "Land Parcel Identification System" (LPIS), containing all agricultural plots in EU countries as georeferenced vector field boundaries together with information on cultivated crops. LPIS provides the field information in different types as "Agricultural parcel" (AP), "Farmer block" (FB), Physical block" (PB) and "Cadastral parcel" (CP) (Grandgirad and Zielinski, 2008). The following analysis is based on the LPIS type "Agricultural parcel", which means "a continuous area of land, declared by one farmer, which does not cover more than one single crop group […]. Member states may lay down additional criteria for further delimitation of an agricultural parcel." (European Union, 2013). The three regions provide crop specific data for each field. Since the European agrarian subsidies are based on this data and because field boundaries, as well as crops, are changing by growing season, the data is updated annually and carefully checked by regional agricultural authorities. We use 2018 data for this study because the data is available as "Agricultural parcels" for all three selected regions. They describe a field with one crop, which is independent on the cadastral situation. The regions 1) State of Lower Saxony (LS) (Lower Saxony Ministry of Food Agriculture and Consumer Protection, 2018), 2) Free State of Bavaria (BY) (Bavarian Bureau for Agriculture, 2018) in Germany and 3) the Netherlands (NL) (Ministerie van Economische Zaken - Rijksdienst voor Ondernemend Nederland) were selected (Fig. 1) based on (1) availability of data (IACS-LPIS-data usually is not publically available, in our case data from Netherlands (Basisregistratie Gewaspercelen BRP") and Lower Saxony ("Schlaege 2018") is publically available) and (2) a broad range for Central and Western European farming systems. The three study areas are similar in size (NL: 42,508 km^2, LS: 47,614 km^2, BY: 70,550 km^2, see Table 1) and fraction of agricultural land. Agriculture land use in the three selected regions is dominated by grassland and staple crops like maize, wheat, barley etc. as well as potatoes (see Fig. 2). The IACS-LPIS data contains more than 200 crop types. For a better comparison the crop types are aggregated to crop groups (see Fig. 2).

Table 1
Sizes of the land area, agriculture area and number and average sizes of fields in the analyzed regions derived from EU–IACS-LPIS data.

	Bavaria	Lower Saxony	Netherlands
Land Area Size	7.055 Mio. ha	4.761 Mio. ha	4.250 Mio. ha
Agriculture Area	3.173 Mio. ha	2.595 Mio. ha	1.880 Mio. ha
% Agricultural Area	44.97%	54.51%	44.24%
Number of Fields	1.9 Mio.	0.9 Mio.	0.7 Mio.
Ø Field Size	1.6 ha	2.8 ha	2.4 ha

Table 1 shows statistics of the IACS-LPIS data sets of the three study regions. Bavaria and the Netherlands have similar shares of agricultural land whereas in Lower Saxony the share of agricultural land is largest with more than 54%. With 1.6 ha the average field size is smallest in Bavaria pointing at a large share of small farms managed part-time as well as the influence of topography, which limits field sizes in some parts of the State. In Lower Saxony, the average field size is largest (2.8 ha) which is a consequence of larger commercial farms. Average field size in the Netherlands (2.4 ha) is between Bavaria and Lower Saxony.

2.1. Analysis approach

The vector field boundaries from the IACS-LPIS data sets were rasterized at 5, 10, 20, 30 and 50 m resolutions using the Sentinel-2 pixel locations and geometry. The conversion into pixel-based raster dataset

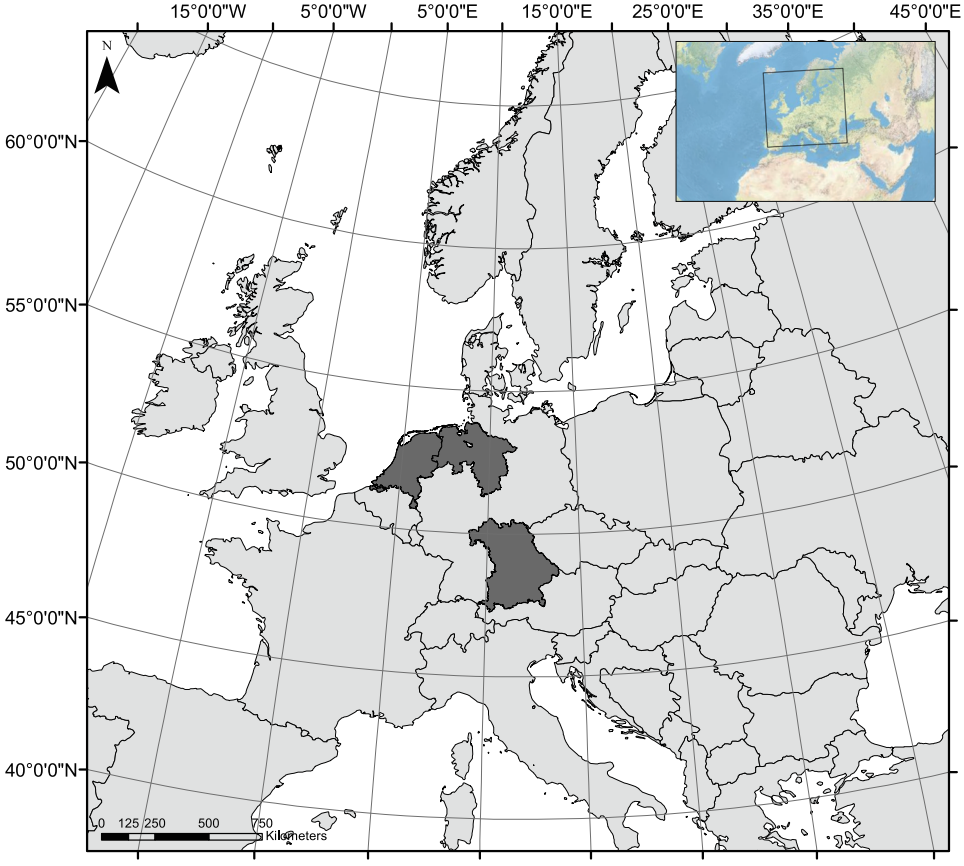

Fig. 1. Location of the three study regions in Central Europe in dark grey.

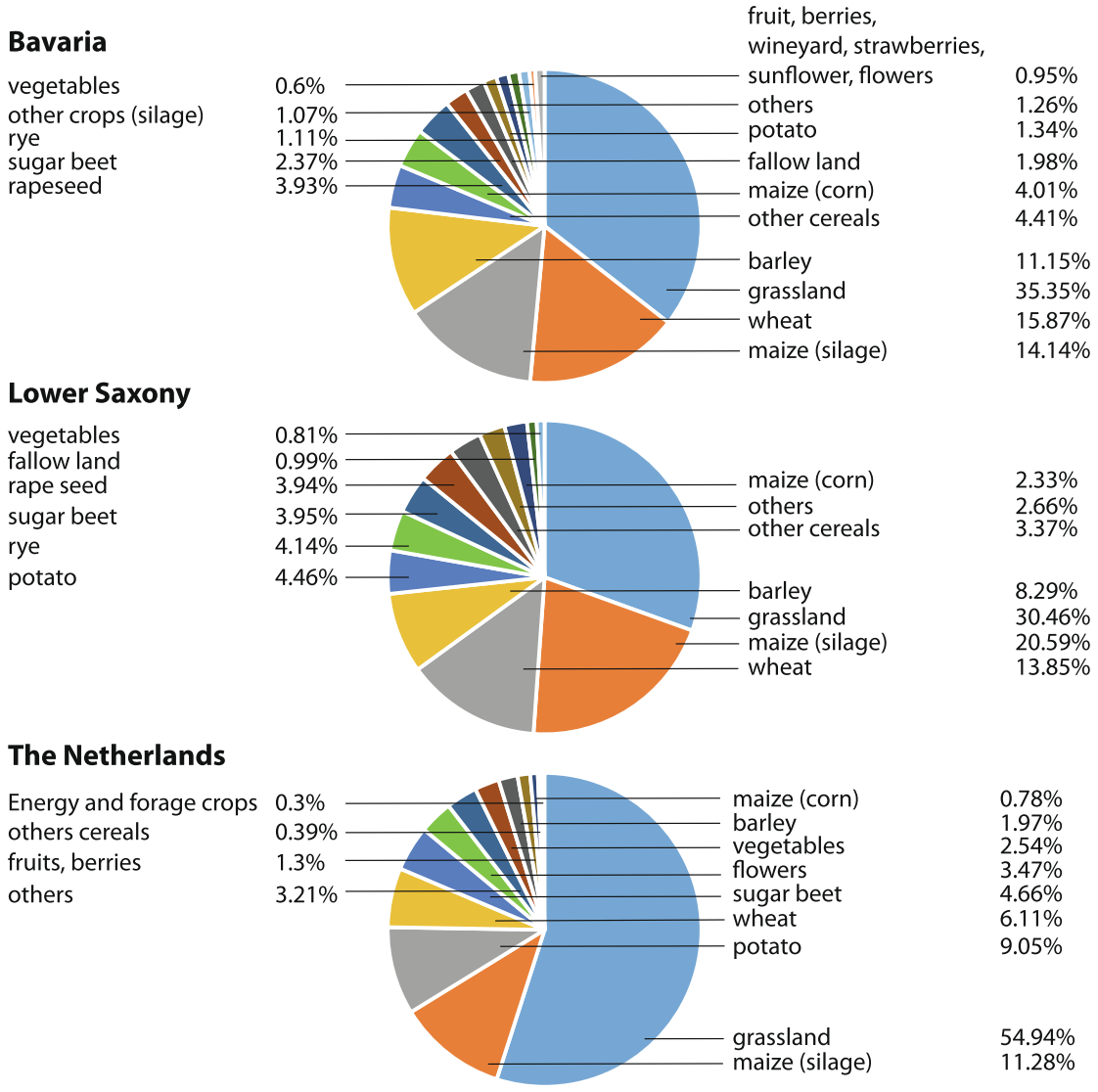

Fig. 2. Crop composition in the three study regions Bavaria, Lower Saxony, and the Netherlands in 2018 (Source: EU-IACS-LPIS).

is carried out using a modified Bresenham's line algorithm (Bresenham, 1965), which assumes the pixel center to be the valid pixel coordinate. This approach tends to increase the rasterized fields beyond the vector field boundaries by maximum half of the chosen resolution. The protrusion of the pixels beyond the field boundaries consequently leads to pixels containing a mix of the spectral reflection of the field crops and their surrounding area. To ensure pure agriculture pixels the vector field boundaries are shrunk before rasterization by half the size of the spatial resolution. Assuming square pixels, the reduction value is calculated via Eq. (1), which is based on the Pythagorean theorem:

$$\text{reduction value} = \sqrt{2 * \left(\frac{\text{resolution}}{2}\right)^2} \quad (1)$$

Fig. 3 shows an exemplary result of shrinking vector field boundaries to ensure that only pixels are rasterized, which completely lie within the vector field boundaries. The shrinking of the fields changes the shape of the original field boundary polygons and may lead to new island polygons. Small fields collapse depending on size and shape and do not include a valid pixel.

Fig. 4 shows the resulting difference between rasterization using the classical Bresenham's line algorithm based on the original polygons (center approach) and on the shrunken field boundaries (pure-pixel approach) where the whole pixels' area is located inside the vector field boundaries.

3. Results

The rasterization is carried out for each of the 3.5 million 2018 IACS-LPIS fields in the study regions and each selected spatial resolution of 5, 10, 20, 30 and 50 m pixel size. It results in five raster-data sets containing the spectrally pure pixels in each agricultural field at five different spatial resolutions. The number of pure pixels per field serves as parameter for the suitability of the selected spatial resolution to analyze crop type and in-field heterogeneities in the context of site-specific smart farming.

Fig. 5 shows an example cut-out of the rasterized pixels at the selected spatial resolutions. The lowest level in Fig. 5 shows the spatial resolution of 5 m (green) with reducing resolution to 10 m (blue), 20 m (orange) and 30 m (black) and 50 m (purple) in the following layers. The expected change in pixel size and pixel pattern can be seen in Fig. 5 as well as a considerable increase of white area not covered with pure pixels and some fields, which completely lose their pixels with decreasing spatial resolution. The approach clearly reduces the sampled

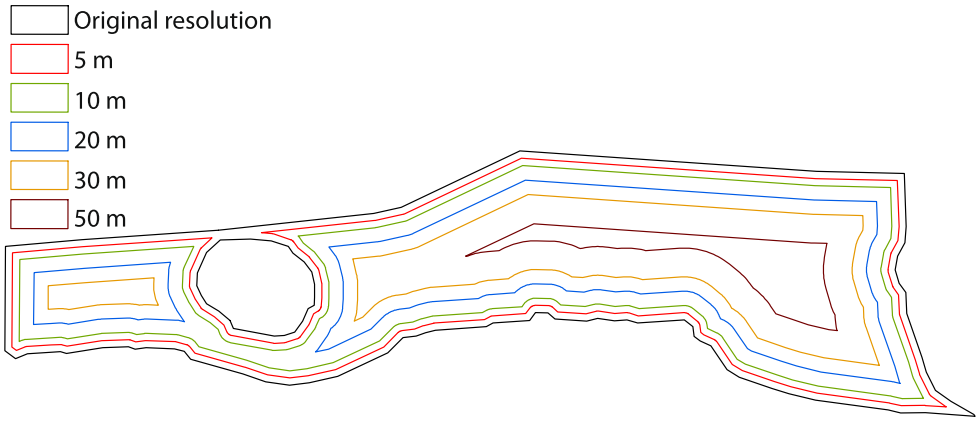

Fig. 3. Exemplary polygon to demonstrate the shrinking of the field boundaries to ensure that only pixels, which are completely within the vector field boundaries are rasterized. The figure shows the original shape of the field in black and the shrunken field boundaries depending on the spatial resolution. At 50 m raster resolution the polygon left from the gap disappears by the approach.

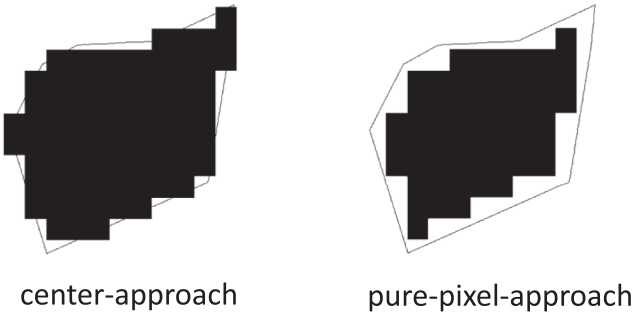

Fig. 4. Center-approach vs. pure-pixel-approach: Center-approach burns the pixel if the center of the pixel is inside the polygon and thereby increases the size of the field. The pure-pixel-approach burns the pixel only where the pixel is completely inside the field boundaries. This method results in "pure-field-pixel" but leads to a loss of covered field area.

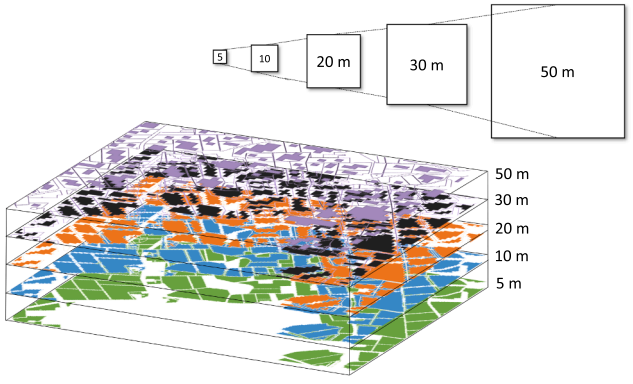

Fig. 5. Exemplarily the change of the field sizes and shapes at different spatial resolutions: 5 m (green), 10 m (blue), 20 m (orange), 30 m (black) and 50 m (purple). (For interpretation of the references to colour in this figure legend, the reader is referred to the web version of this article.)

area in a region because it eliminates all mixed pixels. The reduction of the total sampled agricultural area mainly depends on the field size distribution and the field shape.

Farmers manage fields. Of central importance are therefore (1) the number and total area of fields that are either not covered at all by a pure spectral measurement and (2) the number and total area of fields that contain less than a minimum number of pure pixels. As a consequence, spectral analysis is of limited use to determine crop type in case 1 or in-field spatial heterogeneity in case 2. Consequently, these fields are assumed to be lost to the respective scientific analysis and/or commercial service. Case 1 fields will further be denoted 'lost fields'. Case 2 is not straight forward and requires a threshold number of pixels below which field spatial heterogeneity cannot be determined in a meaningful way for site-specific smart farming. To our knowledge no literature-based general agreement exists on the number of pure samples in a field, which are required to enable site-specific smart farming as defined above. The number depends on the heterogeneity of the considered field as well as on the farming machinery used and management action applied (fertilization, plant protection, irrigation). Practical experience suggests that a minimum of 50 pure pixels per field is desired to determine a spatial distribution of crop growth conditions on which in-field site-specific management actions can be based in a meaningful way and so was selected for this assessment. This is based on the assumption that fields are divided into zones with similar growing conditions and management actions are defined for each zone. We assume that a meaningful division of a field is made up of at least three zones. In order to cluster three different zones in a field with any statistical significance a minimum sample size of 15–20 samples per zone is necessary. This results in a minimum number of ~50 pure spectral samples per field to develop site-specific smart farming services. Fields with an insufficient number of pure pixels for site-specific farming will further be denoted 'no site-specific farming'. Analysis based on thresholds of 1, 10, 20, 30 and 100 pixels are provided in the supplement (S8).

Fig. 6 shows the fractional histograms of pure pixels per field for the three test regions and the selected resolutions of 5, 10, 20, 30 and 50 m. The zero pixels per field column (blue) in the histograms represent the percentage of lost fields, the red line marks the threshold of 50 pure pixels below which a field is denoted 'no site-specific farming'.

Fig. 6 clearly shows the changing shape of the histograms with decreasing spatial resolution. At a resolution of 5 m the percentage of lost fields is small (< 3%) and the increasing pure pixel number classes tend to be equally populated for all three test regions. Percentages of lost fields sharply increase and the population of the classes becomes more right-skewed with decreasing resolution along the lines of the histogram matrix.

In addition to the results for the 'no site-specific farming' case results for fields with 1, 10, 20, 30 and 100 pure pixels are provided in the supplement (S8) together with the numerical values of the histograms (S5-S7). This enables further analysis with additional threshold values. The results show that the monotonously increasing fraction of fields that are lost to site-specific smart farming does not provide any intrinsic indicator for an optimum number of pure samples per field. Table 2 shows the percentage of 'lost fields' and 'no site-specific farming' fields and the related agricultural area in the three test regions as a function of spatial resolution.

As can be expected, Fig. 6 and Table 2A show, that the percentage of 'lost fields' and 'no site-specific farming' fields both increase with decreasing spatial resolution. Table 2A shows, that in all test regions only

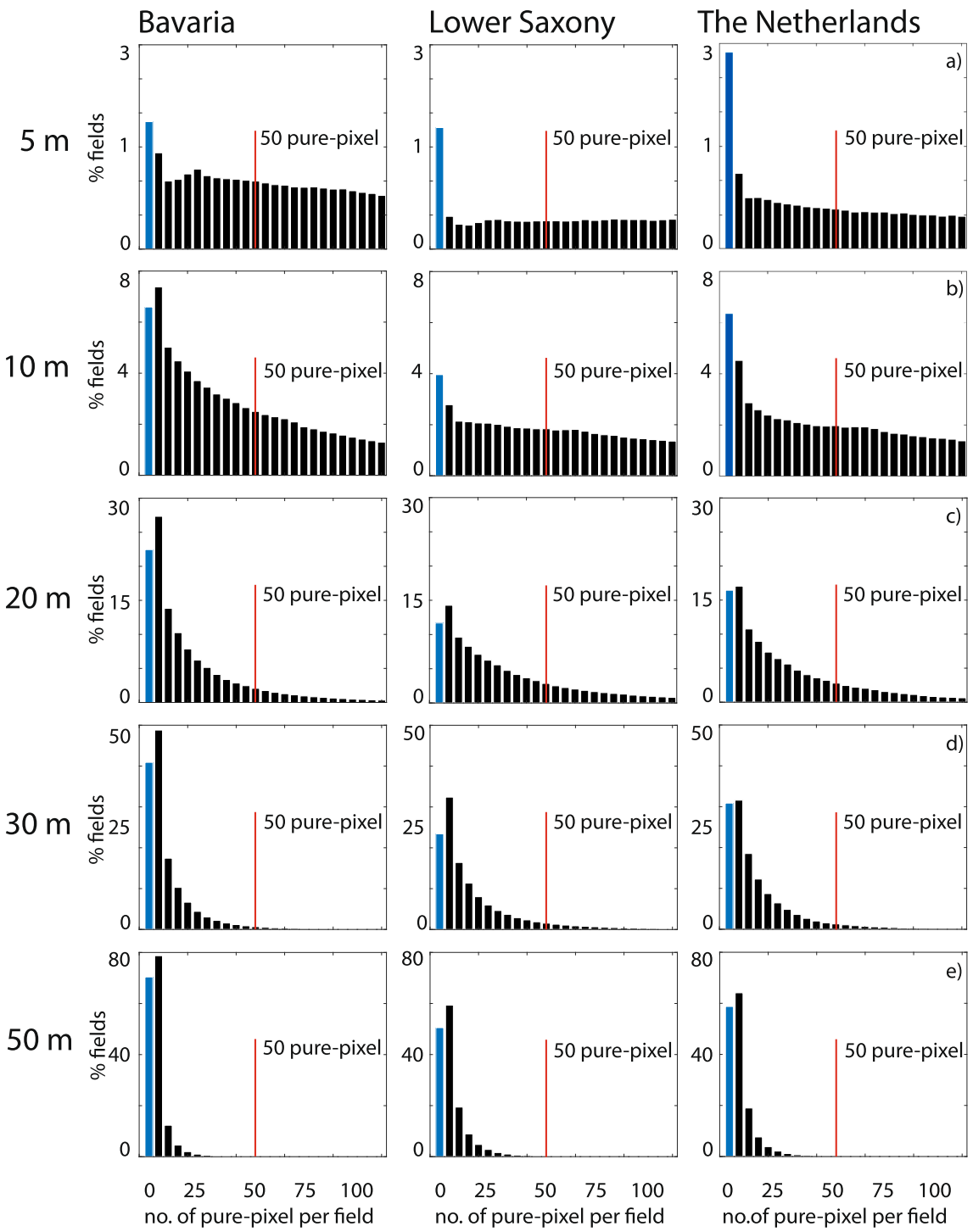

Fig. 6. Fractional histograms of the number of pure pixels per agricultural field for the three test regions Bavaria, Lower Saxony and the Netherlands (columns) and the selected rasterization resolutions of 5, 10, 20, 30 and 50 m (lines).

2–3% of all fields are lost to spectral analysis at a spatial resolution of 5 m. This percentage roughly doubles to around 5% at the 10 m resolution of the contemporary Sentinel-2 VIS-NIR bands. It further increases to 10–20% for the 20 m Sentinel-2 NIR-SWIR bands and the upper resolution of CHIME. 25–40% of all fields in the test regions are lost to a spectral analysis on at least one pure pixel at a spatial resolution of 30 m, which is today's LANDSAT, the lower proposed CHIME and upper proposed LSTM resolution. At LSTM's lower proposed resolution of 50 m, 50–70% are lost. The loss of fields with at least one pure pixel is largest in Bavaria with its compartmentalized agriculture and less severe in Lower Saxony with its large commercial farms. In the Netherlands, the effect lies between the two extremes.

Table 2A also shows the analysis of the percentages of fields that fall in the 'no site-specific farming' category. The general tendency is similar to the 'lost' fields although the level of rejection is considerably higher. 5–12% of the agricultural fields fall into the 'no site-specific farming' category at a spatial resolution of 5 m. This percentage increases to 22–50% at the current Sentinel-2 VIS-NIR spatial resolution of 10 m, further increases to a stunning 70–85% at the current Sentinel-2 NIR-SWIR and upper CHIME spatial resolution of 20 m. It reaches

Table 2
Percentage of (A) 'lost fields' (with no pure pixel inside) and 'no site-specific farming' fields (<50 pure pixels inside) and percentage of (B) agricultural area connected to the 'lost fields' and 'no site-specific farming' fields in (A) for each test region and selected spatial resolution.

A	Bavaria:		Lower Saxony:		Netherlands:	
	% lost fields (no pure pixel inside)	% no site-specific farming fields (< = 50 pure pixels inside)	% lost fields (no pure pixel inside)	% no site-specific farming fields (< = 50 pure pixels inside)	% lost fields (no pure pixel inside)	% no site-specific farming fields (< = 50 pure pixels inside)
5 m	1.69%	12.17%	1.78%	5.72%	2.87%	9.54%
10 m	6.41%	49.79%	3.96%	23.14%	6.36%	28.84%
20 m	22.27%	86.40%	11.67%	69.65%	16.43%	75.27%
30 m	40.73%	97.72%	23.40%	91.51%	30.86%	94.42%
50 m	70.22%	99.93%	50.52%	99.57%	58.76%	99.74%
B	Bavaria:		Lower Saxony:		Netherlands:	
	% area lost fields (no pure pixel inside)	% area no site-specific farming fields (< = 50 pure pixels inside)	% area lost fields (no pure pixel inside)	% area no site-specific farming fields (< = 50 pure pixels inside)	% area lost fields (no pure pixel inside)	% area no site-specific farming fields (< = 50 pure pixels inside)
5 m	0.08%	0.98%	0.12%	0.37%	0.21%	0.63%
10 m	0.49%	10.53%	0.29%	3.74%	0.51%	4.95%
20 m	3.58%	55.43%	1.58%	33.52%	2.34%	39.82%
30 m	10.82%	85.86%	4.86%	68.56%	7.61%	75.20%
50 m	33.91%	98.76%	18.88%	96.34%	25.35%	96.17%

92–98% for the current LANDSAT and discussed lower CHIME and upper LSTM resolution of 30 m and 99% for the discussed lower LSTM resolution of 50 m.

Table 2B shows the percentage area represented by the lost fields of Table 2A. In general, the fraction of the area is lower than the fraction of fields because small fields tend to get lost first. At the resolution of 10 m, the fields that are lost because they do not contain a single pure pixel is ~1% of the total agricultural area in all three regions. The lost area increases to 1–3% at 20 m, 5–10% at 30 m and to 19–34% at 50 m resolution.

The analysis of the agricultural area assumed lost for site-specific smart farming (<50 pure pixels inside) shows a different perspective. Here at 5 m resolution, the lost area is below 1%. This value increases to 4–10% at 10 m resolution. 20 and 30 m resolution show a strong increase of lost area to 33–55% (20 m) and 68–86% (30 m) respectively. At 50 m resolution, 96–99% of the area is lost to smart farming, which makes a resolution of 50 m unsuitable for site-specific farming services in the selected test regions in Western and Central Europe.

Field sizes and shapes may vary considerably depending on land use and crop selection. Specialty crops like wine, hops and vegetables, etc. tend to be cultivated on smaller fields with more intensive management and higher revenues per hectare. Staple crops like maize, cereals as well as potatoes and sugar beet, etc. tend to be cultivated on larger fields with more mechanization and smaller revenues per hectare. We therefore analyze the resolution dependent fraction of 'lost' and 'no site-specific farming' fields for the major agricultural crops in the selected regions. We exemplary present the results for Bavaria since it is the most compartmentalized of the chosen regions and may therefore serve as a lower baseline for estimating the potentials of different resolutions for high- resolution remote sensing based agriculture services (crop specific analyses of the Netherlands and Lower Saxony are attached in the supplement). Fig. 7a and b show the percentage of 'lost fields' and 'no site-specific farming' fields in Bavaria for different crop types as a function of spatial resolution.

In Fig. 7a and b, the position of the crop categories is ordered by the respective percent loss of fields. The colors of the bars represent different spatial resolutions. Fig. 7 shows that different crops are unequally affected by the reduction in the spatial resolution regarding the percentage of (a) lost fields as well as (b) no site-specific farming fields. Two categories can be distinguished. First staple crops like cereals and maize as well as sugar beet, which generally populate the left side of the graphs. They show relatively small percentages of both 'lost' and 'no site-specific farming' fields. Second specialty crops like wine, flowers fruits and vegetables, with higher percentages of 'lost' and 'no site-specific farming' fields, which tend to populate the right side of the graphs. Fig. 7 clearly shows that the current Sentinel-2 configuration allows field-based crop type identification for more than 90% of the staple crops in Central Europe. For about 20–40% of specialty crops, no identification is possible because of small field sizes. On the other hand, the 20 m NIR-SWIR spectral information of Sentinel-2 is insufficient to determine heterogeneity for site-specific agricultural services on approx. 60–80% of Central European fields (Fig. 7b). Specifically, for staple crops, the percentage of 'no site-specific farming' fields decrease considerably when moving to 10 and decisively when moving to 5 m spatial resolution.

Fig. 8a and b show the corresponding crop-specific agricultural area affected by the choice of resolution. Again, similar to the results show in Table 2B, Fig. 8a shows that the fractional agricultural area related to the lost fields is smaller than the fractional number of lost fields for all categories. Fig. 8 also confirms the distinction between crop categories found in Fig. 7: areal loss in staple crops is smaller for coarser resolutions than for specialty crops like wine, hops, vegetables, flowers or fruits.

Fig. 8b shows the lost area of the 'no site-specific farming fields' (<50 pure pixels). The results show that the 10 m resolution of the current Sentinel-2 fleet is able to cover about 80% of the crops area, the fraction of the specialty crops is lower, the fraction of the lost area of the staple crops lies under 10%. Decrease of spatial resolution of 20 m increases loss to about 40% at staple crops and a decrease to 30 m increases losses to 80%. At the spatial resolution of 50 m nearly no field of any crop is suitable for agricultural remote sensing services based on pure pixels.

Table 3 summarizes the three test regions to one overview result, which includes all three Central and Western European study regions. Columns 2 and 3 show the resulting fraction of fields, column 4 and 5 the fraction of agricultural area affected by the selected spatial resolution. Table 3 clearly shows that with a resolution of 5 m 90% and more fields and more than 99% of the agricultural area can be accessed with high-resolution satellite remote sensing systems even for sophisticated agricultural services. Current Sentinel-2 due to its limited spatial resolution cannot cover roughly half of the Western and Central European study sites' agricultural fields or a quarter of their agricultural area with site-specific smart farming services. At the spatial resolution of 30 m or even of 50 m, more than 90% of the fields and roughly 85%

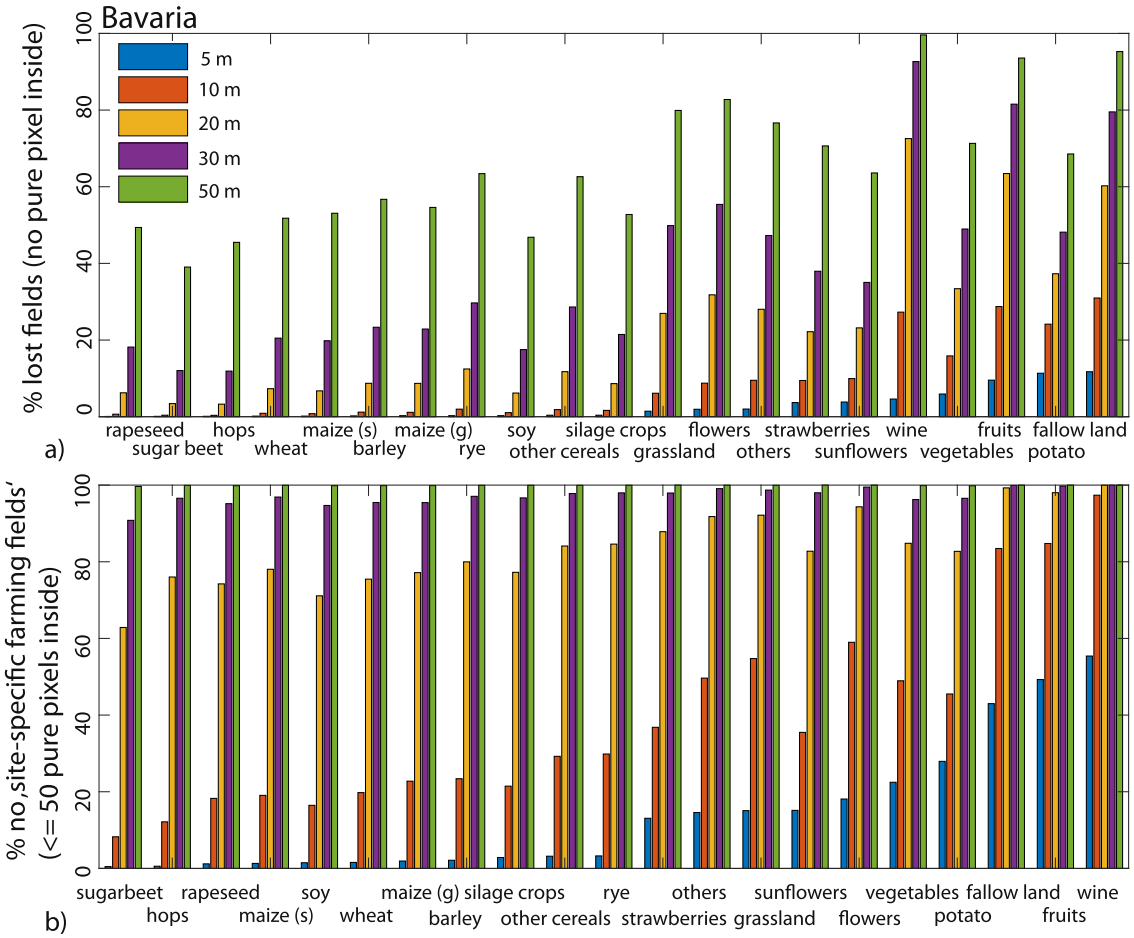

Fig. 7. Percentage of (a) 'lost fields' and (b) 'no site-specific farming' fields of different crop types in Bavaria for the selected rasterization resolutions of 5, 10, 20, 30 and 50 m. Maize (s) = silage maize, maize (g) = maize grain, silage crops = silage crops without maize.

of the area are lost to site-specific smart farming services. Nevertheless, it should be stated that the fraction of fields and related area on which time series of images can be used to identify crops on one pure pixel is much larger making resolutions of 30 m and above much more suitable for EU-CAP monitoring purposes.

4. Discussion

The impact of pixel spacing / spatial resolution of existing and anticipated space borne sensors on the potential coverage of agriculture with EU's Common Agricultural Policy (CAP) and site specific smart farming related remote sensing services was analyzed in a real-world scenario. We used the 2018 vector field boundaries and crop types of 3.5 million fields (management units) in the German States of Bavaria and Lower Saxony and the Netherlands. We determined, for spatial resolutions of 5, 10, 20, 30 and 50 m, the fraction of fields with (1) no pure pixel and (2) less than 50 pure pixels. We assume case 1 fields excluded from CAP-related and case 2 fields excluded from site-specific smart farming remote sensing services. The composition of the analyzed fields is representative for large parts of Western and Central Europe's agriculture. Nevertheless, we want to point out that there are regions within EU with smaller (e.g. Romania, Southern Poland, northwest Spain) and larger (e.g. Hungary, Czech Republic, South Spain, East Germany) average field sizes (Kuemmerle et al., 2013).

The spatial resolution range from 5 to 50 m represents the global present and future land surface Earth Observation free and open data infrastructure. It covers both existing systems like Sentinel-2 and LANDSAT and anticipated systems like the future generation Sentinel-2 as well as the Copernicus hyperspectral CHIME and thermal LSTM candidate missions. Their data will operationally be available with dense temporal coverage for a foreseeable future and therefore is ideally suited to develop the science behind operational agricultural services for public and private users. Ultra-high resolution space borne sensors, which offer data at spatial resolutions of the order of 1 m on a commercial basis currently lack the long term operational commitment as well as the combined spectral and temporal coverage to base e.g. site-specific smart services on their data. A spatial resolution of the order of 1 m is also an order of magnitude larger than the swath width of the usual agricultural machinery, which is 10 m. Sensors, which offer this resolution therefore often over perform when it comes to site-specific smart farming services.

The analysis of the loss of coverage of agricultural fields and their related area with spatial resolution was carried out for the major staple and specialty crops on all agricultural fields in the selected regions subsidized by EU. This gives insight into the relation of crop-specific analyses, which are important because from an application point of view it makes a difference whether fields with highly-valued crops (e.g. specialty crops like wine, hops, vegetables) or lower-valued staple crops (e.g. maize, cereals) and potato are lost. The first category produces more revenue per hectare and therefore tends to be managed more intensively. In this category, the overall economic impact of improvements of crop management (water saving in irrigation, more efficient fertilization, early detection of pests, etc.) with agricultural remote sensing services is potentially higher. On the other hand, staple crops generally cover much larger areas and therefore, potentially, site-specific agricultural management based on agricultural services can improve efficiency and achieve positive environmental impact on much larger areas.

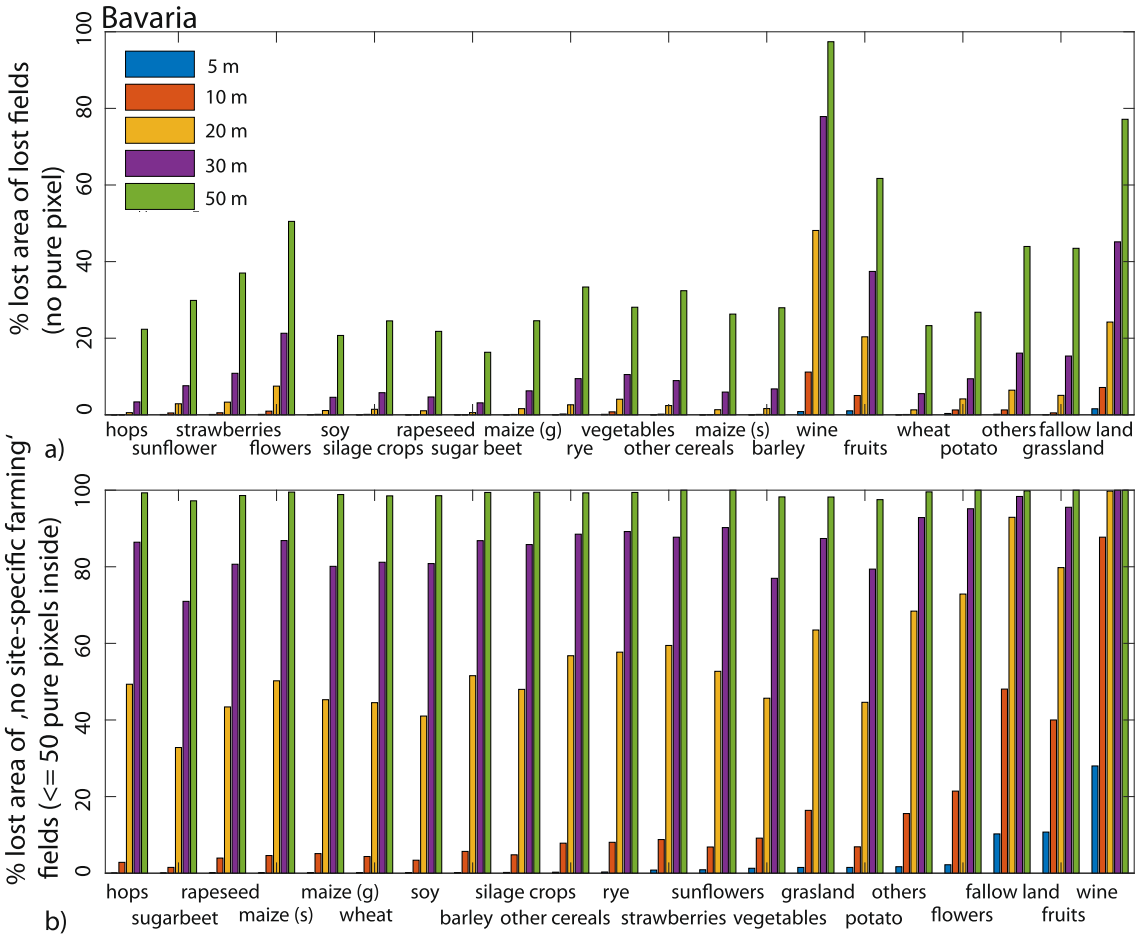

Fig. 8. Percentage of (a) 'area of lost fields' and (b) 'area of no site-specific farming' fields of different crop types in Bavaria for the selected rasterization resolutions of 5, 10, 20, 30 and 50 m. Maize(s) = silage maize, maize(g) = maize grain, silage crops = silage crops without maize.

Table 3
Percentage of 'lost fields' (with no pure pixel inside) and 'no site-specific farming' fields (<50 pure pixels inside) for all regions analyzed.

	All regions:			
	% lost fields (no pure pixel inside)	% no site-specific farming fields (< = 50 pure pixels inside)	% area lost fields (no pure pixel inside)	% area no site-specific farming fields (< = 50 pure pixels inside)
5 m	1.79%	10.02%	0.13%	0.69%
10 m	5.79%	37.75%	0.43%	6.85%
20 m	18.40%	79.89%	2.60%	44.16%
30 m	34.34%	95.48%	8.01%	77.37%
50 m	62.90%	99.80%	26.70%	97.30%

We found, as can be expected, a strong decrease of loss of coverage of fields and the related area with increasing spatial resolution. Since there are more small fields than large fields, the decrease in loss of coverage is more pronounced for the number of fields than for their related area. At the lowest resolution of 50 m ~ 60% of the fields and 25% of the agricultural area do not contain a single pure pixel. This resolution also does not allow to derive site-specific smart farming services in all three test regions. The situation becomes slightly less serious with the current LANDSAT and lower CHIME and upper LSTM candidate Missions' resolution of 30 m. The fraction of analyzed fields, which do not contain a single pure spectral measurement, decreases to from ~60 to 35% with 8% of the area lost. With the spatial resolution of today's Sentinel-2 sensors still a notable fraction of 18% (at 20 m) and 6% (at 10 m) of the fields and 2.6% (at 20 m) and 0.4% (at 10 m) of the related agricultural area are still too small to contain at least a single pure pixel. As a conclusion, with the spatial resolution of current Sentinel-2-time series reliable quantitative image analysis like crop type specification to serve EU's CAP is not possible for roughly every 5th analyzed field. An increase of spatial resolution to 5 m would in turn allow finding at least one pure pixel in almost all analyzed fields.

Since the criterion for a field to be accessible for site-specific smart farming services was defined to be at least 50 pure pixels it can generally be expected that both a larger fraction of fields and a larger area is lost for site-specific smart farming services. With resolutions of 30 m and below only the 5% largest fields, which cover 20% of the area, are accessible for these services. This, together with the low temporal revisit frequency explains why LANDSAT data is not suitable for developing smart farming services for the analyzed fields. Sophisticated site-specific agricultural services like the provision of spatial chlorophyll distributions within a field go beyond simple computation of NDVI. They rely on the complete set of all Sentinel-2's 10 and 20 m resolution VIS-SWIR bands. They depend on some sort of resolution merge between 10 m VIS/NIR bands and 20 m NIR/SWIR bands which inevitably degrades the spatial resolution of the merged pixels to somewhere between 10 and 20 m. At the 20 m resolution the fraction of fields, which are potentially accessible with site specific smart farming services is 20% and the covered area is 66%. On the other hand, a spatial resolution of equal or better than 10 m completely changes the situation. Site-specific smart farming services can then potentially be made available ~2/3rd of the analyzed fields and for more than 93% of the related agricultural area. Most importantly, at this resolution staple crops in the selected European regions would almost completely be covered.

Finally, with a resolution of 5 m 90% of the analyzed fields, which cover more than 99% of the agricultural area in the selected regions contain more than 50 pure pixels and are therefore accessible for site-specific smart farming services. A major part of the specialty crops would then also be covered. With a spatial resolution of 5 m in all bands and the current spectral coverage and revisit time a future 2nd generation Sentinel-2 would allow developing site-specific smart farming services for almost all farmers in the selected European study regions. It would make next Sentinel-2 s the information backbone necessary for smart farming to completely cover Europe's agriculture and to realize the environmental and commercial benefits, that potentially go along with it.

CHIME in its upper resolution of 20 m would enable to use high-valued, pure and complete spectral information to develop new sophisticated Copernicus based agricultural services, that go far beyond current smart farming approaches, on 1/3rd of all fields and 55% of the agricultural area in the selected European study regions. These numbers are reduced to well below 10% of fields and 23% of the area when choosing CHIME's lower resolution of 30 m which is equivalent to that of the existing and upcoming hyperspectral missions PRISMA (Labate et al., 2009) and EnMAP (Guanter et al., 2015). Although the pivotal role that CHIME will potentially play for developing advanced next-generation site-specific agricultural services is not questioned by this choice in resolution, an increase beyond the spatial resolution of existing and upcoming hyperspectral missions would be a decisive difference for both science and application and an important success-factor for CHIME. It strongly enlarges both the number of accessible crops and fields and as a result accelerates the transition towards next-generation site-specific farming. LSTM in its upper resolution of 30 m has the same coverage in terms of fields and area than CHIME's lower resolution. Implementing LSTM's lower resolution of 50 m would increase the fractions of fields and covered area for which no sufficient unmixed thermal information on in-field heterogeneity can be measured for the analyzed fields to 58–70% and 99% respectively. That means that only a few very large fields would be accessible.

5. Conclusion

Any increase in spatial resolution extends both the customer base and the accessible acreage for Copernicus-based CAP as well as site-specific agricultural services in Central Europe. The effect is most pronounced between a resolution of 20 and 5 m for the number of fields because it allows tapping into a large number of specialty fields. The increase in covered acreage is most pronounced between 20 and 10 m because it allows extending services to cover almost all non-specialty crop fields in Central Europe. This is an essential step in commercial terms because it would provide small farmers with the information to catch up in raising the efficiency of fertilizer, pesticide and irrigation water use. It also touches social aspects in providing to a large base of small part-time Central European farmers the basic information needed for fully digitized farm management, which eases their documentary and bureaucratic burdens thereby supporting them in their struggle to survive and to play a positive role in protecting rural lifestyles. The benefit of a resolution increase of Sentinel-2 for central European agriculture applications goes far beyond economic and social terms. It also is an essential step in environmental terms because it provides a cost-efficient path to site-specific, optimized fertilizer application on many small fields, which currently contribute strongly to Central Europe's groundwater resources.

The current Sentinel-2 workhorses have already proven the usefulness and cost-effectiveness for site-specific agricultural services in Central Europe (Bach et al., 2018). The results of the study clearly show the added value in terms of coverage of an increase in spatial resolution from today's effective 10–20 m to ideally 5 m for all spectral bands on a future Sentinel-2 follow-up.

Funding

This research was funded by the Bavarian Environment Agency (Landesamt für Umwelt, LfU) under the grant number 81-44214.9-89131/2017, 81-4421.9-89123/2017 and 81-4421.992819/2017. The APC was funded by Ludwig-Maximilians-University Munich.

CRediT authorship contribution statement

Jonas Meier: Conceptualization, Methodology, Software, Validation, Formal analysis, Investigation, Data curation, Writing - original draft, Visualization. **Wolfram Mauser:** Conceptualization, Methodology, Writing - original draft, Resources, Supervision, Project administration, Funding acquisition. **Tobias Hank:** Conceptualization, Writing - review & editing, Supervision. **Heike Bach:** Conceptualization, Writing - review & editing, Supervision.

Declaration of Competing Interest

The authors declare that they have no known competing financial interests or personal relationships that could have appeared to influence the work reported in this paper.

Acknowledgements

The authors would like to thank the Bavarian Bureau for Agriculture (Landesamt für Landwirtschaft, LfL) for providing the 2018 IACS-LPIS data of Bavaria within the project "VieWBay" of the Bavarian State Ministry for the Environment and Consumer Protection. The responsibility for the content of this publication lies with the authors.

Appendix A. Supplementary material

Supplementary data to this article can be found online at https://doi.org/10.1016/j.compag.2019.105205.

References

Lesiv, M., Laso Bayas, J.C., See, L., Duerauer, M., Dahlia, D., Durando, N., Hazarika, R., Kumar Sahariah, P., Vakolyuk, M.y., Blyshchyk, V., et al., 2019. Estimating the global distribution of field size using crowdsourcing. Glob. Change Biol. 25, 174–186.

Fritz, S., See, L., McCallum, I., You, L., Bun, A., Moltchanova, E., Duerauer, M., Albrecht, F., Schill, C., Perger, C., et al., 2015. Mapping global cropland and field size. Glob. Change Biol. 21, 1980–1992.

Graesser, J., Ramankutty, N., 2017. Detection of cropland field parcels from landsat imagery. Remote Sens. Environ. 201, 165–180.

Wolfert, S., Ge, L., Verdouw, C., Bogaardt, M.-J., 2017. Big data in smart farming – a review. Agric. Syst. 153, 69–80.

Walter, A., Finger, R., Huber, R., Buchmann, N., 2017. Opinion: Smart farming is key to developing sustainable agriculture. Proc. Natl. Acad. Sci. 114, 6148–6150.

Hank, T.B., Berger, K., Bach, H., Clevers, J.G.P.W., Gitelson, A., Zarco-Tejada, P., Mauser, W., 2018. Spaceborne imaging spectroscopy for sustainable agriculture: Contributions and challenges. Surv. Geophys.

European Commission. The common agricultural policy at a glance. https://ec.europa.eu/info/food-farming-fisheries/key-policies/common-agricultural-policy/cap-glance_en (2019/04/30).

Skogstad, G., Verdun, A., 2009. The common agricultural policy: Continuity and change. J. Eur. Integr. 31, 265–269.

ESA, 2015. Sentinel-2 user handbook. European Space Agency (ESA).

Nieke, J., Rast, M., 2018. Towards the copernicus hyperspectral imaging mission for the environment (chime). Valencia, Spain, 22-27 July 2018, pp. 157–159.

Koetz, B., Bastiaanssen, W., Berger, M., Defourney, P., Bello, U.D., Drusch, M., Drinkwater, M., Duca, R., Fernandez, V., Ghent, D., et al., 2018. In High spatio-temporal resolution land surface temperature mission - a copernicus candidate mission in support of agricultural monitoring, IGARSS 2018 - 2018 IEEE International Geoscience and Remote Sensing Symposium, 22-27 July 2018, 2018; pp. 8160–8162.

Yan, L., Roy, D.P., 2014. Automated crop field extraction from multi-temporal web enabled landsat data. Remote Sens. Environ. 144, 42–64.

Schmidt, M., Pringle, M., Devadas, R., Denham, R., Tindall, D., 2016. A framework for large-area mapping of past and present cropping activity using seasonal landsat images and time series metrics. Remote Sens. 8, 312.

Gehlke, C.E., Biehl, K., 1934. Certain effects of grouping upon the size of the correlation coefficient in census tract material. J. Am. Stat. Assoc. 29, 169–170.

Openshaw, S., Tylor, P.S., 1979. A million or so correlation coefficients: Three

experiments on the modifiable areal unit problem. In: Wrigley, N. (Ed.), Statistical applications in the spatial sciences. Pion, London.
Lower Saxony Ministry of Food Agriculture and Consumer Protection, 2018. Integrated administration and control system of lower saxony (schlaege 2018). Landentwicklung und Agrarförderung Niedersachsen. https://sla.niedersachsen.de/landentwicklung/LEA/.
Openshaw, S., 1984. The modifiable areal unit problem. Geo Books, Norwich.
Löw, F., Duveiller, G., 2014. Defining the spatial resolution requirements for crop identification using optical remote sensing. Remote Sens. 6, 9034–9063.
European Commission, 2016. Copernicus agriculture and forestry applications user requirements workshop. Directorate-General for Internal Market, Industry, Entrepreneurship and SMEs. DG GROW Aerospace, Maritime and Defence Industries, Brussels.
European Union, 2013. No 1306 Chapter II Article 67. In: REGULATION (EU) No 1306/2013 OF THE EUROPEAN PARLIAMENT AND OF THE COUNCIL of 17 December 2013 on the financing, management and monitoring of the common agricultural policy and repealing Council Regulations (EEC) No 352/78, (EC) No 165/94, (EC) No 2799/98, (EC) No 814/2000, (EC) No 1290/2005 and (EC) No 485/2008, II. 1306. European Union, 67.
Fisher, J.R.B., Acosta, E.A., Dennedy-Frank, P.J., Kroeger, T., Boucher, T.M., 2018. Impact of satellite imagery spatial resolution on land use classification accuracy and modeled water quality. Remote Sens. Ecol. Conserv. 4, 137–149.
Pax-Lenney, M., Woodcock, C.E., 1997. The effect of spatial resolution on the ability to monitor the status of agricultural lands. Remote Sens. Environ. 61, 210–220.
Zhou, K., Cheng, T., Zhu, Y., Cao, W., Ustin, S.L., Zheng, H., Yao, X., Tian, Y., 2018. Assessing the impact of spatial resolution on the estimation of leaf nitrogen concentration over the full season of paddy rice using near-surface imaging spectroscopy data. Front. Plant Sci. 9, 964.
Sprintsin, M., Karnieli, A., Berliner, P., Rotenberg, E., Yakir, D., Cohen, S., 2007. The effect of spatial resolution on the accuracy of leaf area index estimation for a forest planted in the desert transition zone. Remote Sens. Environ. 109, 416–428.
Atkinson, P.M., 1997. Selecting the spatial resolution of airborne mss imagery for small-scale agricultural mapping. Int. J. Remote Sens. 18, 1903–1917.
Grandgirad, D., Zielinski, R., 2008. Land parcel identification system (lpis) - anomalies' sampling and spatial pattern. Joint Research Center, Ispra.
Bavarian Bureau for Agriculture. Integrated administration and control system (iacs), land parcel identification system (lpis) - bavaria. 2018.
FAO. Faostat; Food and Agriculture Organization of the United Nations (FAO): 2019.
Ministerie van Economische Zaken - Rijksdienst voor Ondernemend Nederland. Basisregistratie gewaspercelen (brp). https://nationaalgeoregister.nl/geonetwork/srv/dut/catalog.search#/metadata/b812a145-b4fe-4331-8dc6-d914327a87ff?tab=relations.
Bresenham, J.E., 1965. Algorithm for computer control of a digital plotter. IBM Syst. J. 4, 25–30.
Kuemmerle, T., Erb, K., Meyfroidt, P., Müller, D., Verburg, P.H., Estel, S., Haberl, H., Hostert, P., Jepsen, M.R., Kastner, T., et al., 2013. Challenges and opportunities in mapping land use intensity globally. Curr. Opin. Environ. Sustain. 5, 484–493.
Labate, D., Ceccherini, M., Cisbani, A., De Cosmo, V., Galeazzi, C., Giunti, L., Melozzi, M., Pieraccini, S., Stagi, M., 2009. The prisma payload optomechanical design, a high performance instrument for a new hyperspectral mission. Acta Astronaut. 65, 1429–1436.
Guanter, L., Kaufmann, H., Segl, K., Foerster, S., Rogass, C., Chabrillat, S., Kuester, T., Hollstein, A., Rossner, G., Chlebek, C., et al., 2015. The enmap spaceborne imaging spectroscopy mission for earth observation. Remote Sens. 7, 8830–8857.
Bach, H., Mauser, W., 2018. Sustainable agriculture and smart farming. In: Mathieu, P.-P., Aubrecht, C. (Eds.), Earth observation open science and innovation. Springer International Publishing, Cham, pp. 261–269.

APPENDIX II

The results of the first publication regarding the detected irrigated area is summarized in a supplement. All available regional and global data set of irrigated area are compared to the developed global irrigation map in the first publication.

Meier, J.; Zabel, F.; Mauser, W. (2018): A global approach to estimate irrigated areas – a comparison between different data and statistics. Supplement. *Hydrol. Earth Syst. Sci.*, *22*, https://doi.org/10.5194/hess-22-1119-2018-supplement

Supplement of Hydrol. Earth Syst. Sci., 22, 1119–1133, 2018
https://doi.org/10.5194/hess-22-1119-2018-supplement

Hydrology and Earth System Sciences
Open Access
EGU

Supplement of

A global approach to estimate irrigated areas – a comparison between different data and statistics

Jonas Meier et al.

Correspondence to: Jonas Meier (jonas.meier@lmu.de)

S. 1 Supplementary materials

Table S1: Comparison of different information about irrigated areas in the USA.

	New irrigation map[km²]	Ozdogan et al. [km²]	USGS [km²]
California	41,186	26,808	42,087
Texas	30,220	18,312	23,957
Arkansas	19,785	10,610	18,899
Idaho	16,475	8,348	14,569
Oregon	10,268	3,974	7,689
Florida	9,097	4,160	8,053
Kansas	16,146	12,131	12,464
Colorado	16,013	12,043	13,517
Nebraska	36,778	33,118	35,329
Wyoming	7,412	4,370	4,371
Washington	9,232	6,324	6,394
Utah	6,092	3,300	5,423
Missouri	5,632	3,047	5,301
Nevada	3,841	1,306	2,335
Montana	10,336	8,001	6,637
Arizona	4,955	3,050	4,019
Mississippi	6,542	4,755	7,244
Minnesota	2,382	854	2,185
New Mexico	4,985	3,665	3,553
Wisconsin	1,514	558	1,643
Michigan	1,939	1,208	2,048
New Jersey	542	192	402
Oklahoma	2,533	2,197	2,161
New York	312	164	437
Georgia	5,941	5,802	5,787
Connecticut	75	0	105
Rhode Island	25	0	25
Massachusetts	59	53	163
New Hampshire	1	0	24
Vermont	1	0	16
District of Columbia	0	0	0
West Virginia	0	0	15
Illinois	2,019	2,072	1,955
Maine	1	92	193
Delaware	398	600	538
Pennsylvania	116	330	276

Iowa	635	851	757
Indiana	1,440	1,973	1,607
Ohio	146	721	230
Maryland	328	1,047	425
Virginia	286	1,018	473
South Carolina	848	1,844	623
North Dakota	974	2,536	947
Kentucky	236	2,234	244
Alabama	389	3,345	615
South Dakota	2,000	5,484	785
North Carolina	1,174	5,091	1,085
Tennessee	348	4,267	372
Louisiana	4,858	10,767	3,747
Sum	286,516	222,625	251,724

Table S2: Comparison of different information about irrigated areas in China.

	New Irrigation Map [km²]	Zhang et al. [km²]	FAO [km²]
Xinjiang Uygur'	99,645	30,629	46,291
'Henan'	79,933	51,069	38,626
'Shandong'	73,327	48,110	44,855
'Hebei'	51,821	44,830	44,750
'Jiangxi'	47,970	18,935	34,876
'Anhui'	36,251	31,902	23,093
'Jiangsu'	34,501	38,606	28,422
'Hunan'	27,129	26,616	25,984
'Sichuan'	25,082	23,418	21,407
'Shaanxi'	24,668	13,123	12,116
'Hubei'	23,879	20,712	20,825
'Guangdong'	21,004	14,778	20,423
'Heilongjiang'	20,725	20,327	20,031
'Jilin'	18,837	13,119	18,187
'Gansu'	18,826	9,430	11,531
'Yunnan'	17,246	14,032	13,282
'Liaoning'	16,072	14,381	10,663
'Shanxi'	15,860	11,043	10,174
'Nei Mongol'	15,549	21,062	13,859
'Guangxi'	15,203	14,707	12,083
'Zhejiang'	14,818	13,421	14,687
'Fujian'	9,603	9,294	9,382
'Guizhou'	7,080	6,550	5,150
'Chongqing'	5,972	6,230	4,325

'Ningxia Hui'	5,473	4,012	4,972
'Qinghai'	4,188	2,114	3,016
'Tianjin'	4,178	3,434	3,219
'Beijing'	3,401	3,274	3,524
'Xizang'	3,371	1,417	2,899
'Shanghai'	2,996	2,868	3,083
'Hainan'	2,732	1,795	1,892
Sum	747,342	535,237	527,631

Table S3: Comparison of different information about irrigated areas in India.

	New irrigation map [km²]	Ambika et al. [km²]
'Andaman and Nicobar'	13	
'Andhra Pradesh'	62,676	60,800
'Arunachal Pradesh'	167	1,200
'Assam'	2,120	11,700
'Bihar'	65,738	27,100
'Chandigarh'	13	10
'Chhattisgarh'	14,313	33,400
'Dadra and Nagar Haveli'	33	50
'Daman and Diu'	10	0
Delhi	528	200
'Goa'	279	500
'Gujarat'	51,915	44,200
'Haryana'	36,671	30,900
'Himachal Pradesh'	1,937	2,800
'Jammu and Kashmir'	4,483	3,600
'Jharkhand'	4,745	14,000
'Karnataka'	31,535	39,500
'Kerala'	3,605	5,800
'Madhya Pradesh'	125,178	56,000
'Maharashtra'	55,178	35,900
'Manipur'	323	600
'Meghalaya'	638	1,200
'Mizoram'	46	700
'Nagaland'	282	1,200
'Odisha'	18,998	33,700
'Puducherry'	233	200
'Punjab'	47,274	43,800
'Rajasthan'	72,676	83,400
'Sikkim'	110	300

'Tamil Nadu'	31,998	32,700
'Tripura'	705	1,300
'Uttar Pradesh'	200,979	142,800
'Uttarakhand'	5,329	4,800
'West Bengal'	36,884	25,700
Sum	877,611	740,060

Table S4: Global comparison of irrigation maps. The values of GRIPC are weighted by an averaged field size factor of 0.83.

	New irrigation map [km²]	GMIA (downscaled) [km²]	FAOSTAT (average 1999-2012) [km²]	AQUASTAT (average 1998-2012) [km²]	GRIPC [km²]	GIAM [km²]
Afghanistan	36,043	33,484	32,063	32,080	5,618	10,081
Åland Islands	18	18	0		0	
Albania	5,446	3,433	3,457	3,390	3,313	2,238
Algeria	7,309	6,064	5,692	8,997	10,913	1,443
Angola	859	836	845	855	632	233
Argentina	17,907	16,922	18,981	23,570	22,040	93,043
Armenia	2,740	2,705	2,740	2,735	810	1,067
Aruba	0	0	0		0	
Australia	36,479	36,045	25,119	24,650	58,062	118,652
Austria	1,068	1,068	1,072	1,014	2	1,165
Azerbaijan	16,175	14,169	14,296	14,257	15,964	8,356
Bahamas	0	0	10	10	83	
Bahrain	15	15	40	41	1	
Bangladesh	53,291	48,033	48,195	50,500	62,804	52,351
Barbados	9	9	50	54	11	
Belarus	822	822	1,166	866	1	841
Belgium	298	298	251	232	4	3,248
Belize	44	44	33	35	63	39
Benin	467	114	178	177	136	152
Bhutan	250	248	285	298	289	10
Bolivia	1,311	1,274	2,618	2,619	2,549	2,141
Bosnia and Herzegovina	180	53	30	30	109	108
Botswana	51	51	16	14	85	54
Brazil	48,828	39,731	44,929	42,930	86,575	41,951
Bulgaria	6,157	5,625	2,530	1,211	4,144	13,018
Burkina Faso	897	228	385	396	15	157
Burma	46,405	21,193	21,208	20,500	32,660	44,530
Burundi	213	213	226	214	78	118

Cambodia	5,466	5,406	3,256	3,189	21,477	7,363
Cameroon	943	266	275	257	666	527
Canada	11,918	11,918	8,421	12,180	4,754	26,583
Cape Verde	23	19	33	35	24	0
Central African Republic	4	0	10		0	12
Chad	1,748	320	291	303	3,692	252
Chile	18,910	18,503	11,042	11,090	13,902	15,149
China	746,284	596,413	615,240	585,695	681,448	1,119,888
Colombia	8,353	8,340	9,662	9,935	5,714	5,462
Congo	20	20	20		516	0
Costa Rica	990	990	1,020		350	126
Cote d'Ivoire	639	622	730		695	951
Croatia	419	58	131	138	236	352
Cuba	8,672	8,672	8,700	5,576	7,441	4,869
Cyprus	583	583	445	555	1,189	71
Czech Republic	520	520	375	354	0	5,180
Democratic Republic of the Congo	124	122	110		1,947	218
Denmark	4,199	4,199	4,425	4,542	2,757	11,647
Djibouti	3	3	10	10	3	9
Dominican Republic	2,871	2,853	2,909	2,881	160	709
Ecuador	8,212	8,008	11,361	11,767	483	2,886
Egypt	37,319	33,451	35,009	35,160	20,667	21,441
El Salvador	492	492	450	452	6	116
Eritrea	232	231	211		21	170
Estonia	0	0	40	9	2	246
Ethiopia	6,623	3,086	2,900	2,896	2,492	1,842
Fiji	24	24	37	35	5	0
Finland	819	819	822	778	0	1,253
France	33,500	29,743	26,438	26,380	12,960	23,996
French Guiana	57	57	56		151	29
French Polynesia	0	0	10		13	
Gabon	41	41	40		34	0
Gambia	24	24	29	36	6	399
Georgia	4,299	4,150	4,384	4,328	3,522	1,285
Germany	4,961	4,961	5,516	5,466	502	21,977
Ghana	646	631	322	309	414	606
Greece	19,557	15,636	15,037	13,910	13,213	9,077
Grenada	0	0	10	4	0	0
Guadeloupe	71	71	66		2	19
Guam	0	0	2		0	0
Guatemala	1,361	1,361	2,875	3,248	85	694
Guernsey	0	0	0		0	
Guinea	973	906	950	949	553	3,026

Guinea-Bissau	348	209	249		58	1,080
Guyana	1,316	1,316	1,463	1,430	1,565	963
Haiti	929	929	959	970	572	508
Honduras	774	774	847	888	150	706
Hong Kong	21	21	0		43	
Hungary	3,181	3,181	1,847	1,956	493	2,417
Iceland	0	0	0		0	
India	879,572	612,289	642,777	642,960	880,684	1,012,349
Indonesia	62,199	61,733	63,594	67,220	30,383	31,729
Iran (Islamic Republic of)	99,493	91,973	86,256	84,985	32,917	26,233
Iraq	36,118	35,407	35,250		15,194	22,200
Ireland	4	4	0	11	0	0
Israel	1,852	1,786	2,199	2,250	2,833	998
Italy	49,632	38,573	39,324	38,593	26,230	28,306
Jamaica	241	241	250	307	30	49
Japan	23,722	23,721	25,563	26,500	12,835	25,251
Jordan	919	898	846	802	1,588	727
Kazakhstan	57,177	26,566	20,161	19,720	42,375	72,277
Kenya	4,040	960	981	1,301	55	854
Kiribati	0	0	0		6	
Korea, Democratic People's Republic of	13,991	13,991	14,600		8,573	14,673
Korea, Republic of	7,482	7,482	8,441	8,435	15,000	11,925
Kuwait	105	105	87	86	10	373
Kyrgyzstan	11,277	10,339	10,323	10,220	5,408	7,009
Lao People's Democratic Republic	3,171	3,121	3,024	3,028	7,215	1,056
Latvia	0	0	9	8	0	127
Lebanon	1,090	1,059	1,040	1,040	1,216	247
Lesotho	19	19	30	26	0	57
Liberia	12	12	30		67	2
Libyan Arab Jamahiriya	4,770	4,711	4,700	4,350	3,830	2,307
Lithuania	0	0	55	45	0	573
Luxembourg	0	0	365	0	0	0
Madagascar	11,445	11,445	10,860	10,860	6,123	724
Malawi	498	497	671	643	165	33
Malaysia	3,422	3,422	3,752	3,800	633	2,588
Mali	2,864	2,486	2,993	3,035	468	564
Malta	23	23	27	28	51	0
Martinique	51	51	64		1	
Mauritania	469	469	450	450	89	151
Mauritius	190	190	207	212	244	53
Mexico	71,197	68,352	63,636	63,600	63,787	38,547
Mongolia	7,687	759	840		1,924	4,223
Montenegro	71	36	23	24	96	103

Morocco	15,734	15,091	14,439	14,827	23,925	10,451
Mozambique	1,280	1,199	1,174	1,181	601	564
Namibia	86	86	79	76	15	105
Nepal	18,163	11,048	12,201	11,680	16,401	12,520
Netherlands	4,158	4,158	4,434	4,805	141	8,702
New Caledonia	0	0	97		24	
New Zealand	5,342	5,197	5,406	5,435	4,658	1,254
Nicaragua	884	883	1,441	1,467	1,010	164
Niger	744	744	816	823	494	41
Nigeria	6,277	3,172	2,907	2,918	14,507	1,979
Norway	1,149	1,149	1,148	1,142	2	21
Oman	1,044	599	593	589	148	179
Pakistan	192,534	165,867	191,007	189,050	130,583	140,362
Palestine	243	242	230	220	1,127	75
Panama	329	329	335	321	3,807	491
Paraguay	605	585	808	1,016	8,665	286
Peru	18,178	17,951	22,721	25,800	1,705	3,560
Philippines	17,470	17,293	14,527	18,790	19,279	15,426
Poland	1,045	1,045	1,039	967	30	3,515
Portugal	8,993	8,361	6,341	6,879	3,406	3,589
Puerto Rico	358	358	219	219	6	120
Qatar	139	137	130	129	3	385
Republic of Moldova	2,915	2,915	2,475	2,677	300	2,941
Reunion	79	79	84		19	7
Romania	21,392	21,235	31,519	13,720	5,426	23,752
Russia	21,651	20,171	44,770	23,750	78,337	138,869
Rwanda	91	91	92	91	50	801
Saint Helena	2	0	0		0	
Saint Lucia	35	35	30	30	0	0
San Marino	2	2	0		5	11
Sao Tome and Principe	80	80	100		0	0
Saudi Arabia	15,195	14,050	16,190	16,200	1,931	6,787
Senegal	1,252	1,250	1,170	1,197	827	2,114
Serbia	1,973	1,648	931	920	276	1,719
Seychelles	1	1	3	3	3	1
Sierra Leone	295	295	299		2,489	218
Slovakia	2,211	2,211	1,599	1,547	5	1,099
Slovenia	152	152	60	65	59	4
Somalia	8,304	2,094	2,000	2,000	12	3,725
South Africa	15,266	15,250	15,332	15,840	8,332	8,210
Spain	42,126	36,856	37,674	36,733	34,065	34,217
Sri Lanka	5,398	5,391	5,700	5,700	12,291	9,480
Sudan	19,896	18,851	19,900	18,901	8,686	17,371

Suriname	444	444	549	542	616	198
Swaziland	421	421	499	499	128	198
Sweden	1,607	1,607	1,616	1,535	475	839
Switzerland	552	552	503	580	12	295
Syrian Arab Republic	15,931	15,248	13,418	13,490	15,892	5,670
Taiwan	4,088	4,058	3,795		3,564	4,990
Tajikistan	7,271	6,949	7,301	7,307	5,947	3,832
Thailand	67,449	60,696	61,148	57,005	74,231	66,106
The former Yugoslav Republic of Macedonia	1,887	1,305	1,096	914	1,345	1,698
Timor-Leste	341	341	343	347	47	38
Togo	86	86	70		20	217
Trinidad and Tobago	30	30	64	70	0	19
Tunisia	4,841	4,685	4,230	4,452	3,821	1,091
Turkey	61,036	54,001	51,139	51,615	22,122	17,534
Turkmenistan	33,644	20,162	19,544	19,910	11,483	15,224
Uganda	120	80	120	101	4	300
Ukraine	24,073	24,073	22,327	22,563	11,770	29,956
United Arab Emirates	2,414	2,396	1,863	1,593	41	938
United Kingdom	2,430	2,430	1,899	1,145	233	9,707
United Republic of Tanzania	1,802	1,737	1,795	1,843	567	470
United States	285,447	279,020	267,401	267,630	226,636	280,455
Uruguay	2,395	2,395	2,149	2,095	5,400	3,814
Uzbekistan	56,300	38,845	42,082	41,980	36,596	36,015
Venezuela	7,226	7,168	8,843	8,126	6,275	8,949
Viet Nam	47,074	42,847	42,739	45,850	54,965	43,840
Yemen	12,630	8,658	6,221	6,801	1,632	917
Zambia	1,459	1,440	1,513	1,559	20	8
Zimbabwe	1,851	1,846	1,740	1,735	163	47
Sum	3,674,478	3,007,038	3,076,937	2,962,922	3,141,000	3,983,979

APPENDIX III

The map of global irrigated area developed in the first publication is available for non-commercial use (CC-NY-NC-3.0) and can be downloaded.

Meier, J.; Zabel, F.; Mauser, W. (2018): Global Irrigated Areas. *PANGAEA*, https://doi.org/10.1594/PANGAEA.884744